Performance Study of One-Dimensional Models for Stratified Thermal Storage Tank

by

Eberhard Markus Kleinbach

A thesis submitted in partial fulfillment of the requirements for the degree of

Master of Science

(Chemical Engineering)

at the

University of Wisconsin-Madison

1990

Abstract

The performance of a solar domestic hot water system (SDHW) is affected by the temperature distribution in the storage tank. Therefore, accurate modeling of a SDHW system requires an accounting for the thermal stratification in the storage tank.

TRNSYS, a transient system simulation program developed by the Solar Energy Laboratory, has been proven to be an accurate program in predicting and analyzing solar thermal and other energy systems.

TRNSYS uses two basic concepts for stratified storage tank models. In the multi-node approach, the tank is divided into N nodes, with energy balances written for each node. This results in a set of N differential equations that can be solved for the temperatures of the nodes as a function of time. In the plug flow approach, segments of liquid of different temperatures and sizes are assumed to move through the tank in plug flow manner. The sizes of the fluid elements are determined by the simulation time step and the flow rates. Whenever the incoming fluid from the heat source is colder than the fluid at the top of the tank, "plume entrainment" occurs. Plume entrainment has been built into both the multi-node and the plug flow model.

So far there have been no guidelines concerning the employment of the TRNSYS tank models under various operating conditions. Therefore, a performance study of the TRNSYS tank models has been carried out using experimental data from two different sources. Data for low heat source flow rates were obtained from Queen's University,

Kingston, Ontario and data for high heat source flow rates were obtained from Colorado State University, Fort Collins, Colorado. Three numbers have been defined to describe the performance of the different tank models in predicting the experimental data. The results are discussed in detail and recommendations as to which tank model should be used under which conditions are given.

The results suggest that the use of the fully mixed tank model is never appropriate. Relationships between the number of nodes to be used for the multi-node models and the mean number of tank turnovers have been developed which are useful as a guideline for choosing the most appropriate number of nodes for given operating conditions. The plug flow model with plume entrainment is suggested as an alternative to the multi-node models for a mean number of tank turnovers less than five.

Acknowledgements

It's hard to believe but it is true: the thesis is done. The sixteen months of studying at the University of Wisconsin are over; and time has passed quickly.

My first thanks go to my advisors Professor William A. Beckman, Professor Sanford A. Klein and Professor John A. Duffie. Bill, the director of the Solar Lab, was always asking for "any progress" when I walked into my weekly advisor meetings. During the meetings he always gave his best to help me to go in the right direction. His questions helped me to explore every detail of this project. Sandy had enlightening ideas, questions and answers which were essential for the progress of this project. He provided necessary motivation for the next steps. Jack, the founder of the Solar Lab, helped me to get started in this project and to understand the basic ideas of the use of solar energy. I enjoyed working with all three of them. Together with Professor John W. Mitchell they made the Solar Lab a great place to be, not only because of their picnics and parties.

It will not be easy to leave the Solar Lab. The pleasant atmosphere, the good computer equipment and the fun during times of hard work made it very enjoyable here. Thanks to my fellow graduate students and the whole Solar Lab staff for their helpfulness with computer and other problems. The weekly seminars gave insight in what went on in the Lab and gave me some additional good experience.

Besides the people of the Lab several other friends have all contributed to a good time here. Thanks to my roommates and the people from Geneva Chapel, I never felt like a stranger. Having a good beer at the "Essenhaus" every now and then with my German friends was a nice change during long weeks of studying. I also appreciate the letters and

greetings which I received from friends at home who kept in touch and showed their interest in what I am doing here.

Thanks to Queen's University, Kingston, Ontario and Colorado State University, Fort Collins, Colorado for providing the experimental data which made this study possible.

I am also grateful to Professor Michael Zeitz, the organizer of this successful and unique exchange program between the Universität Stuttgart and the Department of Chemical Engineering at the University of Wisconsin in which I participated. The financial support for this work was supplied during the first two semesters by the German Academic Exchange Service (DAAD). During the remaining time funds were made available through the U.S. Department of Energy.

Last but not least, I want to thank my parents and my brothers for their loving support with letters, packages, phone calls and dollars. The family vacation that we spent together in the western part of the United States was certainly one of the highlights. I am looking forward to see you all again in the reunified Germany.

Table of Contents

List of Figures

List of Tables

Nomenclature

Roman Symbols

Text Symbol	Dimension	Meaning
a	[kJ/(°C h)]	coefficient in the discrete equations
A	[m^2]	cross-sectional area of the tank
A_c	[m^2]	total collector aperture area
b	[kJ/h]	coefficient in the discrete equations
c	[-]	fraction of volume
C	[-]	(entrainment) constant
C_f	[kJ/(kg °C)]	specific heat capacity of the fluid
d	[m]	penetration depth of the stream
D	[m]	inlet pipe diameter
D_T	[m]	outer diameter of the tank
F_h	[-]	heat exchanger penalty factor
F_R	[-]	collector heat removal factor
H	[m]	height of the tank
H_{in}	[m]	heat source inlet above bottom of tank
g	[m/s^2]	acceleration of gravity
Δh_i	[m]	separation between centers of segments i and i+1
i	[-]	number of node under consideration

i_d	[-]	number of node where the stream merges with the tank
I_T	[kJ/(h m2)]	total radiation incident on the collector per unit area
j	[-]	summation variable
k_f	[kJ/(h m °C)]	thermal conductivity of the fluid
K_S	[-]	Phillips stratification coefficient
L	[-]	number of node that contains the thermostat
$\dot{m}$	[kg/h]	mass flow rate
$\dot{m}_{coll}$	[kg/h]	mass flow rate in the collector loop
$\dot{m}_{heat}$	[kg/h]	mass flow rate in the heat source loop
$\dot{m}_{load}$	[kg/h]	mass flow rate in the load loop
$\dot{m}_S$	[kg/h]	mass flow rate of the stream
$\dot{m}_T$	[kg/h]	mass flow rate of the tank
M_{heat}	[kg]	total daily mass of the fluid coming from the heat source
M_i	[kg]	mass of the fluid in the ith node
M_{load}	[kg]	total daily mass of the fluid removed to the load
M^P	[kg]	mass of fluid in the control volume
M_T	[kg]	mass of the fluid in the tank
N	[-]	number of nodes (segments)
$\overline{N}$	[-]	average number of segments
P	[-]	performance number
P_{best}	[-]	best value of P (for a particular test)
P_T	[m]	perimeter of the tank
$\dot{Q}_{aux,i}$	[kJ/h]	rate of auxiliary energy input into node i

Q_{cond}	[kJ]	conducted heat
QD	[-]	relative error in the delivered energy
Q_{del}	[kJ]	delivered energy
$\dot{Q}_{del}$	[kJ/h]	rate of delivered energy
Q_{entr}	[kJ]	entrained enthalpy
Q_{env}	[kJ]	losses to the environment
$\dot{Q}_{env}$	[kJ/h]	rate of the losses to the environment
QI	[-]	relative error in the energy input into the tank
Q_{in}	[kJ]	energy input into the tank
$\dot{Q}_{in}$	[kJ/h]	rate of energy input into the tank
Q_S	[kJ]	enthalpy of the stream
Q_T	[kJ]	enthalpy of the tank flow
$\dot{Q}_u$	[kJ/h]	rate of useful energy gain
Ri	[-]	Richardson Number
r_{ins}	[-]	ratio of thickness of top insulation to thickness of side insulation for upright tanks or ratio of insulation thickness of top to bottom for horizontal tanks
S_i	[m^2]	cross-sectional area between segments i and i+1
ST	[(°C)^2]	stratification coefficient defined by Wu and Bannerot
t	[h]	time
t_1	[h]	time at the beginning of the time step
Δt	[h]	time step
Δt_{max}	[h]	maximum allowable time step
t_{off}	[h]	time when the flow from the heat source

		ends
t_{on}	[h]	time when the flow from the heat source begins
Δt_{sol}	[h]	time step used to solve plume entrainment
T	[-]	mean number of tank turnovers
ΔT	[°C]	temperature difference between the temperature of the inlet fluid and the initial tank temperature
ΔT_{actual}	[°C]	actual temperature difference between the top and the bottom of the storage tank
T_{bottom}	[°C]	temperature of the bottom node
ΔT_c	[°C]	temperature difference between the tank and the environment
ΔT_{db}	[°C]	temperature deadband of the auxiliary heater
T_{del}	[°C]	temperature of the fluid delivered to the load
T_{env}	[°C]	temperature of the environment
T_{fl}	[°C]	average flue temperature when the auxiliary is not operating
T_{heat}	[°C]	temperature of the fluid entering the tank from the heat source
T_i	[°C]	temperature of the ith node
ΔT_{ideal}	[°C]	ideal temperature difference between the top and the bottom of the storage tank
T_{init}	[°C]	initial temperature of the preheat portion of the tank
T_{mains}	[°C]	temperature of the fluid replacing that extracted to the load

T_{mean}	[°C]	mean tank temperature
$T_{mean,actual}$	[°C]	actual mean temperature in the storage medium
$T_{mean,ideal}$	[°C]	ideal mean temperature for a linear temperature profile in the storage medium
T_{ret}	[°C]	temperature of the fluid returned to the heat source
T_S	[°C]	temperature of the stream
T_{set}	[°C]	set point temperature of the auxiliary heater
T_T	[°C]	temperature of the tank
$\overline{T}_T$	[°C]	mean temperature of the tank layer under consideration
T_{top}	[°C]	temperature of the top node
u	[1/h]	coefficient in first order differential equation
U	[kJ]	internal energy of the tank
ΔU	[kJ]	change in the internal energy of the tank
U_L	[kJ/(m^2 h °C)]	overall heat loss coefficient between the collector and the environment per unit area
U_T	[kJ/(m^2 h °C)]	overall heat loss coefficient between the tank and the environment per unit area
UA	[kJ/(h °C]	overall heat loss coefficient between the tank and the environment
UA_{fl}	[kJ/(h °C)]	overall heat loss coefficient to the exhaust flue of an in-tank gas auxiliary heater
$UA_{fl,i}$	[kJ/(h °C)]	overall heat loss coefficient to the gas flue of an in-tank auxiliary heater for node i
UA_i	[kJ/(h °C]	overall heat loss coefficient between node i

		and the environment
v	[°C/h]	coefficient in first order differential equation
$\dot{V}_{coll}$	[m^3/s]`	volume flow rate in the collector loop
V_{heat}	[m^3]	volume of fluid added from the heat source to the tank
$\dot{V}_{heat}$	[m^3/s]	volume flow rate in the heat source loop
V_i	[m^3]	volume of node i
V_{load}	[m^3]	volume of fluid returned from the load
$\dot{V}_{load}$	[m^3/s]	volume flow rate in the load loop
V_T	[m^3]	volume of the tank
w	[m/s]	fluid velocity at the inlet port
x	[m]	vertical coordinate measured from the top of the tank
Δx	[m]	height of control volume

Greek Symbols

Text Symbol	Dimension	Meaning
α_i	[-]	control function for node i
β	[1/°C]	thermal expansion coefficient of the fluid
β_i	[-]	control function for node i
γ_i	[kg/h]	control function for node i
δ_i	[-]	control function for node i

ε	[-]	control function
η	[-]	collector efficiency
ξ	[-]	Koldhekar stratification coefficient
ρ_f	[kg/m^3]	density of the fluid
τ	[h]	time (integration variable)
$(\tau\alpha)$	[-]	transmittance-absorptance product
ξ	[m]	vertical coordinate measured from the top of the tank (integration variable)

Additional Subscripts and Superscripts

Text Symbol	Meaning
0	previous time step
exp	experimental
N	north; node above
P	polar; node under consideration
S (subscript)	stream
S (superscript)	south; node below
sim	simulated
T	tank

Chapter 1

Introduction and Literature Review

1.1 Energy Storage

For time-dependent energy resources, e.g. solar energy, there is a necessity of energy storage if these resources are to meet substantial portions of energy needs that are also time-dependent but in a different fashion. A variety of ways to store thermal energy is conceivable, e.g. in the form of sensible heat of a liquid or solid medium, as heat of fusion in a chemical system or as chemical energy of products in a reversible chemical reaction. In some cases energy conversion may be required.

The choice of the storage medium depends on the nature of the process considered. For water heating systems, energy storage as sensible heat of stored water is logical. Water as storage medium also has the advantages of high specific heat (which prevents the storage device to become overly bulky), benign character, low cost and availability in abundance.

The performance of a thermal storage device is affected by a number of factors. The more important ones are (i) its thermal capacity; (ii) the temperature range over which it operates; (iii) means of addition or removal of heat and the temperature differences associated thereafter; (iv) the temperature stratification in the device and (v) the thermal losses from the device. This thesis is particularly concerned with the phenomenon of thermal stratification in hot liquid storage tanks.

1.2 Thermal Stratification

The term "thermal stratification" suggests a discontinuous temperature field. Though such is impossible the term corresponds well with our image of the phenomenon. In general thermal stratification means that the temperature of the fluid increases with the elevation.

1.2.1 Factors affecting Thermal Stratification

Stratification in a thermal storage tank will depend mainly on the design of the tank, the size, location and design of the inlets and outlets and the flow rates of entering and leaving streams. Lavan and Thompson [1] carried out an experimental study of thermally stratified hot water storage tanks. They concluded that stratification improves with increasing height to diameter ratio of the tank, increasing temperature difference between the inlet and the exit water, increasing inlet and outlet port diameters and decreasing flow rates. Best results were obtained when the inlet and outlet ports are near the end walls and when the flow is directed towards these walls. Gari and Loehrke [2] investigated specially designed inlet manifolds which introduce water into the tank with minimum mixing between fluids of unlike temperatures.

There are four primary "destratification factors" which contribute to the loss and/or degradation of the stored energy. These are : (i) the heat losses to the ambient; (ii) heat conduction from the hot layer to the cold layer; (iii) vertical conduction in the tank wall which along with (i) induce convective currents (mixing) and (iv) mixing introduced during charge and discharge cycles.

Much work has been done to investigate the effects of factors (i) to (iii). Computational analyses by Miller [3] have shown that if the tank wall conductivity is close to that of the water and if in addition the heat losses to the ambient are small, then the temperature is

essentially constant in the radial direction and negligible convection currents arise. The calculation of vertical temperature profiles, as outlined by Jaluria and Gupta [4] for this case, is straightforward. These calculations also show that the degradation process is very slow, requiring several days. Since many charge and discharge cycles usually occur during this time frame, conduction through water is not considered as a major source of destratification. However, for a Plexiglas tank with no insulation, heat losses from the sides severely degrade stratification [4]. The effect of such heat losses is particularly important for small tanks. Alternatively, if the tank walls are highly conductive, then the walls will approach the average temperature in the tank. Hess and Miller [5] have shown that this causes convective currents which destroy stratification. Experimental and numerical work revealed that the thermocline in an aluminum tank degraded ten times faster than that in a glass tank [3]. Later experiments by Sherman et al. [6] confirmed that the thermocline degradation is indeed considerably accelerated by highly conductive walls.

The effect of inlet jet mixing during charging (iv) has been investigated by Sliwinski et al. [7]. They have found that the height of the mixing region, when non-dimensionalized by division by the tank height, appears to be a unique function of the Richardson number, defined by

$$Ri = \frac{g \beta \Delta T H}{w^2} \tag{1.1}$$

where g = acceleration of gravity

β = thermal expansion coefficient of the fluid

ΔT = temperature difference between the temperature of the inlet fluid and the initial tank temperature

w = fluid velocity at the inlet port

H = height of the tank

The experiments performed by Sliwinsky et al. propose that the height of the mixing region rises sharply for Ri < 0.5. This critical Richardson number, however, may be dependent on the inlet port configuration. Experiments by Loehrke and Holzer [8] showed that good stratification was not achieved at a Richardson number as high as 4.7, since the incoming flow was turbulent. A second mixing phenomenon, called "plume entrainment" will be discussed in section 2.3.

1.2.2 Effect of Stratification on the Performance of Solar Domestic Hot Water (SDHW) Systems

The thermal performance of a SDHW system, an example is shown in Fig. 1.1, depends on the temperature distribution in the storage tank, which is affected mainly by the collector flow rate. High collector flow rates (about 50 kg/(h m^2 collector area)) were traditionally used in forced flow SDHW because a high collector flow rate improves the collector efficiency curve by increasing the collector heat removal factor as explained in Duffie and Beckman [9]. However, high collector flow rates will cause the storage tank to be at nearly uniform temperature due to a large amount of mixing.

A thermally stratified storage tank, obtainable at low collector flow rates, can improve system performance. This has been noted by several researchers as early as 1979 [10 - 13]. However, there is a discrepancy between various studies as to the degree of system performance enhancement possible. Some studies indicate improvements as high as 20 % while others show no improvement potential. Although the collector heat removal factor decreases by reducing the collector flow rate, the collector efficiency may be increased by supplying the collector with cold water from the bottom of a stratified tank because of lower collector thermal losses. This becomes clear by looking at Eqn (1.2) for the efficiency of a flat-plate collector as evaluated by Hottel and Whillier [14] as

$$\eta = \frac{\dot{Q}_u}{A_c I_T} = F_R (\tau\alpha) - F_R U_L \frac{(T_{ret}-T_{env})}{I_T} \qquad (1.2)$$

where η = collector efficiency

$\dot{Q}_u$ = rate of useful energy gain

A_c = total collector aperture area

I_T = total radiation incident on the collector per unit area

F_R = collector heat removal factor

$(\tau\alpha)$ = transmittance-absorptance product

U_L = overall heat loss coefficient between the collector and the environment per unit area

T_{ret} = temperature of the fluid returned to the heat source (in this case collector)

T_{env} = temperature of the environment

It is apparent that the trade off between the reduced collector heat removal factor and the reduced collector losses must be addressed when identifying an optimal collector flow rate. In general the optimal collector flow rate will be the maximum flow rate possible that does not cause hot water to circulate through the collector either by tank mixing or overcharging. In practice the optimal collector flow rate is found to be about one seventh of the traditionally used flow rate.

The reduction of the collector flow rate has two additional effects. Firstly, the collector outlet temperature and therefore the temperature at the top of the storage tank will be increased. This increases the quality (i.e. thermodynamic availability) of the energy available. Secondly, substantial savings may be realized through initial system cost reductions; low flow systems allow major reductions in piping, pumping, plumbing and heat exchanger costs.

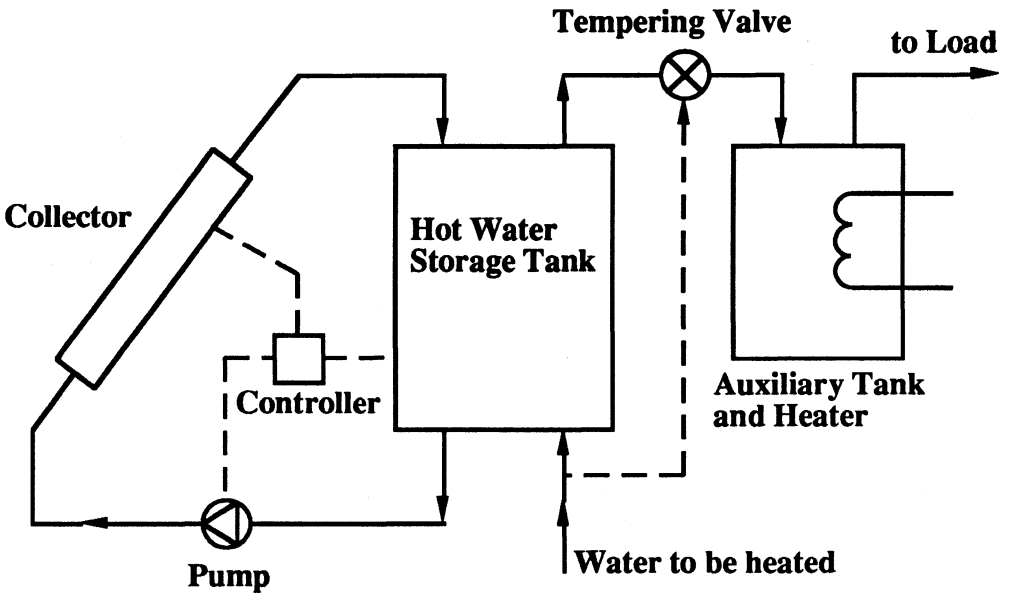

Fig. 1.1 Typical Solar Domestic Hot Water System

1.2.3 Stratification Description

Several attempts to define a stratification coefficient have been made in order to quantitatively determine the effect of a stratified thermal storage tank on the overall performance of a SDHW system. Three models of interest have been developed by Phillips and Dave [15], Wu and Bannerot [16] and Koldhekar [17].

The Phillips stratification coefficient, K_S, is defined as the ratio of the actual useful energy gain to the useful energy gain that would be achieved if there were no stratification in the storage tank and can be written as

$$K_S = \frac{F_R F_h A_c [(\tau\alpha) I_T - U_L (T_{ret}-T_{env})]}{F_R F_h A_c [(\tau\alpha) I_T - U_L (T_{mean}-T_{env})]} \qquad (1.3)$$

where F_h = heat exchanger penalty factor

T_{mean} = mean tank temperature.

This ratio utilizes the Hottel, Whillier [14] and Bliss [18] model for defining the useful energy gain. The Phillips stratification coefficient is reported as an all day integrated value based on the solar input hours only.

The model defined by Wu and Bannerot was originally confined to the study of horizontally placed storage tanks. The stratification factor, ST, is defined as the mass weighted mean square difference between the temperature of the water in the ith element and the average temperature of the water in the tank and is therefore

$$ST = \sum_{i=1}^{N} \frac{M_i (T_i - T_{mean})^2}{M_T} \tag{1.4}$$

where N = number of fluid elements in the tank

M_i = mass of the fluid in the ith element

T_i = temperature of the fluid in the ith element

M_T = total mass of the fluid in the tank.

T_{mean} = mean tank temperature

A fully mixed tank has a stratification coefficient of zero whereas a stratified tank would have a stratification coefficient greater than zero. The actual value of ST for the stratified case is based on the individual tank geometry and the temperature distribution inside the tank. This coefficient is a measure of the instantaneous stratification in the storage tank and has units of $(°C)^2$.

The stratification number defined by Koldhekar, ξ, is the product of two ratios: the ratio of the actual temperature difference, ΔT_{actual}, to the ideal temperature difference,

ΔT_{ideal}, between the top and the bottom of the storage tank and the ratio of the actual average temperature, $T_{mean,actual}$, to the average temperature for a linear temperature profile, $T_{mean,ideal}$, in the storage medium. In equation form this is written as

$$\xi = \frac{\Delta T_{actual}\, T_{mean,actual}}{\Delta T_{ideal}\, T_{mean,ideal}} \tag{1.5}$$

This number provides an indication of the energy content available from the storage tank and the temperature level at which the energy is available. The ideal top temperature is limited by the boiling point of the water and the ideal bottom temperature is limited by the temperature of the mains water. A value of zero indicates a fully mixed tank. For a stratified tank this stratification number is greater than zero and is also dependent on the temperature scale used.

1.2.4 Modeling Stratification in a Hot Liquid Storage Tank

1.2.4.1 Review of proposed Models

A number of models have been developed to account for thermal stratification in hot liquid storage tanks. However, the levels of sophistication with which these models were developed are quite different. One-dimensional, two-dimensional and three-dimensional models exist. The simpler and therefore computationally less expensive models are suitable to be used for simulating annual performance of energy systems, e.g. SDHW systems. The more detailed models require significantly more computing time but can shed considerable light on the phenomena inside the tank, such as temperature and velocity distributions.

Traditionally, thermally stratified storage tanks have been modeled one-dimensionally by assuming the tank to be made up of N uniform temperature, fixed location disks [19, 20] as described in section 2.1. Energy balances (involving entering and leaving streams, losses to the environment and possibly auxiliary energy input) for each of these disks are solved each simulation time step. Alternatively, isothermal disks of variable sizes (governed mainly by the flow rates and the simulation time step) moving in plug flow manner through the tank were modeled [20, 21] as described in section 2.2. A minimum amount of mixing is introduced in both models when the incoming fluid streams are directed to the level where they are closest to the disk temperatures (variable inlets). More mixing is introduced when the incoming fluid streams enter the tank at fixed locations and temperature inversions are corrected by mixing of appropriate disks (fixed inlets).

Since it is desirable to achieve a plug-type flow by placing the inlet hot (cold) liquid at the uppermost (lowermost) portion of the tank or by using specially designed inlet manifolds [2] with minimum mixing with the existing fluid in the tank, one-dimensional modeling efforts are somewhat justified.

Han and Wu [22] proposed a one-dimensional model which includes the mixing effects due to viscous entrainment by the incoming stream of the tank. The model incorporates heat source and load circuits. Mass and energy balance equations are derived for both circuits and solved using an implicit finite difference technique. An additional equation describing the rate of entrainment is provided. A boundary condition parameter is introduced to account for mixing in the upper and lower regions of the tank due to the introduction of heat source and load flows, respectively. Another model by Phillips and Pate [23] and Lightstone [24] which also accounts for viscous entrainment is presented in section 2.3.

The model of Cole and Bellinger [25] is a one-dimensional analytical model with empirically derived parameters. These are a mixing parameter which accounts for the mixing due to the introduction of the fluid into the tank, a normalized film heat transfer

coefficient which accounts for the fluid-wall thermal interaction and a capacity ratio which takes the effect of the wall heat capacity on stratification into account. Heat losses to the surroundings were neglected and a constant flow rate assumption was imposed. Also, constant inlet temperature and uniform initial temperature assumptions were made.

The model of Zurigat et al. [26] is a one-dimensional finite difference model which accounts for turbulent mixing in the tank and heat losses to the ambient. The energy equation for turbulent flow is solved by splitting it into two equations representing the conduction and convection cases, and handling them with different computational time steps. This technique was shown to completely eliminate the numerical diffusion in the finite difference solution. By introducing an effective diffusivity factor the turbulent energy equation is reduced to the laminar one, magnifying the molecular diffusivity by that factor. The model incorporates three different inlet geometries; a side inlet, an impingement inlet and a perforated inlet. There are several other one-dimensional models, e.g [27 - 30], in the literature which are not described in this review.

More complex models have appeared in the literature. The two-dimensional model of Cabelli [31] has incorporated two flow circuits and two geometric configurations with horizontal and vertical entries into the tank. The values of the Reynolds numbers used were limited by the mesh size to magnitudes smaller than those expected in practical situations. This discrepancy was treated later by Guo and Wu [32] who developed a two-dimensional model applicable for higher Reynolds numbers. In their work, the Richardson number, Ri, was identified as the important parameter for characterization of the physical conditions of the flow pattern and the temperature stratification inside the storage tank. At $Ri << 1$, the forced convection becomes important and leads to a complete mixing case. In the two-dimensional model of Chan et al. [33] different inlet and outlet locations were tested and compared with respect to thermal efficiency.

A three-dimensional model has been developed by Sha et al. [34] to study improved storage tank designs. The model incorporates a simple eddy diffusivity turbulence model and is restricted to a cylindrical tank geometry.

1.2.4.2 Validation of Models

The validation of the models for thermally stratified storage tanks was commonly, e.g. [26, 27, 35, 36], done by comparing the thermocline (region of steepest temperature gradient inside the tank) predictions with the experimentally measured thermocline during single charge or discharge experiments. During these experiments, hot (cold) fluid is used to displace the cold (hot) fluid existing in the tank which results in the development of a thermocline inside the tank. The idea behind this method of testing the models is that if a model is capable of accurately predicting the thermocline during charging or discharging then it will also predict the correct temperature of the fluid being displaced (and therefore the temperature of the fluid leaving the tank) as a function of time. In this thesis a different approach of validating the storage tank models under investigation, without using the thermocline, will be used (cf. section 4.2); mainly because the experiments on which the comparisons for the models are based are not single charge or discharge experiments (cf. chapter 3).

1.3 Goal of Project

So far there have been no recommendations concerning the employment of different storage tank models in energy systems simulation programs, e.g TRNSYS [20]. The goal of this project is to compare the TRNSYS tank models (introduced in chapter 2) with experimental

data for a wide range of conditions in order to give some recommendations as to which tank model should be used under which operating conditions. The recommendations to be given will be based on the accuracy of predicting the experimental data and the computational efficiency of the models under investigation.

Chapter 2

Models used in this project

In this chapter the storage tank models under investigation are introduced. Both the multi-node model and the plug flow model have been extended by building in "plume entrainment". All the models are available in the TRNSYS [20] simulation program, developed by the Solar Energy Laboratory.

TRNSYS has been proven to be an accurate program in predicting and analyzing solar thermal and other energy systems. It has a modular structure and consists of individual subroutines which represent real physical devices or utility components. The components can be connected together to form complex systems.

2.1 Multi Node Model

In the multi-node approach [19,20], the tank is modeled as N fully mixed volume segments (nodes) as shown in Fig. 2.1. The degree of stratification is determined by the choice of N. Higher values of N result in more stratification. A maximum number of 15 nodes can be chosen in the current implementation. For the special case of N = 1 the tank is modeled as a fully mixed tank and no stratification effects are possible. Unequally sized nodes can be specified in this model.

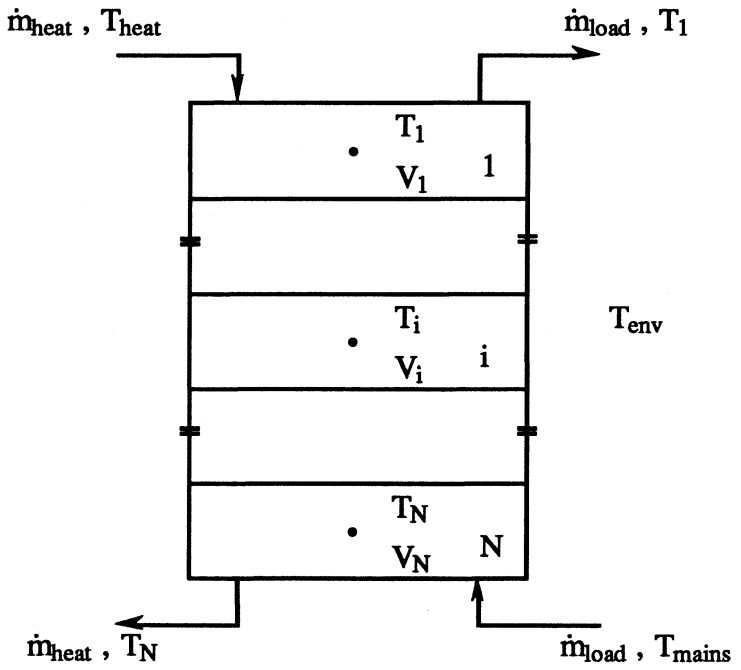

Fig. 2.1 Multi-Node Model

where $\dot{m}_{heat}$ = mass flow rate in the heat source loop

$\dot{m}_{load}$ = mass flow rate in the load loop

T_{heat} = temperature of the fluid entering the tank from the heat source

T_{mains} = temperature of the fluid replacing that extracted to the load

T_i = temperature of the ith node

T_{env} = temperature of the environment

An assumption employed in the multi-node model is that the fluid streams flowing up and down from each node are fully mixed before they enter each node. In terms of Fig. 2.2 this implies that $\dot{m}_1$ is added to $\dot{m}_4$,$\dot{m}_2$ is added to $\dot{m}_3$, and a resultant flow, either up or down is determined before an energy balance on the nodes is done. With this assumption, the heat source flow and the load flow are treated simultaneously.

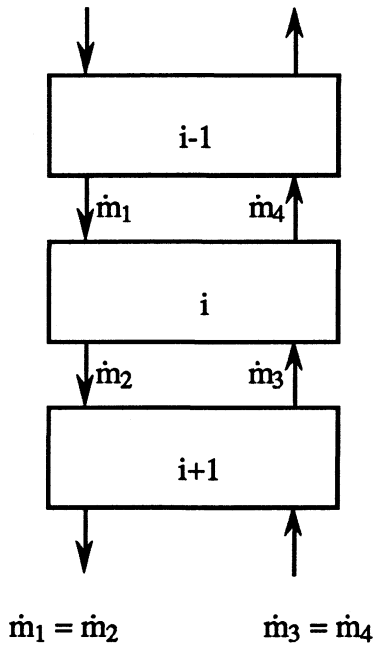

Fig. 2.2 Internal Flows associated with Node i

An energy balance on the ith segment (neglecting losses, entering streams from heat source or load and auxiliary energy input) is then

$$M_i C_f \frac{dT_i}{dt} = \begin{cases} (\dot{m}_1 - \dot{m}_3) C_f (T_{i-1} - T_i) & \dot{m}_1 \geq \dot{m}_3 \\ (\dot{m}_3 - \dot{m}_1) C_f (T_{i+1} - T_i) & \dot{m}_1 < \dot{m}_3 \end{cases} \qquad (2.1.1)$$

where M_i = mass of the fluid in the ith node

C_f = specific heat capacity of the fluid

The model has the option of specifying fixed or variable inlet positions. For fixed inlet positions, the fluid from the heat source enters just below the auxiliary, if present, or at the top of the tank. The mains water enters at the bottom of the tank. At the end of the time step any temperature inversions that result from these flows are eliminated by total mixing of appropriate nodes. For variable inlet positions, the flows enter the nodes that are closest in density and therefore temperature and no temperature inversions are created. This mode of operation preserves the maximum possible degree of stratification.

The model optionally includes an electric resistance heating element, subject to temperature and/or time control. For tank models in which $N > 1$, the position (node number) of the heating element and the thermostat must be specified. The auxiliary heater employs a temperature deadband ΔT_{db}. The heater is on if it was on for the previous time step and the thermostat temperature is less than the set point temperature T_{set} or if the temperature of the node containing the thermostat is less than $(T_{set}-\Delta T_{db})$. The node containing the auxiliary is heated first until it reaches the temperature of the node above. These two nodes are then heated together until they reach the temperature of the node above them. This process continues until either the maximum heater input is used or the set temperature is reached.

The model allows for losses to the exhaust flue of an in-tank gas auxiliary heater. The overall heat loss coefficient to the gas flue, UA_{fl}, and the average flue temperature when the auxiliary is not operating, T_{fl}, have to be specified. The overall loss from any node above and including the auxiliary heater occurs from the exterior and interior of the tank. Temperature inversions due to top losses and bottom gains (higher UA-values for top and bottom nodes) are eliminated by fully mixing of appropriate nodes.

An energy balance written about the ith tank node is then

$$M_i C_f \frac{dT_i}{dt} = \alpha_i \dot{m}_{heat} C_f (T_{heat}-T_i) + \beta_i \dot{m}_{load} C_f (T_{mains}-T_i)$$

$$+\delta_i \gamma_i C_f (T_{i-1}-T_i) + (1-\delta_i) \gamma_i C_f (T_i-T_{i+1})$$

$$+ \varepsilon \dot{Q}_{aux,i} - (1-\varepsilon) UA_{fl,i} (T_i-T_{fl}) - UA_i (T_i-T_{env}) \qquad (2.1.2)$$

where α_i = 1, if fluid from heat source enters node i, 0 otherwise

β_i = 1, if fluid returning from load enters node i, 0 otherwise

$$\gamma_i = \dot{m}_{heat} \sum_{j=1}^{i-1} \alpha_j - \dot{m}_{load} \sum_{j=i+1}^{N} \beta_j$$

$$\delta_i = \begin{cases} 1, \text{ if } \gamma_i > 0 \\ 0, \text{ if } \gamma_i \le 0 \end{cases}$$

ε = 1, if auxiliary is on, 0 otherwise

$\dot{Q}_{aux,i}$ = rate of auxiliary energy input into node i

$UA_{fl,i}$ = overall heat loss coefficient to the gas flue of an in-tank auxiliary heater for node i

UA_i = overall heat loss coefficient between node i and the environment

Eqn (2.1.2) represents a set of N first order ordinary differential equations that can be solved analytically for the temperatures of the N nodes as a function of time. The procedure is to start with the node which has the largest entering flow stream and then work throughout the tank. Eqn (2.1.2) can be rewritten as

$$\frac{dT_i}{dt} = u\,T_i + v \qquad \text{with} \quad u < 0 \ \text{and} \ v > 0 \tag{2.1.3}$$

which has the solution

$$T_i\,(t+\Delta t) = \left(T_i\,(t) + \frac{v}{u}\right) e^{u\,\Delta t} - \frac{v}{u} \tag{2.1.4}$$

The average temperature over the time step Δt is defined as

$$\overline{T}_i = \frac{1}{\Delta t}\int_0^{\Delta t} T_i\,(t+\tau)\,d\tau = \frac{1}{\Delta t}\int_0^{\Delta t} \left(\left(T_i\,(t) + \frac{v}{u}\right) e^{u\,\tau} - \frac{v}{u}\right) d\tau \tag{2.1.5}$$

which upon integration yields

$$\overline{T}_i = \frac{T_i\,(t) + \frac{v}{u}}{u\,\Delta t}\left(e^{u\,\Delta t} - 1\right) - \frac{v}{u} \tag{2.1.6}$$

The auxiliary is added, if necessary, after the changes in tank temperatures due to flows and losses have been computed. This is done by increasing the final and average temperatures resulting from the solution of Eqn (2.1.2) with $\varepsilon = 0$ by the amount that would result with auxiliary input. To compute the energy flows that occur during one time step (rate of energy input into the tank, $\dot{Q}_{in}$, rate of delivered energy, $\dot{Q}_{del}$, and the rate of the losses to the environment, $\dot{Q}_{env}$) the model uses the analytical mean value over the time step. The change in the internal energy of the tank, ΔU, is computed with the initial and final values of the temperatures in the time step. The energy quantities are then defined by the following formula

$$\dot{Q}_{in} = \dot{m}_{heat}\,C_f\,(T_{heat} - T_N) \tag{2.1.7}$$

$$\dot{Q}_{del} = \dot{m}_{load}\, C_f\, (T_1 - T_{mains}) \tag{2.1.8}$$

$$\dot{Q}_{env} = \sum_{i=1}^{N} UA_i\, (T_i - T_{env}) + (1-\varepsilon) \sum_{i=1}^{L} UA_{fl,i}\, (T_i - T_{fl}) \tag{2.1.9}$$

$$\Delta U = \rho_f\, C_f \sum_{i=1}^{N} V_i\, (T_i \mid_{t_2=t_1+\Delta t} - T_i \mid_{t=t_1}) \tag{2.1.10}$$

where V_i = volume of node i

ρ_f = density of the fluid

t_1 = time at the beginning of the time step

L = number of node that contains the thermostat.

T_{fl} = average flue temperature when the auxiliary is not operating

2.2 Plug Flow Model

The plug flow model [20,21] simulates the behavior of a temperature stratified storage tank using a variable number of variable size segments. The number of segments and their volumes actually employed cannot be controlled but vary depending primarily on the tank volume, the net (heat source plus load) flow and the simulation time step. The maximum number of segments in the current plug flow model is 50 (this upper bound is maintained by merging of small segments, if necessary). The segments of liquid are assumed to move

through the tank in plug flow and the model is essentially a bookkeeping method to keep track of the segments. Fig. 2.3 illustrates the concept of this tank model.

In this example the tank is initially divided into four segments of volume V_i, represented by segments on the horizontal axis, and temperature T_i. In one time step, the heat source delivers a volume of liquid, V_{heat}, equal to $\dot{m}_{heat}\Delta t/\rho_f$ at a temperature T_{heat}. Assuming that T_{heat} is greater than T_1, then a new segment is added at the top of the tank and the entire profile is shifted down. At the same time, a volume of fluid, V_{load}, returns from the load, with V_{load} equal to $\dot{m}_{load}\Delta t/\rho_f$ and temperature T_{mains}. If T_{mains} is less than T_4, then a segment is added at the bottom of the tank and the whole profile is shifted upward. These steps are shown sequentially, although they occur simultaneously. The net shift of the initial profile is equal to the difference between the total heat source volume and load volume, V_{heat}-V_{load} (downward if positive).

The segments and/or fractions of segments whose positions fall outside the bounds of the tank are returned to the heat source and load. The average temperature of the fluid delivered to the load for the example of Fig. 2.3 is

$$T_{del} = \frac{V_{heat}\, T_{heat} + (V_{load}-V_{heat})\, T_1}{V_{load}} \qquad (2.2.1)$$

and the average heat source return temperature, T_{ret}, is equal to T_{mains}.

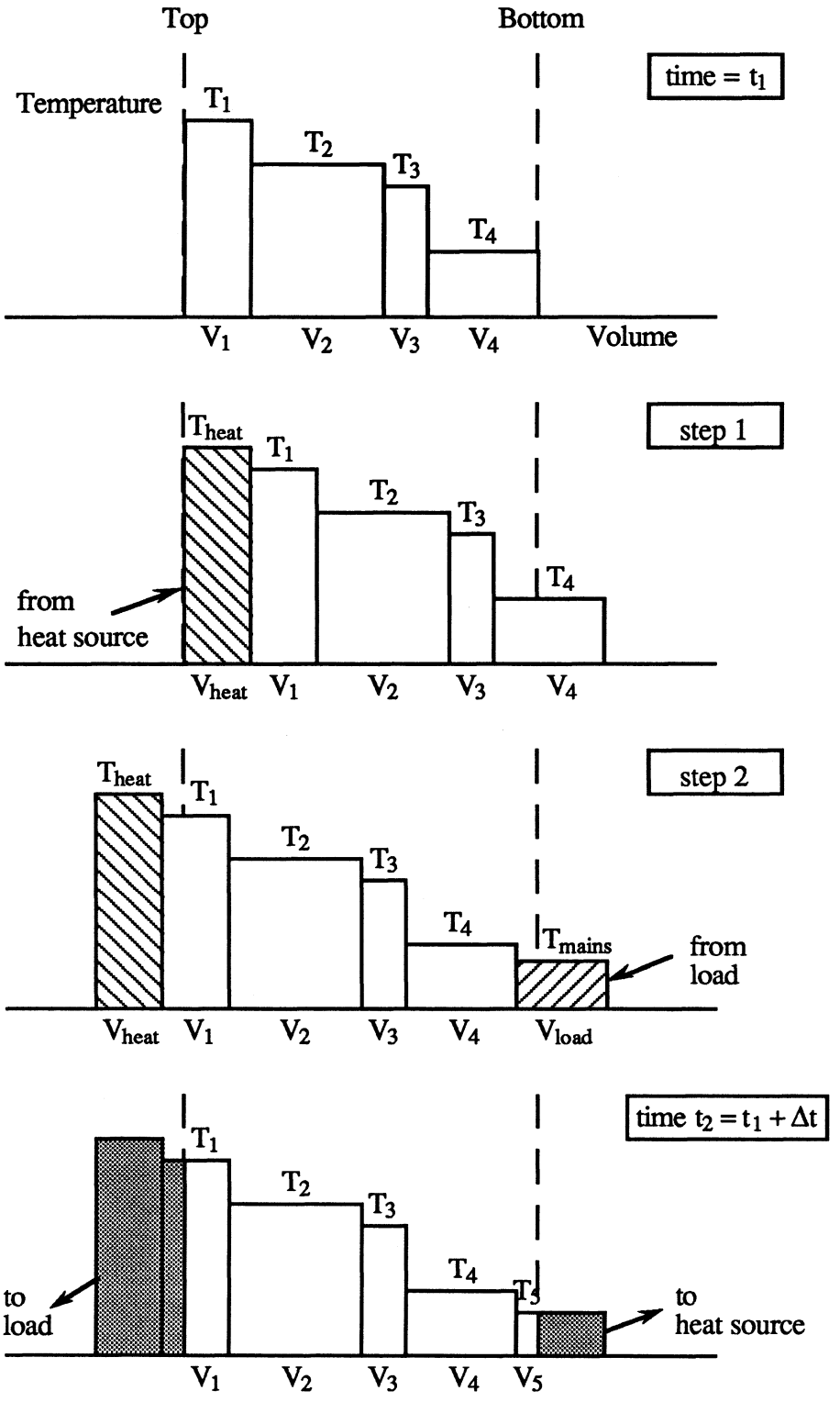

Fig. 2.3 Concept of the Plug Flow Model

In general, for N segments the average delivery and heat source return temperature are computed as follows

If $V_{heat} < V_{load}$ then

$$T_{ret} = T_{mains} \tag{2.2.2}$$

$$T_{del} = \frac{T_{heat}\, V_{heat} + \sum_{i=1}^{j-1} T_i\, V_i + c\, T_j\, V_j}{V_{load}} \tag{2.2.3}$$

where c and j must satisfy

$$0 \le c \le 1 \tag{2.2.4}$$

$$V_{heat} + \sum_{i=1}^{j-1} V_i + c\, V_j = V_{load} \tag{2.2.5}$$

If $V_{heat} > V_{load}$ then

$$T_{del} = T_{heat} \tag{2.2.6}$$

$$T_{ret} = \frac{T_{mains}\, V_{load} + \sum_{i=j+1}^{N} T_i\, V_i + c\, T_j\, V_j}{V_{heat}} \tag{2.2.7}$$

where c and j must satisfy

$$0 \leq c \leq 1 \tag{2.2.8}$$

$$V_{load} + \sum_{i=j+1}^{N} V_i + c\, V_j = V_{heat} \tag{2.2.9}$$

The model provides the option of fixed and variable inlet positions. The fixed inlet position option forces the inlet water to enter the tank section in which the inlet is physically located, regardless of the temperature of the water in the tank at this position. This introduces some mixing at the inlets. Temperature inversions are eliminated by fully mixing of appropriate segments beginning at the inlets in the direction of the inversion. The heat source inlet position can be specified and division of the existing segment might be necessary. The load flow enters at the bottom of the tank. With the variable inlet position, the inlet water is directed to the level to which it is closest in density and therefore temperature and thus no temperature inversions are created (maximum possible degree of stratification). For both options the incoming fluid mixes with adjacent segments if its temperature is within 0.5 °C, otherwise a new segment is created.

The optional auxiliary heater is modeled as in the multi-node model. If necessary, the segment containing the auxiliary is split into two segments at the actual position of the auxiliary. If a load flow is occuring and the auxiliary is able to heat the outlet segment, then the delivered fluid is heated with a linear temperature profile over the time step. The overall heat loss coefficient to the exhaust flue of an in-tank gas auxiliary heater, UA_{fl}, when the auxiliary is not operating can be included. In this case the average flue temperature is assumed to be the temperature of the environment.

The model was developed for upright and horizontal cylindrical tanks. Also the ratio of thickness of top insulation to thickness of side insulation for upright tanks or the ratio of insulation thickness of top to bottom for horizontal tanks, r_{ins} (=1, if tank is concentric in

insulation jacket), can be specified. It is important to note that the value of the overall heat loss coefficient, UA, depends on the value of r_{ins}.

Storage losses from the tank and conduction between segments are evaluated before the temperature profile has been adjusted for flows and auxiliary energy input. This is accomplished by solving the following differential equation for each segment

$$\rho_f V_i C_f \frac{dT_i}{dt} = - (UA_i+UA_{fl,i}) (T_i-T_{env}) + k_f S_{i-1} \frac{T_{i-1}-T_i}{\Delta h_{i-1}} - k_f S_i \frac{T_i-T_{i+1}}{\Delta h_i} \qquad (2.2.10)$$

where k_f = thermal conductivity of the fluid

S_i = cross-sectional area between segments i and i+1

Δh_i = separation between centers of segments i and i+1.

When conduction is included, the set of coupled first order ordinary differential equations is solved analytically by successive substitution with at most 20 iterations. Conduction down the walls of the tank can be included by using an effective conductivity. Temperature inversions due to top losses and bottom gains (higher UA-values for top and bottom segments) are eliminated by fully mixing of appropriate segments.

The losses are then calculated as

$$\dot{Q}_{env} = \sum_{i=1}^{N} UA_i (T_i-T_{env}) + (1-\varepsilon) \sum_{i=1}^{L} UA_{fl,i} (T_i-T_{env}) \qquad (2.2.11)$$

using the analytical mean value for T_i.

The rate of energy input into the tank, $\dot{Q}_{in}$, and the rate of delivered energy, $\dot{Q}_{del}$, are computed as

$$\dot{Q}_{in} = \dot{m}_{heat} C_f (T_{heat}-T_{ret}) \qquad (2.2.12)$$

$$\dot{Q}_{del} = \dot{m}_{load}\, C_f\, (T_{del}-T_{mains}) \qquad (2.2.13)$$

The change in internal energy of the tank is

$$\Delta U = \rho_f\, C_f \left(\sum_{i=1}^{M} (V_i\, T_i) \mid_{t_2=t_1+\Delta t} - \sum_{i=1}^{N} (V_i\, T_i) \mid_{t=t_1} \right) \qquad (2.2.14)$$

2.3 Plume Entrainment Model

2.3.1 Introduction

The previously discussed models account for mixing at the inlets (only if the fixed inlet option is chosen) by fully mixing of adjacent segments whenever temperature inversions occur. The multi node model also introduces some mixing by taking into account the thermal capacitance of each node (cf. Eqn (2.1.2)) and by considering flow from one node to another inside the tank. The plug flow model introduces some mathematical dispersion by entering segments that are already at a mixed temperature, by allowing variable size and number of segments and by merging segments. However, neither model attempts to mathematically describe what physically is happening. This has been done by Phillips and Pate [23] and Lightstone [24].

In the late afternoon when the availability of solar energy has decreased and the top portion of the tank is still hot as a result of higher energy input earlier in the day, the temperature of the incoming fluid is cooler than the upper portion of the tank. This is especially the case for low flow systems which, in general, exhibit a higher degree of stratification in the storage tank than high flow systems. As a result, a downward directed

buoyancy force will drive the incoming fluid down the tank and because of its turbulent motion and viscosity, the hot fluid in the tank will be entrained in the falling plume. Thus, the incoming stream is heated up and it will fall down to the position in the tank where its density and therefore temperature matches that of the tank. This is known as "plume entrainment" and it will decrease the degree of stratification in the tank.

This effect can be significant as shown by the experimental work of Phillips and Pate. Their flow visualization experiments showed that water at 10°C introduced with a very low velocity in a tank with an approximately linear temperature profile (top at 55°C and bottom at 14°C) fell only to a level in the tank where the temperature was about 45°C. This indicates that the plume must have entrained enough hot water from the tank to raise its temperature by at least 35°C. The plume will, in fact, have had its temperature raised by a greater amount then that since an upward directed buoyancy force is needed to balance the downward directed momentum forces. Also a simple order-of-magnitude analysis of conduction in water can rule out conduction as the major mechanism for energy transport between the incoming stream and the tank.

2.3.2 Mathematical Model

In the following, the mathematical model of plume entrainment based on energy and mass balances will be described.

The storage tank is modeled as having two separate sections: the plume or stream region and the rest of the tank. These regions will be referred to as the stream (S) and the tank (T) regions as shown in Fig. 2.4. The vertical coordinate x is measured from the top of the tank downward. The distance from the top of the tank to where the stream merges with the tank (i.e. the penetration depth of the stream) is denoted as d and is defined as the smallest value of x for which the stream temperature exceeds the tank temperature. It will

be assumed that, except in the vicinity of the stream, there are no horizontal temperature gradients in the tank, which is justified by the experimental work of Pate [37]. Therefore a one-dimensional model can be formulated. It will further be assumed that the cross-sectional area of the stream is much smaller than that of the tank. Thus, both axial conduction and thermal capacity of the stream can be neglected and the tank cross-sectional area can be considered to be constant.

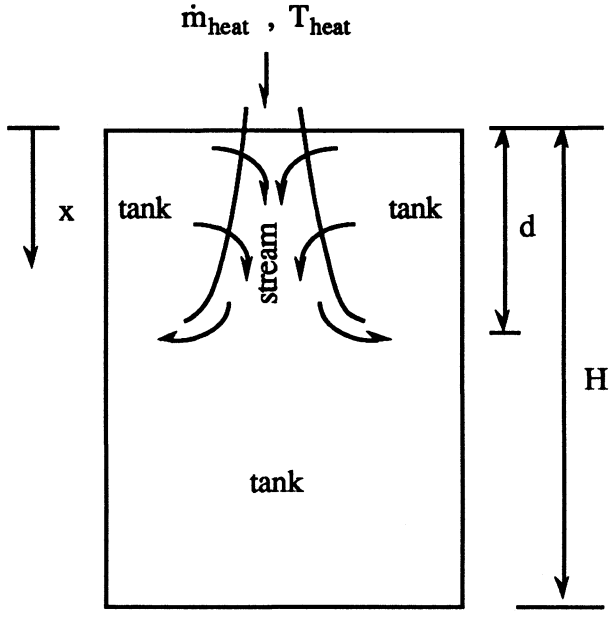

Fig. 2.4 Stream and Tank Regions

2.3.2.1 Energy equations

The energy balances for the stream and the tank are found by dividing the tank and the stream into control volumes and writing an energy balance for each control volume as shown in Appendix A.

The resulting energy equations derived by Phillips and Pate are for the stream

$$C_f \frac{\partial(\dot{m}_S T_S)}{\partial x} = C_f T_T \frac{\partial \dot{m}_S}{\partial x} \tag{2.3.1}$$

and for the tank

$$\rho_f A C_f \frac{\partial T_T}{\partial t} = - C_f \frac{\partial(\dot{m}_T T_T)}{\partial x} + C_f T_T \frac{\partial \dot{m}_T}{\partial x} + k_f A \frac{\partial^2 T_T}{\partial x^2} - U_T P_T (T_T - T_{env}) \tag{2.3.2}$$

where $\dot{m}_S$ = mass flow rate of the stream

T_S = temperature of the stream

$\dot{m}_T$ = mass flow rate of the tank

T_T = temperature of the tank

A = cross-sectional area of the tank

k_f = thermal conductivity of the fluid.

U_T = overall heat loss coefficient between the tank and the environment per unit area

P_T = perimeter of the tank

Note that the term $- C_f \partial(\dot{m}_T T_T) / \partial x$ represents the advection into the control volume from the tank, while $+ C_f T_T \partial \dot{m}_T / \partial x$ represents the energy lost from the tank into the stream.

2.3.2.2 Flow Rates and Boundary Conditions

Conservation of mass for the tank requires that

$$\frac{\partial \dot{m}_S}{\partial x} = - \frac{\partial \dot{m}_T}{\partial x} \qquad (2.3.3)$$

In order to solve the system for the four unknowns $\dot{m}_S$ (x,t), $\dot{m}_T$ (x,t), T_S (x,t) and T_T (x,t) one additional equation is needed which describes how mass from the tank is entrained into the falling stream. As explained by Pate, solutions for entrainment rates of a plume in a stratified environment are very complex. In the model presented here it is assumed that the mass entrained into the falling stream is independent of temperature. The plume is treated as a momentum driven jet. The theory of isothermal entrainment has been summarized by Schlichting [38]. It has been shown that, for developed axisymmetric flow,

$$\frac{\partial \dot{m}_S}{\partial x} = C \frac{\dot{m}_{heat}}{D} \qquad (2.3.4)$$

where C = (entrainment) constant

D = inlet pipe diameter (diameter of the stream at x=0)

To obtain numerical values for C under specific conditions the reader is referred to the theoretical work summarized by Schlichting and the experimental work of Hill [39]. In this model C is assumed to be 0.32. This value corresponds to the experimentally found value by Hill.

Eqn (2.3.4) may then be integrated using the boundary condition

$$\dot{m}_S (0,t) = \dot{m}_{heat} (t) \qquad (2.3.5)$$

This results in

$$\dot{m}_S(x,t) = \begin{cases} C\dfrac{\dot{m}_{heat}(t)}{D}x + \dot{m}_{heat}(t) & 0 < x < d \\ 0 & d < x \le H \end{cases} \qquad (2.3.6)$$

Note that a discontinuity exists at x = d where the stream merges with the tank.

Now Eqn (2.3.3) can be integrated with the boundary condition

$$\dot{m}_T(0,t) = -\dot{m}_{load}(t) \qquad (2.3.7)$$

Thus we obtain

$$\dot{m}_T(x,t) = \begin{cases} -C\dfrac{\dot{m}_{heat}(t)}{D}x - \dot{m}_{load}(t) & 0 < x < d \\ \dot{m}_{heat}(t) - \dot{m}_{load}(t) & d < x \le H \end{cases} \qquad (2.3.8)$$

with a discontinuity at x = d.

The boundary condition for the stream temperature is

$$T_S(0,t) = T_{heat}(t) \qquad (2.3.9)$$

The initial temperature profile in the tank is

$$T_T(x,0) = T_T^0(x) \qquad (2.3.10)$$

A boundary condition for the tank temperature is not needed since its value will be determined by the stream.

2.3.3 Numerical Solution

Lightstone solved these equations with the assumptions of no heat conduction ($k_f = 0$) and no load flow ($\dot{m}_{load} = 0$). At this point the losses can also be neglected since they are treated separately in the multi node model and the plug flow model when plume entrainment occurs. The numerical method used is a finite volume approach similar to that described by Patankar [40].

2.3.3.1 Discretization of the Stream Energy Equation

The discretized form of the stream energy equation is found by integrating Eqn (2.3.1) over a control volume as shown in Fig. 2.5.

$$\int_{x}^{x+\Delta x} C_f \frac{\partial(\dot{m}_S T_S)}{\partial \xi} d\xi = \int_{x}^{x+\Delta x} C_f T_T \frac{\partial \dot{m}_S}{\partial \xi} d\xi \qquad (2.3.11)$$

The values of the temperatures are determined at a nodal point in each control volume. Integration yields

$$C_f [(\dot{m}_S T_S)|_{x+\Delta x} - (\dot{m}_S T_S)|_x] = C_f \overline{T}_T (\dot{m}_S|_{x+\Delta x} - \dot{m}_S|_x) \qquad (2.3.12)$$

where $\overline{T}_T$ = mean temperature of the tank layer under consideration.

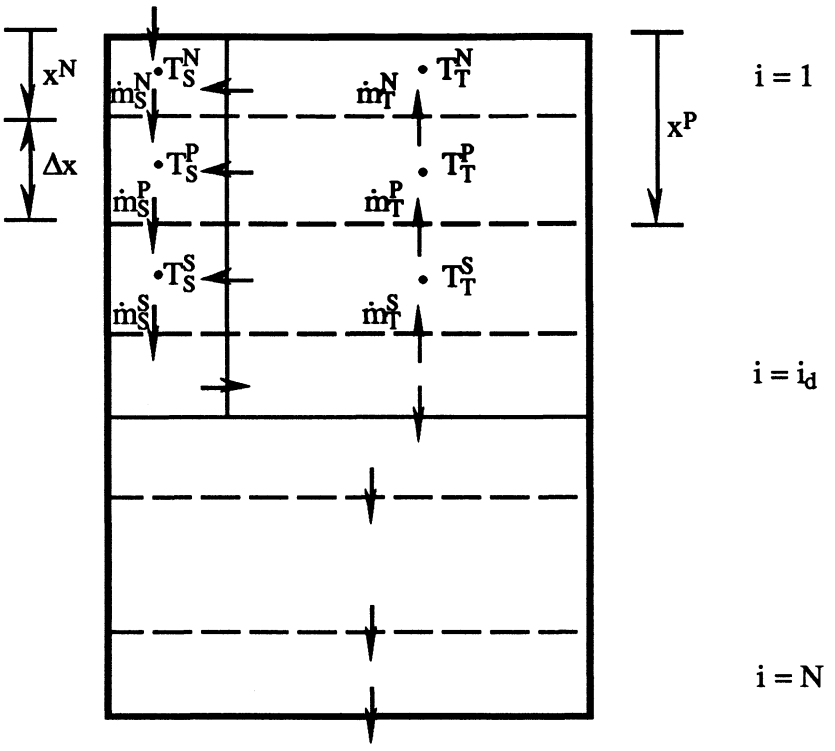

Fig. 2.5 Discretized Grid

Here and in the following equations the superscripts N, P, S are related to the nodal locations N = north; node above

P = polar; node under consideration

S = south; node below.

By fully upwinding the temperatures in the direction of flow and directly calculating the mass flow rates at the control volume faces using Eqn (2.3.6), the control volume interface temperatures and mass flow rates become

$$(\dot{m}_S T_S)\,|_{x+\Delta x} = \dot{m}_S^P\, T_S^P \tag{2.3.13}$$

and

$$(\dot{m}_S T_S)\,|_x = \dot{m}_S^N\, T_S^N \tag{2.3.14}$$

In order to decouple the tank and stream energy equations, the energy lost from the tank into the stream is delayed. The tank temperatures used are those from the previous time step. This gives

$$C_f \overline{T}_T (\dot{m}_S|_{x+\Delta x} - \dot{m}_S|_x) = C_f T_T^{P^0} (\dot{m}_S^P - \dot{m}_S^N) \tag{2.3.15}$$

The discretized form of the stream energy equation is then

$$a_S^P T_S^P = a_S^N T_S^N + b_S \tag{2.3.16}$$

where

$$a_S^P = C_f \dot{m}_S^P \tag{2.3.17}$$

$$a_S^N = C_f \dot{m}_S^N \tag{2.3.18}$$

$$b_S = C_f T_T^{P^0} (\dot{m}_S^P - \dot{m}_S^N) \tag{2.3.19}$$

2.3.3.2 Discretization of the Tank Energy Equation

Separate discrete tank energy equations are derived for three regions in the tank defined by

1. $i < i_d$
2. $i = i_d$
3. $i > i_d$

as shown in Fig. 2.5.

The fact that the nodes are of finite size is important for the node where the stream merges with the tank and discontinuities occur in the equations for the mass flow rates, Eqns

(2.3.6) and (2.3.8). Integration of the tank energy equation for the nodes for which $i < i_d$ over both a time step, Δt, and a control volume with the aforementioned assumptions

$$\int_x^{x+\Delta x}\int_t^{t+\Delta t} \rho_f A C_f \frac{\partial T_T}{\partial \tau}\, d\tau\, d\xi = \int_t^{t+\Delta t}\int_x^{x+\Delta x} -C_f \frac{\partial(\dot{m}_T T_T)}{\partial \xi}\, d\xi\, d\tau +$$

$$\int_t^{t+\Delta t}\int_x^{x+\Delta x} C_f T_T \frac{\partial \dot{m}_T}{\partial \xi}\, d\xi\, d\tau \qquad (2.3.20)$$

gives

$$M^P C_f \left(T_T^P - T_T^{P^0}\right) = - C_f \left[(\dot{m}_T T_T)\,|_{x+\Delta x} - (\dot{m}_T T_T)\,|_x\right] \Delta t +$$

$$C_f T_T^{P^0} (\dot{m}_T\,|_{x+\Delta x} - \dot{m}_T\,|_x)\, \Delta t \qquad (2.3.21)$$

where M^P = mass of fluid in the control volume.

The term representing the energy lost to the stream is delayed so as to be consistent with the stream energy equation. As before, upwinding the temperatures in the direction of flow and noting that by mass conservation the flow in this region is towards the tank top (-) yields

$$(\dot{m}_T T_T)\,|_{x+\Delta x} = \dot{m}_T^P T_T^S \qquad (2.3.22)$$

$$(\dot{m}_T T_T)\,|_x = \dot{m}_T^N T_T^P \qquad (2.3.23)$$

The discretized form of the tank energy equation for the nodes $i < i_d$ is therefore

$$a_T^P T_T^P = a_T^S T_T^S + b_T^P \tag{2.3.24}$$

where

$$a_T^P = C_f \left(\frac{M^P}{\Delta t} - \dot{m}_T^N \right) \tag{2.3.25}$$

$$a_T^S = - C_f \dot{m}_T^P \tag{2.3.26}$$

$$b_T^P = C_f \left(\frac{M^P}{\Delta t} - (\dot{m}_T^N - \dot{m}_T^P) \right) T_T^{P^0} \tag{2.3.27}$$

A similar dicretization of the tank energy equation is done for the nodes with $i = i_d$ and $i > i_d$. For $i = i_d$ the third term in the tank energy Eqn (2.3.2) can be rewritten using Eqns (2.3.1) and (2.3.3) which gives

$$C_f T_T \frac{\partial \dot{m}_T}{\partial x} = - C_f \frac{\partial (\dot{m}_S T_S)}{\partial x} \tag{2.3.28}$$

The stream merges with T_S^P and $\dot{m}_S^P$ into the tank and divides into two mass flows upward and downward the tank (cf. Fig. 2.5). Therefore for $i = i_d$

$$a_T^P T_T^P = b_T^P \tag{2.3.29}$$

where

$$a_T^P = C_f \left(\frac{M^P}{\Delta t} - (\dot{m}_T^N - \dot{m}_T^P) \right) \tag{2.3.30}$$

$$b_T^P = C_f \left(\frac{M^P}{\Delta t} T_T^{P^0} - (\dot{m}_T^N - \dot{m}_T^P) T_S^P \right) \tag{2.3.31}$$

For $i > i_d$ the third term of Eqn (2.3.2) equals 0 since the mass flow rate of the tank is constant. Therefore for $i > i_d$

$$a_T^P T_T^P = a_T^N T_T^N + b_T^P \tag{2.3.32}$$

where

$$a_T^P = C_f\left(\frac{M^P}{\Delta t} + \dot{m}_T^P\right) \tag{2.3.33}$$

$$a_T^N = C_f \dot{m}_T^N \tag{2.3.34}$$

$$b_T^P = C_f \frac{M^P}{\Delta t} T_T^{P^0} \tag{2.3.35}$$

As for the mass flow rates of the stream, the mass flow rates of the tank can be calculated directly using Eqn (2.3.10), by knowing the distance from the tank top to the control volume interface x^P.

2.3.4 Time Step Restrictions

Numerical instabilities, producing non-physical results, can occur if a weight on a variable in the discrete equations is negative. This may be the case in Eqn (2.3.29). If

$$\frac{M^P}{\Delta t} < \left(\dot{m}_T^N - \dot{m}_T^P\right)$$

then a negative weight on the $T_T^{P^0}$ will arise. This implies that the larger $T_T^{P^0}$ is then the smaller T_T^P becomes - a physically unrealistic result. A maximum allowable time step may therefore be calculated as

$$\Delta t_{max} = \frac{M^P}{\dot{m}_T^N - \dot{m}_T^P} = \frac{\rho_f (x^P - x^N) A}{-\frac{C \dot{m}_{heat}}{D} (x^N - x^P)} = \frac{\rho_f A D}{C \dot{m}_{heat}} \qquad (2.3.36)$$

Because of the constant entrainment rate, the maximum allowable time step is independent of grid spacing.

This existence of a time step restriction is due to the explicit scheme used to decouple the stream and tank energy equations. Physically, this limits the mass of the fluid entrained into the stream over a time step to at most the mass of the tank control volume.

2.3.5 Solution Method

For a given tank temperature distribution (determined either through the initial conditions or from the values from the previous time step), the stream temperature field at the end of a time step may be solved directly. This is accomplished by starting with the inlet temperature of the stream and then marching down the tank. The penetration depth of the plume, d, is found by comparing the temperature of the stream at each node, T_S (i,t), with the tank temperature of the node below, T_T (i+1,t^0). When a stream control volume is found such that T_S (i,t) > T_T (i+1,t^0) , then the stream is considered to have reached the depth where it merges with the tank and the temperature of the stream which is merging with the tank, T_S (i_d), is set equal to T_S (i,t). The stream does not exist below this point. The discretized tank temperature equations may then be solved directly by calculating T_T (i_d,t) and then marching upwards and downwards in the tank.

The solution procedure can be summarized as follows:

1. Initial conditions
2. Solve T_S (i,t) (using either initial conditions or values of T_T from the previous time step or iteration) by marching down the tank

3. Determine i_d

4. Solve T_T (i,t) by first calculating T_T (i_d,t) directly and then marching upwards and downwards through the tank from i_d

5. Set T_T (i,t^0) = T_T (i,t)

6. t = t + Δt

7. Go to 2.

2.3.6 Incorporation into TRNSYS

Plume entrainment has been programmed into both the multi-node model and the plug flow model. This was done by modifying the already existing code of the WATSUN simulation package [41]. It was decided to keep as many features of the multi-node model and the plug flow model as possible.

Plume entrainment was programmed using the fixed inlet option as described in sections 2.1 and 2.2, respectively. An additional parameter, the inlet pipe diameter, had to be added. When plume entrainment occurs the maximum allowable time step, Δt_{max}, is determined according to Eqn (2.3.37). The time step used to solve plume entrainment, Δt_{sol}, is found by multiplying the maximum allowable time step by two thirds. If the solution time step is smaller than the simulation time step used by TRNSYS then the simulation time step is subdivided accordingly.

2.3.6.1 Incorporation into the Multi-Node Model

In the multi-node model plume entrainment is used whenever the fluid from the heat source is colder than the temperature of the node where it enters the tank. Before the fluid is

added, the losses are calculated and any temperature inversions resulting from top losses or bottom gains are eliminated by mixing of appropriate nodes.

The fluid from the heat source is added as outlined in section 2.3.5, steps 2 to 4. While adding the fluid from the heat source to the tank, a segment is created at the "bottom" of the tank with mass equal to the sum of the mass of all the fluid added to the tank during the solution for one simulation time step and temperature, T_{ret}, as the arithmetic mean temperature of the temperatures of the bottom node. This segment represents the fluid that has to leave the tank at the bottom because of adding fluid from the heat source and it will be returned to the heat source.

Similarly, after adding the fluid from the heat source, the load flow is added using a finite difference equation which was derived in the same way as Eqn (2.3.33) and is therefore

$$T_T^P = \frac{C_f M^P T_T^{P^0} + \dot{m}_{load} \Delta t_{sol} T_T^S}{C_f M^P + \dot{m}_{load} \Delta t_{sol}} \qquad (2.3.37)$$

with $T_T^S = T_{mains}$ for calculating the temperature of the lowermost node and then working upwards through the tank. Also, a segment is created at the "top" of the tank with mass equal to the sum of the mass of the fluid returned from the load to the tank during the solution for one simulation time step and the temperature, T_{del}, as the mean temperature of the temperatures of the top node. This segment represents the fluid that has to leave the tank at the top because of adding fluid from the load and will be delivered to the load.

The program keeps adding the flows from the heat source and the load alternatively until the consecutively added solution time steps, Δt_{sol}, add up to the simulation time step. This preserves the idea of simultaneous heat source and load flow.

Creating segments at the "top" and the "bottom" of the tank was done in order to achieve an energy balance. It is not possible to combine the numerical solution of adding

the fluid from the heat source with the analytical solution of adding the load flow (as done in the multi-node model) with the idea of simultaneous flows.

Since the addition of auxiliary energy in the multi node model without plume entrainment affects the analytical mean temperature of the nodes and these are used to calculate the energy quantities, a different auxiliary algorithm had to be employed because there is no analytical mean value when plume entrainment occurs. Therefore the same auxiliary algorithm as used in the plug flow model was built in after plume entrainment.

2.3.6.2 Incorporation into the Plug Flow Model

In the plug flow model plume entrainment occurs whenever the fluid entering the tank is sufficiently colder (more than 0.5 °C) than the temperature of the segment where it enters the tank (inlet height can be specified), so that the plug flow model would insert the incoming fluid below that segment. The losses are calculated prior to that decision.

The fluid from the heat source is added as outlined in chapter 2.3.5, steps 1 to 7. While adding the fluid to the tank, a segment is created at the "bottom" of the tank as already described for the multi-node model. This is equivalent to shifting the profile downward as shown in Fig. 2.3. After having accomplished this, the plug flow model performs exactly the same as if there had not been plume entrainment.

2.4 Model Discussion

In this section, the previously introduced models are investigated in order to further characterize and distinguish them. The results presented are examples and depend in their details on the chosen system and its specifications.

2.4.1 Number of Nodes and Inlet Positions

Simulations with a simple system, consisting of a collector as heat source and a tank, as shown in Fig. 2.6, were run with TRNSYS in order to determine how the number of nodes for the multi-node model and the choice of fixed or variable inlet positions influences the predicted amount of stratification in the tank.

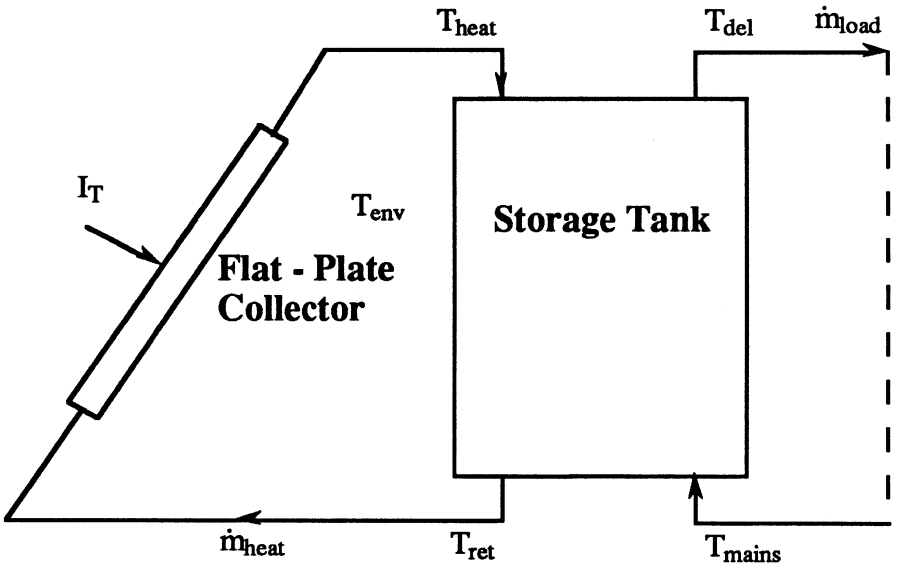

Fig. 2.6 Simple Collector-Tank System

A flat-plate collector was specified for which the rate of the useful energy gain, $\dot{Q}_u$, can be computed using the Hottel-Whillier equation [14]

$$\dot{Q}_u = A_c [F_R (\tau\alpha) I_T - F_R U_L (T_{ret}-T_{env})] \quad (= \dot{m}_{heat} C_f (T_{heat}-T_{ret})) \qquad (2.4.1)$$

where A_c = total collector aperture area

F_R = collector heat removal factor

$(\tau\alpha)$ = transmittance-absorptance product

I_T = total radiation incident on the collector per unit area

U_L = overall loss coefficient between the collector and the environment per unit area.

The collector area was 2.9 m^2, the values of $F_R(\tau\alpha)$ and $F_R U_L$ were 0.604 and 13.276 kJ/(h m^2 °C), respectively. A daily sinusoidal radiation profile between hour 7 and 17 of the day with a total irradiance of 13.5 MJ/(m^2 day) was specified. The collector flow rate, $\dot{m}_{heat}$, was chosen to be 20 kg/h during the time of radiation.

A multi-node tank model with fifteen nodes and volume of 180 liters was used. The temperature of the fluid replacing that extracted to the load, T_{mains}, was 15 °C. Four equal volume load draws of 30 liters each, at a flow rate of 300 kg/h, were performed at the beginning of the hours 9, 12, 15 and 18. The ambient temperature was chosen to be 20 °C. The radiation and the flows were specified using the TRNSYS option of time dependent forcing functions.

The simulations were run with time step 0.1 h until the system reached a steady-periodic state. Fig. 2.7 shows the temperatures of the top node, T_{top}, and bottom node, T_{bottom}, (the difference between them is a measure of the amount of stratification) for fixed and variable inlets.

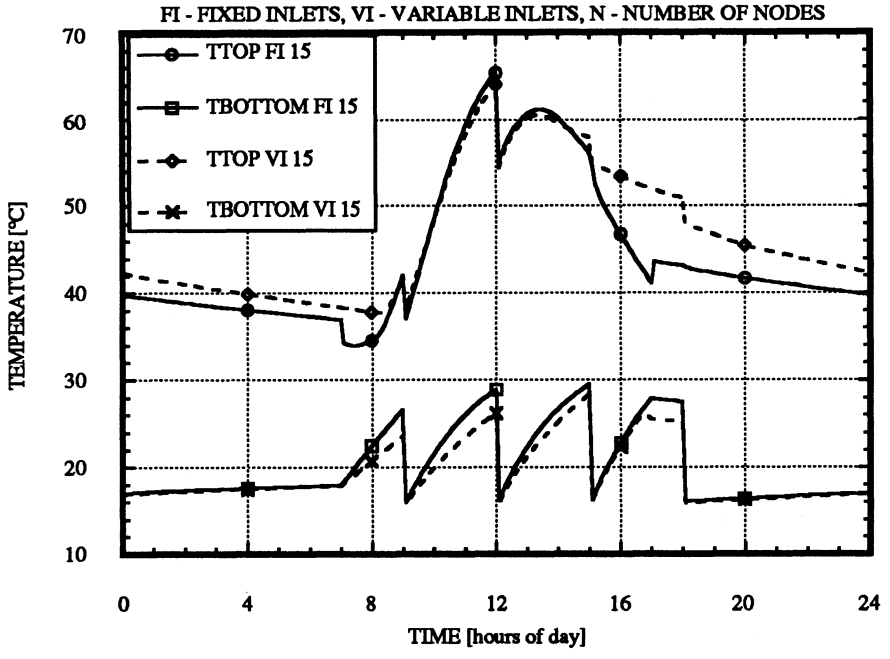

Fig. 2.7 Temperature Profiles for Fixed and Variable Inlet Positions

It can be seen that the temperatures of the top nodes differ most between hours 7 and 9 and hours 15 and 18. The differences are due to the fact that in the early morning and late afternoon the fluid entering the tank is colder than the fluid at the top of the tank because of low solar input. The entering cold fluid decreases the temperature of the top node for the fixed inlet option but not for the variable inlet option where the entering fluid is directed further down. The difference between the top temperatures is maintained during the time of no collector flow and no load draw. The temperatures slightly approach each other because of higher losses for the higher temperature. During the time of high solar input the top temperature profiles are about the same because the entering fluid is hotter than the temperature of the top node which results in no difference between the fixed and the variable inlet options. It can also be seen that there is a decrease in the top temperature

when the load draw occurs. The extent of that temperature drop depends on the flow rates and the volume that is drawn and on the temperatures of the nodes below the top node.

Since the temperature of the fluid replacing that extracted to the load, T_{mains}, is the lowest temperature in the whole system, it is entering the bottom node for both cases. Because the volume drawn during one single draw is 2.5 times higher than the volume of the bottom node and the collector flow rate is much lower than the load flow rate it is clear that the temperature of the bottom node during a draw reaches almost T_{mains} (cf. Eqn (2.1.2)). The higher temperature increase of the bottom node temperature for the fixed inlet option during collector flow is explained by higher temperatures of the nodes above the bottom node. The bottom node also gains energy during the time of no load and collector flow.

The energy inputs into the tank, Q_{in}, by the collector for the fixed and variable inlet option were 22.37 MJ/day and 22.90 MJ/day, respectively. For the delivered energy, Q_{del}, values of 16.99 MJ/day and 17.79 MJ/day, respectively, were obtained. This shows that a higher degree of stratification results in higher energy input because of lower collector losses due to the lower heat source return temperature, T_{ret}, and therefore higher values of delivered energy. Q_{in} and Q_{del} are defined as

$$Q_{in} = \int_{day} \dot{Q}_{in}\, dt = \int_{day} \dot{m}_{heat}\, C_f\, (T_{heat} - T_{ret})\, dt \qquad (2.4.2)$$

$$Q_{del} = \int_{day} \dot{Q}_{del}\, dt = \int_{day} \dot{m}_{load}\, C_f\, (T_{del} - T_{mains})\, dt \qquad (2.4.3)$$

Fig. 2.8 shows the tank temperature profiles for a two-node model and a fifteen-node model with fixed inlets. Plotted are the temperatures of the top nodes, T_{top}, the bottom nodes, T_{bottom}, and the mean tank temperature, T_{mean}, which is defined as

$$T_{mean} = \frac{\sum_{i=1}^{N} T_i V_i}{\sum_{i=1}^{N} V_i} \qquad (2.4.4)$$

There is little difference in the mean tank temperature, which is a measure of the energy stored in the tank, for both models. However there is a considerable difference in the top and the bottom temperatures. The fifteen-node model shows a much larger degree of stratification than the two-node model. The two-node models represents the tank temperature profile using only two mixing temperatures whereas the fifteen-node model uses fifteen mixing temperatures which results in a higher resolution. The nodes in the fifteen-node model are much smaller and therefore have smaller time constants to respond to the temperatures of the entering flow streams (by which the possible amount of stratification will be determined) than the large nodes of the two-node model. This e.g. can be seen from the temperature drop when the load draw occurs. Also, it has to be mentioned that the centers of the nodes under consideration are located differently for both models. The consequence of the model predictions is that the energy input from the collector is lower for the two-node model (Q_{in} = 19.47 MJ/day) because of higher bottom node temperature (more collector losses) than for the fifteen-node model (Q_{in} = 22.37 MJ/day). The delivered energy for the two-node model is lower (Q_{del} = 13.95 MJ/day) because of less energy input and more mixing than for the fifteen-node model (Q_{del} = 16.99 MJ/day).

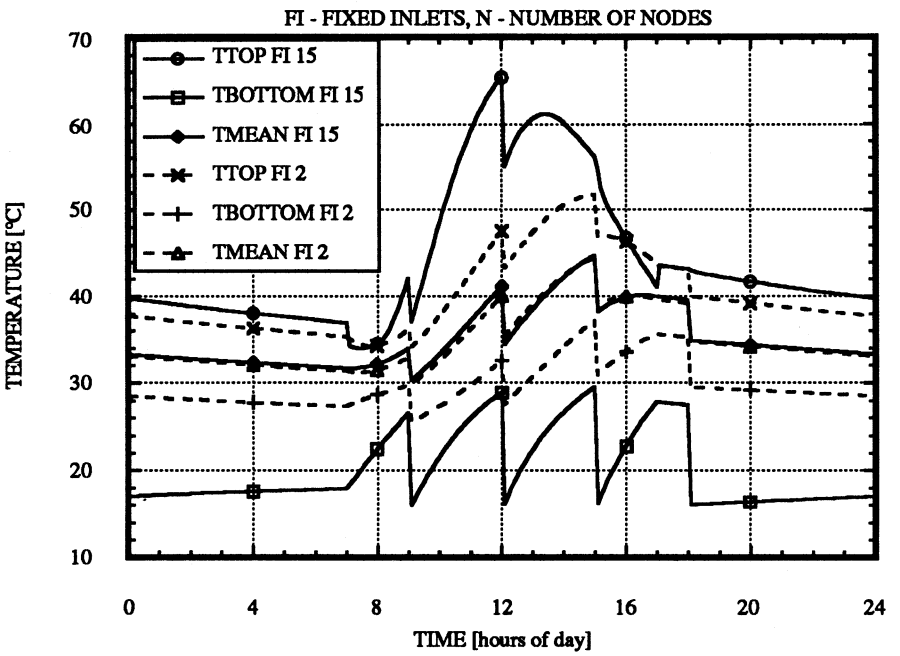

Fig. 2.8 Temperature Profiles for Different Numbers of Nodes

2.4.2 Average Number of Segments

To investigate the number of segments employed in the plug flow model, the same system as introduced before was simulated using the plug flow model. The number of segments affects the temperature distribution predicted by the model. Runs with two different collector flow rates, 20 kg/h and 180 kg/h, were carried out. The values of $F_R(\tau\alpha)$ and F_RU_L for the for the high flow rate were 0.781 and 17.19 kJ/(h m^2 °C), respectively. The sinusoidal radiation profile was integrated for each hour and the load profile was changed to hourly values (by reducing the load flow rate). Fig. 2.9 shows the average number of segments for both values of the collector flow rate. The average number of segments, $\overline{N}$, is defined as

$$\overline{N} = \frac{1}{24\,h} \int_{day} N\,dt \qquad (2.4.5)$$

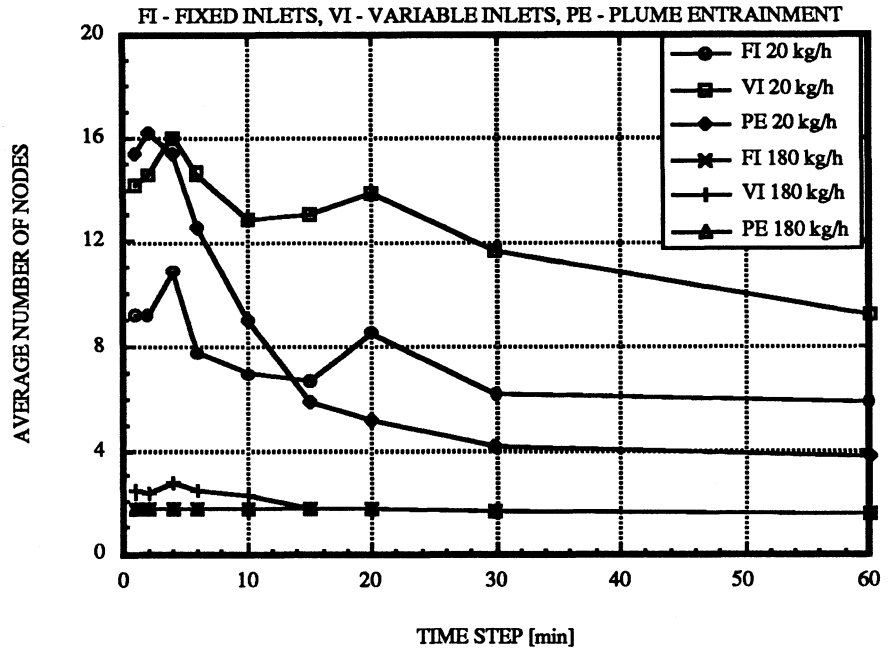

Fig. 2.9 Average Number of Segments for the different Plug Flow Models

Both the simulation time step and the ratio of the tank volume to the collector flow rate (which results in a tank turnover time or mean residence time) strongly influence the average number of nodes. The influence of changing the load profile is not investigated in this example.

The average number of nodes increases with decreasing time step but merging of incoming fluid with existing segments may also reduce the average number of nodes. The probability of merging increases with the number of nodes already in the tank.

The lower average number of nodes for the high flow rate is partly due to the large volume segments that are added, especially for large time steps. There is also less

stratification for higher flow rates (cf Eqn (2.4.1)) which increases the probability for merging segments. Merging will always occur for small time steps when the temperature of the fluid returned to the collector has the same value over several time steps and the radiation does not change.

2.4.3 Fully Mixed Tank Models

Since it is not possible to know a priori how many segments will be used in a simulation with the plug flow model and therefore to find an "equivalent" multi-node model the question arises how both models compare for N = 1. A one-node model can be obtained for the plug flow model by specifying the collector flow rate as 180 kg/h and the time step as 1 h for the 180 liter tank volume. A single load draw between hour 24 and 25 with the draw volume equal to the tank volume and T_{mains} = 20 °C was done. The simulations were carried out for both models under the same conditions starting with tank temperatures of 20 °C at hour 7 for the previously introduced system. The tank temperatures at the end of each time step are shown in Fig. 2.10.

For the first day during collector flow (hour 7 to 17) the tank temperatures of the plug flow model are higher than the tank temperatures of the multi-node model. This observation can be explained by considering how each model determines the tank temperatures.

In the plug flow model the whole tank volume is "taken out" of the tank at the initial temperature of the time step, run through the collector in which the energy is added and put back into the tank.

In the multi-node model the fluid is run "continuously" through the collector during the time step. This is accomplished by using the average tank temperature over the time step according to Eqn (2.1.6) rather than the initial value. The tank "keeps" its fluid and the

entering fluid mixes instantaneously with the tank volume. The fluid returned to the collector has the same temperature as the tank.

This results in a different value of added energy for the two models.

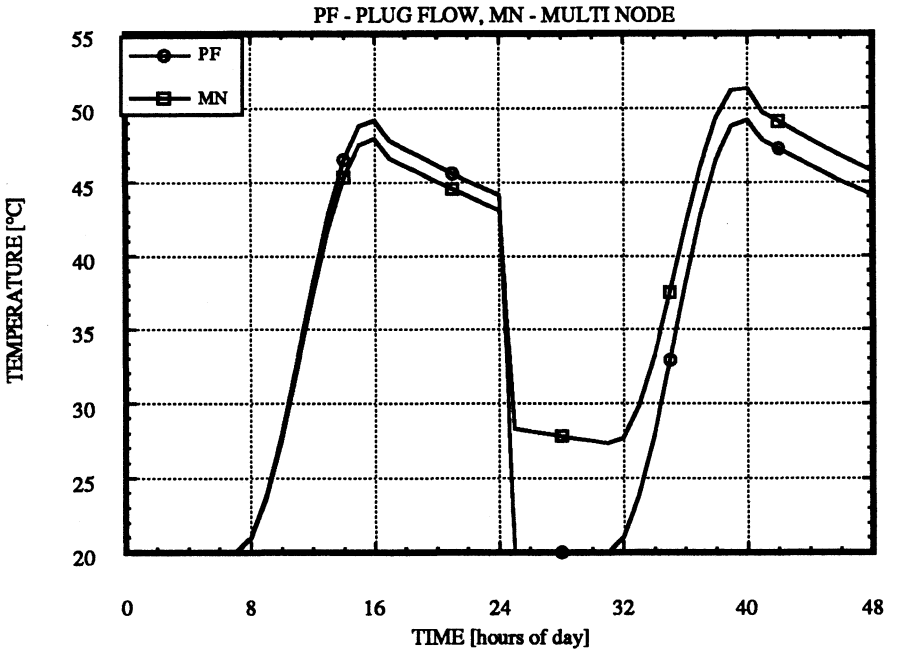

Fig 2.10 Tank Temperatures for the Plug Flow Model and the Multi-Node Model using one Segment

The same principles apply when the load draw occurs. At the end of the load draw the multi-node model has a higher temperature compared to the plug flow. This is a result of the mixing inside the tank during the load draw for the multi node model. The values of the delivered energy for the draw are 17790 MJ and 10900 MJ for the plug flow model and the multi-node model, respectively.

2.4.4 Time Step Dependence

The performance of both the plug flow model and the multi-node model depends on the chosen simulation time step. To investigate this dependence, the same system as used to determine the average number of segments for the plug flow model (hourly profiles) was run with all the tank models for a number of different time steps ranging from 1 to 60 minutes. The values of the delivered energy as defined in Eqn (2.4.3) were taken as the criterion for the time step dependence. The results for two different collector flow rates of 20 kg/h and 180 kg/h are shown in Figs 2.11 and 2.12.

For the collector flow rate of 20 kg/h all the models, except the plug flow model with plume entrainment, exhibit a change in delivered energy with respect to the value for the time step of 60 minutes of less than 1.5 %. The value of delivered energy for the plug flow model with plume entrainment changes by 7.6 %. For the collector flow rate of 180 kg/h all the models, except the plug flow model with variable inlet, show a change of less than 3.3 %. For the plug flow model with variable inlet the relative change in delivered energy is 8.7 %.

In both cases a plug flow model shows the greatest difference. This is related to the change in the average number of segments as a function of the simulation time step as shown in Fig. 2.9. Note that the two models which exhibit the greatest change in the average number of segments also have the poorest time step dependence. This means that for different time steps and therefore different average number of segments the plug flow model is a "different" model.

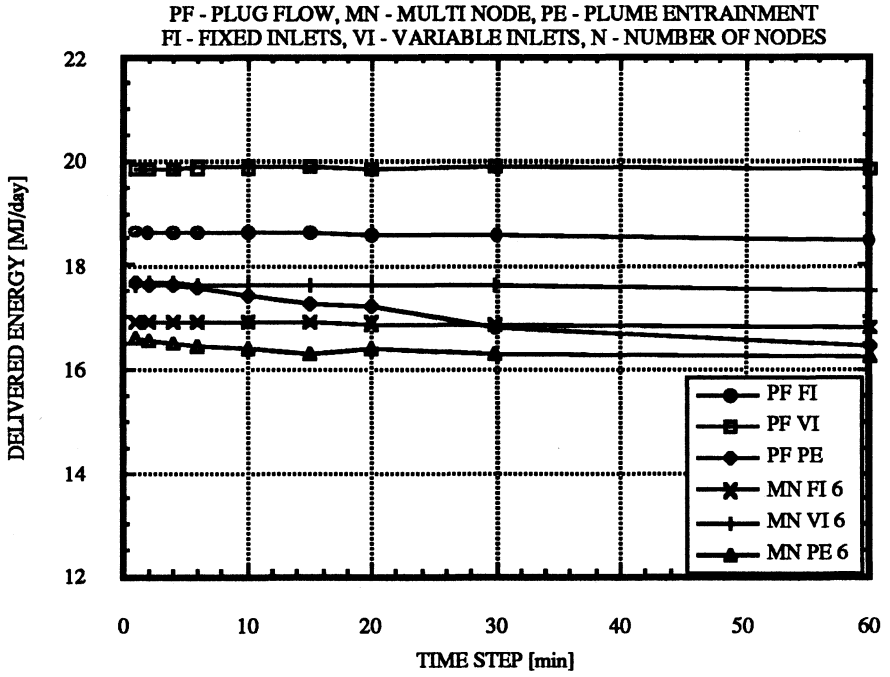

Fig. 2.11 Time Step Dependence of the Tank Models for a Collector Flow Rate of 20 kg/h

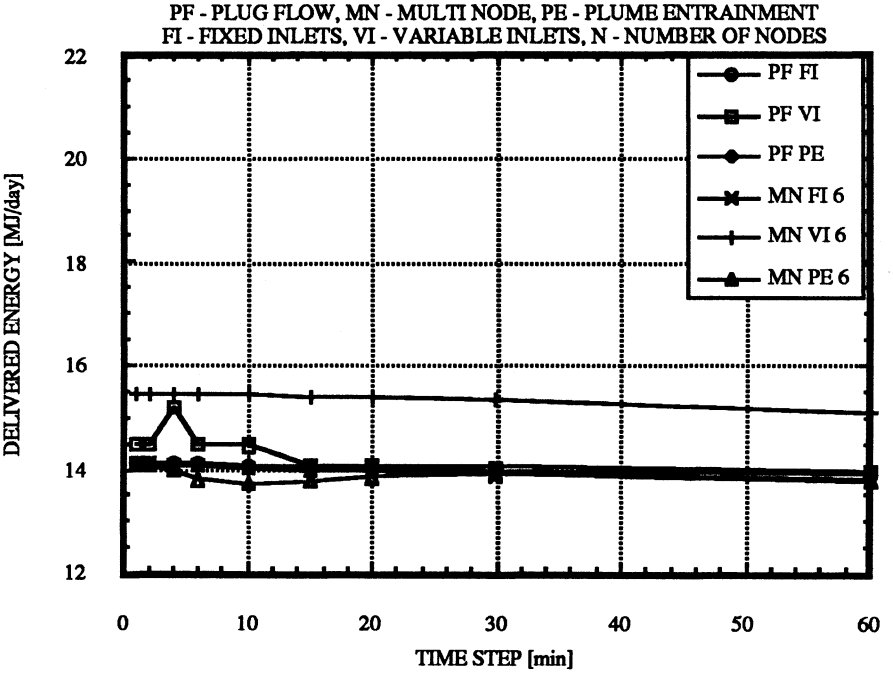

Fig. 2.12 Time Step Dependence of the Tank Models for a Collector Flow Rate of 180 kg/h

Chapter 3

Experimental Data

In this chapter, the two experimental procedures from which the data for the performance study of the TRNSYS tank models were obtained are described. The data for the low heat source flow rate were obtained from Queen's University, Kingston, Ontario [42,43] and the data for the high heat source flow rate were obtained from Colorado State University, Fort Collins, Colorado (CSU) [44].

3.1 Low Flow System

The experimental apparatus consisted of a two component (collector and tank) direct flow SDHW system as shown in Fig. 3.1 and a micro-computer based data acquisition and control system.

The solar collector array was experimentally simulated using a conventional thermal heat source as described in ASHRAE standard 95-1981 [45]. The collector area was 2.9 m^2 and the values of $F_R(\tau\alpha)$ and $F_R U_L$ were 0.743 and 16.34 kJ/(hr m^2 °C), respectively, at a flow rate of 72 kg/h. The collector loop heater was adjusted every minute to deliver energy equal to that of the specified collector operating under a daily irradiance of 12 MJ/day and the measured heat source return temperature. The daily irradiance profile on the collector surface was simulated as a sinusoidal profile between hours 7 and 17 of the day. Effects of different flow rates were accounted for by adjusting the collector heat removal factors, F_R, as described in Duffie and Beckman [9]. The collector loop pump

was turned on at hour 7 and turned off when the rate of the useful energy gain for the collector dropped below zero in the late afternoon (low radiation input and high collector input temperature; cf. Eqn (2.4.1)).

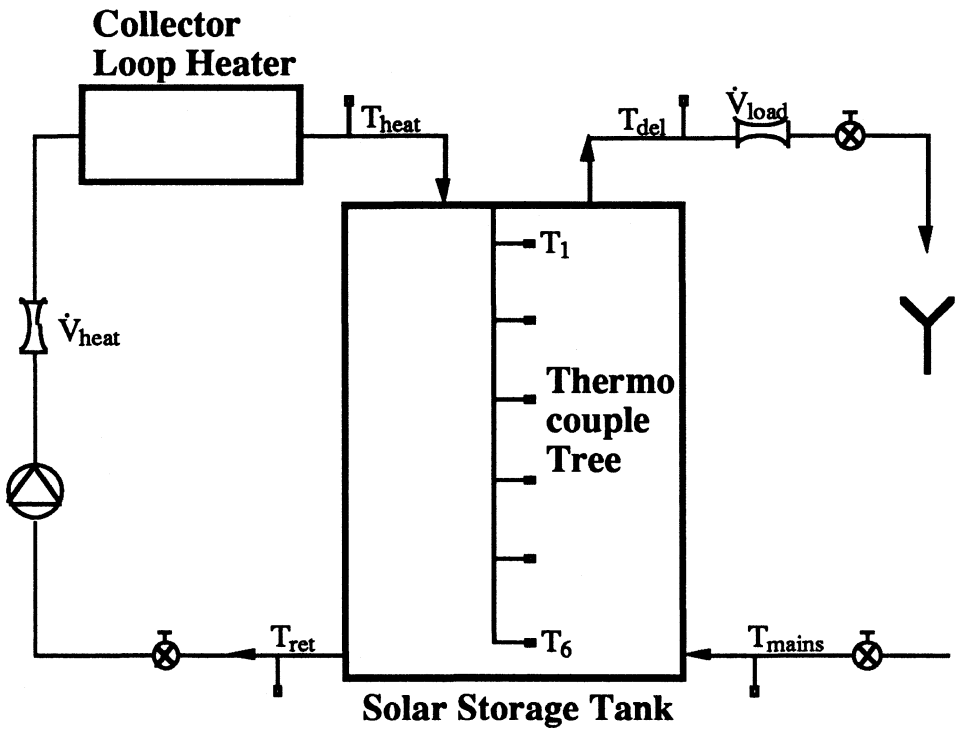

Fig. 3.1 Experimental Set-Up for the Low Flow System

A storage tank with volume equal to 180 liters and length to diameter ratio of 1.84 was used. The UA-value was determined to be 4.57 W/°C by raising the entire tank to a uniform temperature (60°C) and then measuring the rate of temperature decay over one day. This procedure is summarized in Appendix B. The collector and mains water inlet were located radially at the bottom of the tank and the collector outlet and the tank exit were located axially at the top of the tank as shown in Fig. 3.1.

Water was drawn at a flow rate of 6 liters/min from the system. Tests for various collector flow rates and load profiles were performed as shown in Table 3.1.

Test #	$\dot{m}_{heat}$[1] [kg/h]	Load Profile
1	24	Profile 1
2	36	Profile 1
3	48	Profile 1
4	60	Profile 1
5	72	Profile 2
6	84	Profile 3

Hour	Profile 1[2] [liters]	Profile 2[3] [liters]	Profile 3[2] [liters]
7	7	0	10
8	17	0	25
9	17	0	25
10	30	0	45
11	16	0	25
12	7	0	10
13	3	0	5
14	0	0	0
15	0	0	0
16	10	0	15
17	17	0	25
18	30	0	45
19	16	40	25
20	20	40	30
21	7	40	10
22	3	40	5
23	0	40	0
Total Volume	200	200	300

Table 3.1 Experimental Design for the Low Flow System

Successive test days were repeated until the system was determined to be functioning in "steady-periodic" state. This state was identified when the daily delivered energy as defined in Eqn (2.4.2) was found to vary less than 3 % between test days.

---

1) heat source flow rate not quite constant during the experiments
2) drawn at the beginning of the hour
3) drawn in the middle of the hour

The data acquisition and control system supervised load draws, calculated thermal performance (delivered energy) and collected temperature and volume flow rate data every 5 minutes.

Representative experimental tank temperatures are plotted in Fig. 3.2. The tank temperatures measured by the thermocouple tree represent the temperatures of the centers of six equally sized segments in the tank. During the night when there are no flows (hour 22 to 7) a considerable amount of stratification occurs, mainly in the middle part of the tank. The temperature of the bottom part of the tank is close to the mains water temperature because of draws later in the evening when the collector pump was not operating. The temperature of the top part of the tank is close to the temperature after the tank was charged (hour 17) since not all the hot water was taken out of the tank in the evening. The development of the stratification in the evening indicates that the load draw was done in plug flow manner but with some mixing in the zone where the replacement fluid from the load sees the hot water in the tank. Environmental losses and heat conduction cause temperature changes at night. The bottom of the tank gains energy from the environment. The amount of stratification and the mean temperature decrease over night. In the early morning (hour 7 to 8) when the solar input is low, the temperature of the fluid from the collector is lower than the temperature of the upper part of the tank and as a result some mixing occurs at the top of the tank. Between hour 8 and 13 the temperature profile is influenced by the charging and discharging, but without destroying the stratification in the tank because the low collector flow rate causes little mixing at the inlet and also results in a rather high tank turnover time[1)] (5h). A coupling between the bottom and the top temperature can also be observed. Between hour 13 and 16 the tank reaches nearly uniform temperature. The bottom part of the tank is fully charged because no load draws occur. Temperature inversions develop between hour 16 and 17 since the fluid flowing through the collector cools down because of low radiation input and high collector losses

1) defined as the mass of the fluid in the tank divided by the heat source mass flow rate

due to the high collector input temperature (cf. Eqn (2.4.1)). Mixing at the inlets cools down the fluid at the top of the tank but the bottom of the tank stays hot. Several large load draws in the evening result in a stratified temperature field.

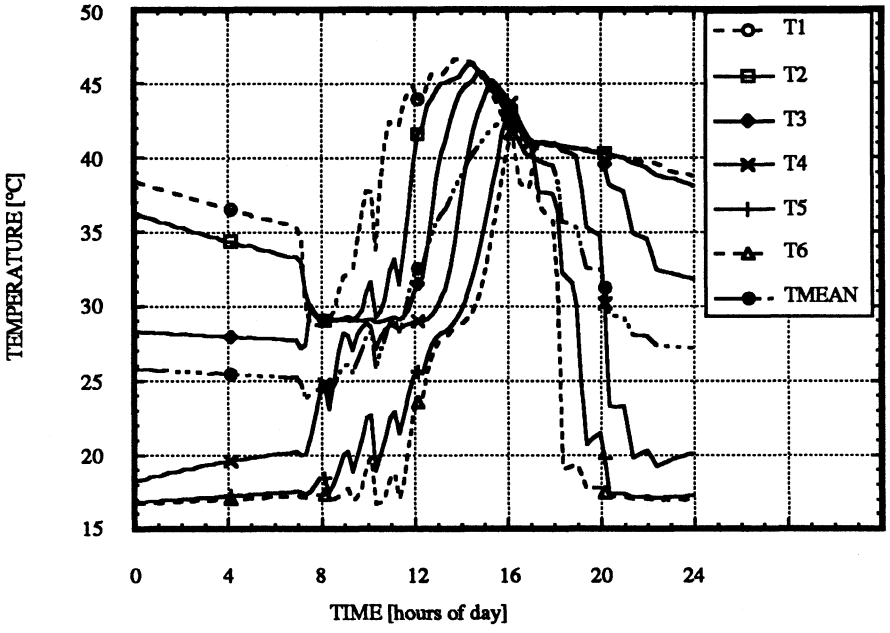

Fig. 3.2 Tank Temperatures for the Low Flow System[1)]

Table 3.2 presents the values of the daily energy input into and the delivered energy from the solar storage tank as well as the change in the internal energy of the tank. The losses, Q_{env}, were calculated as a check on the energy balance. No information about the measurement errors has been obtained.

1) The tank temperatures were obtained from an earlier experiment similar to test #2 in which the collector pump was operating at the same time when the collector was irradiated.

Test #	Q_{in}[1] [kJ]	Q_{del}[2] [kJ]	ΔU[3] [kJ]	Q_{env}[4] [kJ]
1	24577	20988	130	3459
2	23092	18600	5)	4492
3	23456	18760	5)	4696
4	22897	17880	5)	5017
5	23975	20810	303	2862
6	25643	22090	130	3423

Table 3.2 Experimental Results for the Low Flow System

3.2 High Flow System

The data for the high heat source flow rate was taken from a drain-back system as shown in Fig. 3.3. The major components are the collector array and the boiler for the energy input, the drain-back tank as a heat exchanger, the solar storage tank for the energy storage and the auxiliary heater for the addition of electrical auxiliary energy.

---

1) calculated approximating the integral (Eqn (2.4.2)) as a sum with linearly interpolated temperature and flow rate values every 3 minutes, $\rho_f = 1000$ kg/m^3 , $C_f = 4.19$ kJ/(kg °C)

2) according to Queen's University

3) calculated using the tank temperatures at the beginning (hour 0) and the end (hour 24) of the last test day

4) $Q_{env} = Q_{in} - Q_{del} - \Delta U$

5) no tank temperatures were available

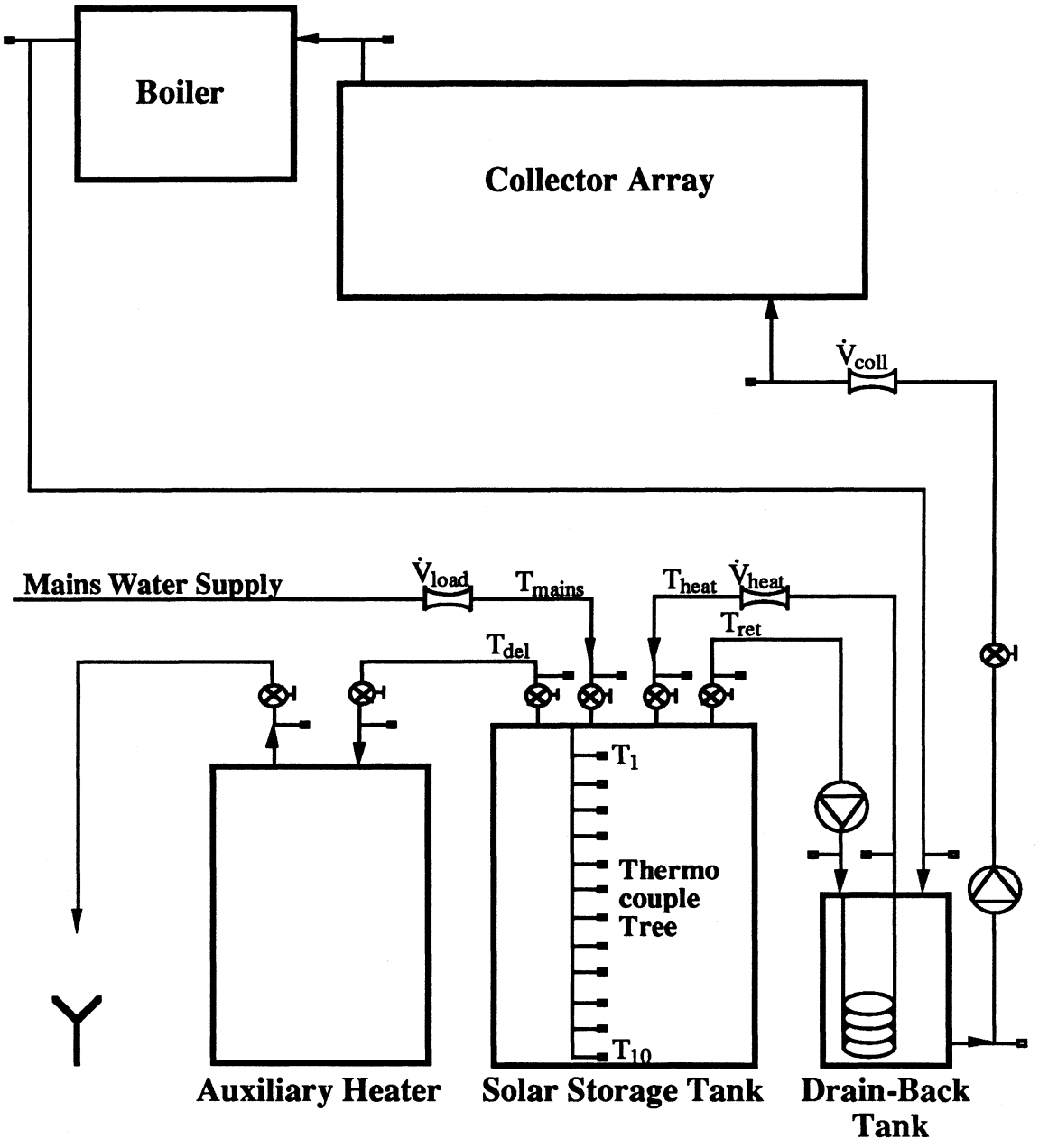

Fig. 3.3 Experimental Set-Up for the High Flow System

The experimental test procedure consisted of a four day test in which the solar radiation and water load profile, ambient temperature (22 ± 2 °C), mains water temperature (22 ± 1 °C) and hot water set point temperature (≥ 48.9 °C) were specified. The tests were completed at the end of four days or when the daily value of the added auxiliary energy was

within 3 % of the previous day's value, whichever came first. The solar storage tank was preheated to about 40 °C at the beginning of the tests to achieve faster convergence. The tests start at hour 17 of the day.

Solar radiation input was simulated with an electric boiler downstream of the collector array which were located in a constant temperature dark room. The boiler input was controlled according to an hourly profile specified by the Solar Rating and Certification Corporation (SRCC) [46] and calculations outlined in ASHRAE standard 95-1987 [47]. The energy input occured between hour 8 and 17 of the day. The value of the total radiation was 17.03 MJ/(m^2 day). The collector parameters, $F_R(\tau\alpha)$ and $F_R U_L$, were 0.602 and 5.56 W/(m^2 °C) at a flow rate of 63.77 kg/(h m^2), respectively. Since the collector was not irradiated, a deadband controller for the collector pumps was emulated through appropriate algorithms in the control software. The collector pumps turned on when the collector sensor temperature exceeded the temperature at the bottom of the storage tank by 20 °F. The pumps remained on until the temperature differential dropped to 5 °F

Daily hot water load was based on energy and was made in three equal draws at hour 8, 12 and 17 of the day. The energy drawn from the system was specified as 49.8 MJ/day. Each draw required about 130 liters of mains water and was performed at a flow rate of 720 kg/h.

The geometry and the piping locations of the solar storage tanks are shown in Fig. 3.4. The UA-values for the large and small solar storage tank are 3.74 W/°C and 3.47 W/°C, respectively. The UA-values were determined by measuring the rate of temperature decay over a 36 hour time period for an initial tank temperature of 60 °C. The procedure is summarized in Appendix B. The volume of the auxiliary tank is 159 liters and the UA-value, determined by a cool-down test, is 1.9 W/°C. The drain-back tank has a volume of 30 liters and a measured heat exchanger effectiveness of 0.6.

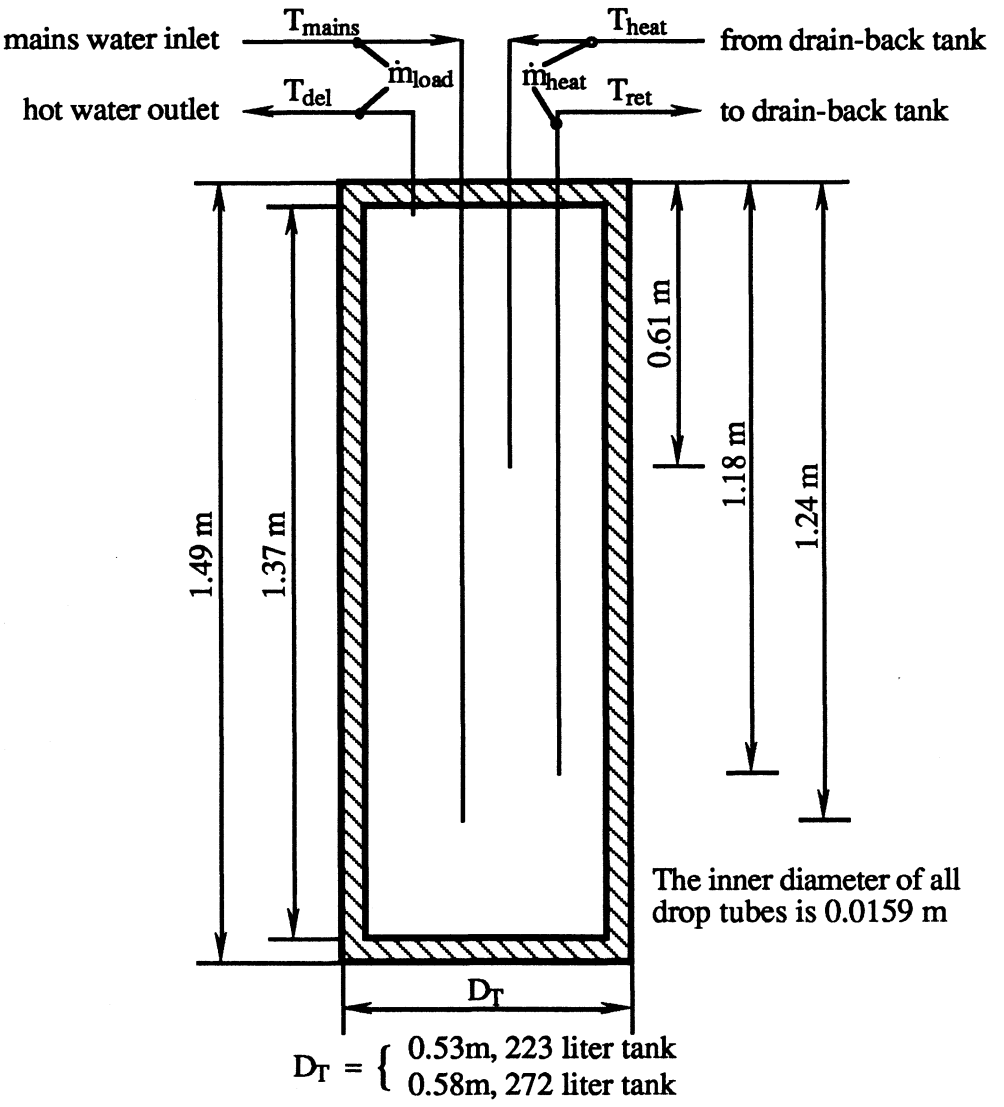

Fig. 3.4 Solar Storage Tank Design for the High Flow System

Eight experiments were designed through combination of two different storage tank volumes, two values of the collector gross area and two different heat source flow rates ($\dot{m}_{heat}$) and collector flow rates ($\dot{m}_{coll}$) as shown in Table 3.3.

Test #	Tank Volume [liters]	Collector Area [m^2]	$\dot{m}_{heat}$[1)] [kg/h]	$\dot{m}_{coll}$[1)] [kg/h]
1	223	2.78	171	205.2
2	223	2.78	342	410.4
3	223	5.56	171	410.4
4	223	5.56	342	205.2
5	272	2.78	171	410.4
6	272	2.78	342	205.2
7	272	5.56	171	205.2
8	272	5.56	342	410.4

Table 3.3 Experimental Design for the High Flow System

Temperatures, volume flow rates, energy usage and energy delivery were monitored throughout the system. The data were sampled 10 times per second. A running average of the ten most recent samples is kept and used when reporting data to file. Data were recorded at varying rates during the tests. During a hot water draw, data were recorded every 15 seconds. Data were recorded every 15 minutes during simulated daylight hours and every 30 minutes during overnight periods.

Fig. 3.5 shows the tank temperatures of the solar storage tank measured by the thermocouple tree for the last day of test #4. The thermocouples were equally spaced with distances of 12.7 cm. The thermocouple tree was centered heightwise in the tank. After the draw at hour 17 a considerable amount of stratification in the tank has developed. Since about half of the tank volume is drawn and the mains water enters the tank at the bottom with downwards directed velocity which causes the hot water at the top to be pushed out in a plug flow manner, the stratification is located mainly in the upper half of the tank. However the temperature profile in the upper half of the tank shows some mixing caused by the load draw since before the draw the tank was at uniform temperature. During the

1) flow rates not quite constant during the experiments

night when there are no flows, temperature changes due to environmental losses and heat conduction can be observed. The amount of stratification and the mean temperature decrease over night. The draw at hour 8 takes the remaining hot water out of the tank so that at the beginning of the energy input the tank is nearly at uniform temperature. The uniform temperature is maintained throughout the day due to the high recirculation flow rate which results in a tank turnover time of about 40 minutes. The stratification created because of the load draw at hour 12 disappears almost immediately.

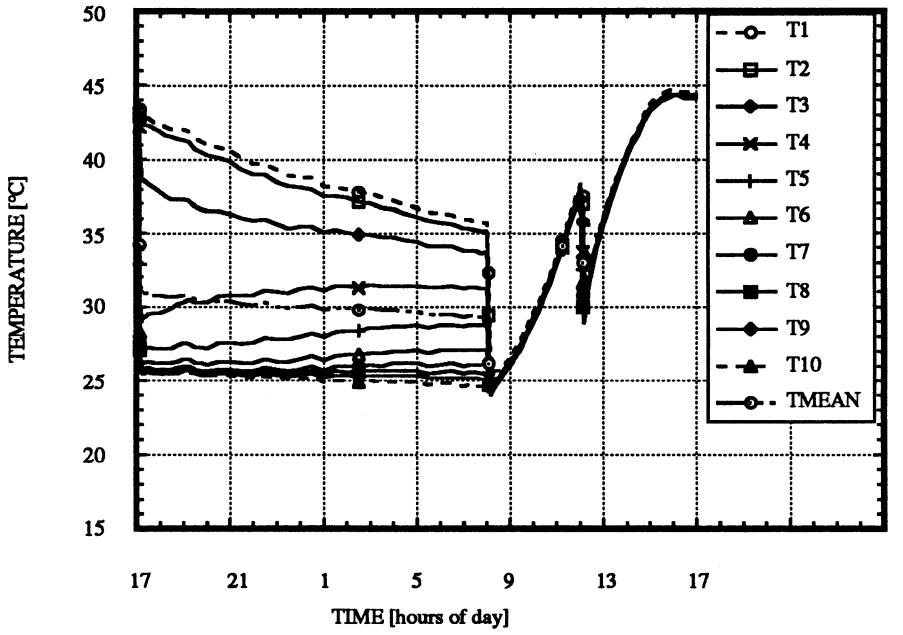

Fig. 3.5 Storage Tank Temperatures for the last Day of Test #4 for the High Flow System

Table 3.4 presents values of the daily energy input into and the delivered energy from the solar storage tank as well as the change in the internal energy of the tank. The losses were calculated as a check on the experimental data. The daily energy input was calculated according to Eqn (2.4.2) with $\dot{m}_{heat} = \dot{V}_{heat}\,\rho_f$. Empirical relationships for ρ_f and C_f as a function of temperature (as also used by CSU to determine the delivered energy) were

employed. The data provided by the measurements and the trapezoid rule to approximate the integral (Eqn (2.4.2)) were used. Thermopile measurements for the temperature differences (T_{heat}-T_{ret}) with an accuracy of 1 % of the temperature difference ± 0.05 °C were available. The measurement error in measuring the volume flow rate was reported to be ± 0.5 %. The values of the delivered energy, Q_{del}, according to Eqn (2.4.3) together with the measurement errors was provided by CSU. The measurement error is based on the maximum errors in the individual measurements. The change in internal energy was calculated using the ten thermocouple temperatures in the tank and ρ_f = 1000 kg/m^3 and C_f = 4.19 kJ/(kg °C) . For test #1 and 3 the calculated losses indicate errors in either Q_{in}, Q_{del} or ΔU outside the range of the specified measurement errors. The values for Q_{env} should be about 2500 kJ and 4000 kJ for test #1 and 3, respectively, to agree with the calculated losses for the other tests (which are mainly a result of the energy input into the system).

Test #	Q_{in} [kJ]	Q_{del} [kJ]	ΔU[1)] [kJ]	Q_{env}[2)] [kJ]
1	17149	16647 ± 345	-297	799
2	20024	16996 ± 346	241	2804
3	27443	25471 ± 452	-175	2147
4	28342	24260 ± 436	664	3418
5	20299	17717 ± 354	295	2287
6	19751	16968 ± 346	360	2423
7	28767	25113 ± 448	-188	3842
8	31433	26712 ± 467	-47	4763

Table 3.4 Experimental Results for the Solar Storage Tank of the High Flow System

1) $\Delta U = U\,|_{\text{end of test}} - U\,|_{\text{end of test - 24 hours}}$
2) $Q_{env} = Q_{in} - Q_{del} - \Delta U$

Chapter 4

Simulation of the Experimental Data

In this chapter the way of performing the simulations to compare the different tank models with the experimental data is developed. Also introduced are three numbers which are used to describe the performance of the tank models in predicting the experimental data.

4.1 System

The experimental set-up for the low flow system (cf. chapter 3.1) was first simulated with a system similar to that shown in Fig. 2.6 by specifying the energy to the collector, the flow rates and the mains water temperature. This represents exactly the way the experiments were performed. With this method of simulating the experimental data, it was realized that the system consisting only of two components (collector and tank) is highly coupled. This means that if the tank model predicts an incorrect temperature returned to the collector then the collector adds an incorrect value of useful energy (cf. Eqn (2.4.1)) which leads to an incorrect collector output temperature. Therefore an incorrect value is used as tank input temperature which then affects the temperature of the fluid delivered to the load and the temperature of the fluid returned to the collector. Although the collector compensates for errors in the collector input temperature to some extent (if T_{ret} is too low then the collector useful energy is too high and vice versa) the coupled system leads to wrong inputs to the tank. This lead to the conclusion that using the approach of simulating

the entire experimental set-up to investigate the performance of the different tank models should not be used.

The idea that, in validating a system component model the system around it should be perfect, motivated a different method of simulating the experimental data. It was decided to leave the collector out in the simulations and force the input values of temperature and flow rate (T_{heat} (t), T_{mains} (t), $\dot{m}_{heat}$ (t), $\dot{m}_{load}$ (t), T_{env} (t)) for the tank to be as measured in the experiments. The resulting system is shown in Fig. 4.1. Forcing the inputs can be done in TRNSYS using the option of time dependent forcing functions and small time steps. Considering only the tank as the system to be simulated is even more important for complex systems such as the high flow system as described in section 3.2.

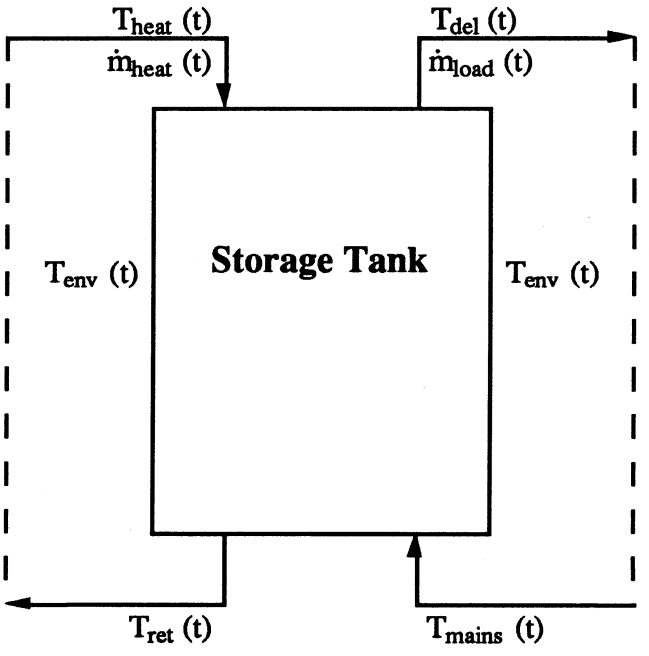

Fig. 4.1 Simulated System

4.2 Performance Numbers

Having found the way of simulating the experiment data the next question is how to describe the performance of the different tank models. This is equivalent to asking which experimental data should be compared with the simulated data. Several attempts were made using data for the low flow system.

Since the performance of a SDHW depends on the amount of stratification in the storage tank, the experimental top and bottom tank temperatures were compared with the simulated ones. In these comparisons no pattern could be recognized. There is also the difficulty that the top and bottom temperatures represented by the models are at different locations for the multi-node model depending on the number of nodes and at variable locations for the plug flow model due to the adaptive size of the segments.

The difficulty of the temperature locations can be avoided by comparing the mean tank temperatures for the experimental and simulated case. There was again no recognizable pattern that allowed any judgement on the performance of the different tank models.

Two main ideas motivated the ultimately used performance study. First, there are two loops for the tank. There is the loop which is connected to the heat source and in which charging of the storage tank takes place and there is the loop in which the load draw occurs (discharging). Both loops are coupled in the sense that it is not possible to take out more energy from the tank than what was put in (minus losses) over a long period of time, i.e. regardless of the change in the internal energy of the tank. Although the two loops are coupled they will be considered separately in the performance study. Second, since the inputs to the tank match exactly the experimental data it was decided to look at the outputs of the tank models ($T_{ret,}$ T_{del}) and compare these with the experimental data. This is motivated by the idea that if the outputs compare well with the experimental data then the storage tank model is appropriate for use as a system component model. This does not

necessarily mean that the temperature profile within the tank is well represented by the model at all times.

Three numbers have been defined in order to compare the simulated outputs with the experimental outputs.

For the load side (discharging) QD is defined as the difference between the predicted and the measured delivered energy divided by the experimentally delivered energy and is therefore

$$QD = \frac{Q_{del,sim} - Q_{del,exp}}{Q_{del,exp}} = \frac{\int_{day} \dot{m}_{load} (T_{del,sim} - T_{del,exp})\, dt}{\int_{day} \dot{m}_{load} (T_{del,exp} - T_{mains})\, dt} \qquad (4.1.1)$$

QD represents the relative error in the delivered energy. QD is a measure of the ability of the model to predict the temperature of the fluid delivered to the load. An overprediction of $T_{del,exp}$ (averaged over time) results in a positive relative error in the delivered energy and vice versa.

For the heat source side (charging) QI is defined as the difference between the simulated and the experimental energy input from the heat source divided by the measured energy input and is therefore

$$QI = \frac{Q_{in,sim} - Q_{in,exp}}{Q_{in,exp}} = \frac{\int_{day} \dot{m}_{heat} (T_{ret,exp} - T_{ret,sim})\, dt}{\int_{day} \dot{m}_{heat} (T_{heat} - T_{ret,exp})\, dt} \qquad (4.1.2)$$

QI represents the relative error for the energy input into the tank. QI is a measure of the ability of the model to predict the temperature of the fluid returned to the heat source. An underprediction of $T_{ret,exp}$ (averaged over time) results in a negative relative error in the energy input into the tank and vice versa. QD and QI are coupled in the same sense as Q_{in} and Q_{del} as described above.

A second number has been defined for the heat source side which is also a measure of the ability of the model to predict the heat source return temperature but does not allow the compensation of positive with negative deviations of $T_{ret,sim}$ from $T_{ret,exp}$. This dimensionless performance number P is

$$P = \frac{\sqrt{\sum_{t=t_{on}}^{t_{off}} \dot{m}_{heat}^2 C_f^2 (T_{ret,exp}-T_{ret,sim})^2 \Delta t^2}}{\int_{day} \dot{m}_{heat} C_f (T_{heat}-T_{ret,exp})\, dt} \qquad (4.1.3)$$

where t_{on} = time when the flow from the heat source begins

t_{off} = time when the flow from the heat source ends.

The denominator represents the experimental energy input into the tank. The numerator is a sum of the squared errors in the energy input into the tank. Eqn (4.1.3) can therefore be rewritten as

$$P = \frac{\sqrt{\sum_{t=t_{on}}^{t_{off}} \Delta Q_{in}^2}}{Q_{in}} \qquad (4.1.4)$$

The values of ΔQ_{in} are determined by both the magnitude of the heat source flow rate, $\dot{m}_{heat}$, and the magnitude of the temperature errors $T_{ret,exp} - T_{ret,sim}$. Therefore P increases if $\dot{m}_{heat}$ increases for the same $T_{ret,exp} - T_{ret,sim}$ or P increases if $T_{ret,exp} - T_{ret,sim}$ increases for the same $\dot{m}_{heat}$. The higher the value of P the poorer is the performance of the tank model under investigation.

4.3 Simulations with TRNSYS

In this section some details about the performed simulations using TRNSYS are given.

The time step used to simulate the low flow data was 3 minutes. This has been seen to be small enough to trace the experimental data used as inputs to the tank reasonably well. For simulating the high flow data a time step of 15 seconds was employed so that during the load draws the measured load flow rate could be tracked. Volume was drawn as measured in the experiments for the high flow system rather than energy. The relative error tolerance controlling the integration error and the relative error tolerance controlling the convergence of input and output variables were both set equal to 0.001. Successive test days were simulated until the system reached a steady-periodic state.

Equally sized nodes were specified for the multi-node model. The use of unequally sized nodes (smaller nodes in the region of the thermocline) can only be motivated by additional information about the temperature profile in the tank during the whole simulation. The thermocline would have to be restricted to a certain region inside the tank. Table 4.1 summarizes the parameters for the multi-node model used in the TRNSYS simulations.

		Low Flow System	High Flow System	
Parameter	Description	Value	Value	Unit
Mode	mode of operation	1, 2 or 3[1)]	1, 2 or 3[1)]	[-]
V_T	tank volume	0.18	0.223 or 0.272[2)]	[m^3]
C_f	fluid specific heat	4.19	4.19	[kJ/(kg °C)]
ρ_f	fluid density	1000	1000	[kJ/m^3]
U_T	loss coefficient[3)]	8.97	5.37 or 5.26[2)]	[kJ/(h °C m^2)]
D	inlet pipe diameter	0.0127	0.0159	[m]
H	tank height	0.92	1.37	[m]

Table 4.1 Parameters for the Simulations with the Multi-Node Model

The plug flow model has the option of specifying the height of the heat source inlet position above the bottom of the tank, H_{in}. This option was used for the solar storage tank of the high flow system (cf. Fig. 3.4). It could be seen that including heat conduction in the plug flow model has little influence on the performance of the model (Q_{del} decreased by less than 1.5 %). For this reason and since the solution procedure can also become computationally expensive when conduction is included (cf. section 2.2) it was decided to omit heat conduction. The ratio of thickness of top insulation to thickness of side insulation was assumed to be 1. This was done because not enough information about the insulation thickness was available. The insulation thickness of commercially used hot water storage tanks, as used in the experiments, generally shows some irregularities (non constant insulation thickness at the top and due to piping locations). It could also be seen that changing r_{ins} by a factor of two result in changes in Q_{del} of less than 0.5 % and in Q_{env}

1) 1- fixed inlet positions, 2 - variable inlet positions, 3 - include plume entrainment
2) small or large solar storage tank, respectively
3) per unit area

of less than 2 %. Table 4.1 summarizes the parameters for the plug flow model used in the TRNSYS simulations. A TRNSYS example deck (input data file) is given in Appendix C.

		Low Flow System	High Flow System	
Parameter	Description	Value	Value	Unit
Mode	mode of operation	1, 2 or 3[1)]	1, 2 or 3[1)]	[-]
V_T	tank volume	0.18	0.223 or 0.272[2)]	[m^3]
H	tank height	0.92	1.37	[m]
H_{in}	heat source inlet	0.92[4)]	0.82[4)]	[m]
C_f	fluid specific heat	4.19	4.19	[kJ/(kg °C)]
ρ_f	fluid density	1000	1000	[kg/m^3]
k_f	heat conductivity	0	0	[kJ/(h m °C)]
Tank	configuration	1[5)]	1[5)]	[-]
UA	loss coefficient	16.45	12.27 or 13.46[2)]	[kJ/(h °C)]
r_{ins}	[6)]	1	1	[-]
T_{init}[7)]	initial temperature	15	≈ 40[8)]	[°C]
D	inlet pipe diameter	0.0127	0.0159	[m]

Table 4.2 Parameters for the Simulations with the Plug Flow Model

1) 1 - fixed inlet positions, 2 - variable inlet positions, 3 - include plume entrainment
2) small and large solar storage tank, respectively
4) above bottom of tank
5) vertical cylinder
6) ratio of thickness of top insulation to thickness of side insulation
7) of the preheat portion of the tank
8) varies according to the experimental procedure

Chapter 5

Discussion of Results

This chapter presents the results obtained by applying the performance study as described in chapter 4 to the experimental data introduced in chapter 3. Also included is a study of computational speed for the investigated models.

5.1 Energy Quantities

In this section, the results based on the relative errors in the energy input into the tank, QI, and relative error in the delivered energy, QD, as defined in Eqns (4.1.1) and (4.1.2) are presented. The reader is reminded that a positive value of QI, corresponding to an overprediction in the energy input into the tank, results from an underprediction of the temperature of the fluid returned to the heat source and vice versa. Similarly, a positive value of QD, corresponding to an overprediction of the delivered energy, is caused by an overprediction of the temperature of the fluid delivered to the load and vice versa. In the figures the results for QI and QD are plotted for the multi-node models with two, three and four nodes. Then the best values of QI and QD for the corresponding numbers of nodes between five and fourteen (or the values of QI and QD for the eight-node model if the best case is not obtained for the multi-node model with a number of nodes between fife and fourteen) are shown. Finally the values of QI and QD for the multi-node models with fifteen nodes are plotted to show the results for the maximum number of nodes.

5.1.1 Comparisons for the Low Flow System

This section presents the results for the relative errors in the energy quantities, QI and QD, obtained with the experimental data measured at Queen's University, Kingston, Ontario. The results obtained with tests #1 to 4 will be analyzed first in order to see the effect on the predictions of the energy quantities when the heat source flow rate, $\dot{m}_{heat}$, is increased for a given load profile (cf. Table 3.1). Figs 5.1 to 5.4 show the values of QI and QD for the tests #1 to 4.

The assumption of a uniform temperature for the fully mixed tank model leads to a significant underprediction of the energy input into the tank. As the heat source flow rate is increased in the different tests the values of QI increase from - 43 % for $\dot{m}_{heat}$ = 24 kg/h to - 36 % for $\dot{m}_{heat}$ = 60 kg/h. This trend indicates decreasing stratification in the tank, as observed in the experiments for increasing heat source flow rate.

The plug flow model with fixed inlets overpredicts the energy input to the tank by + 9 % for $\dot{m}_{heat}$ = 24 kg/h. The value of QI decreases to - 1.5 % as the heat source flow rate increases to $\dot{m}_{heat}$ = 60 kg/h. The plug flow model with variable inlets shows the same trend as the plug flow model with the fixed inlet option in that QI decreases as $\dot{m}_{heat}$ is increased. The values of QI are higher for the plug flow model with variable inlets (+ 12 % for $\dot{m}_{heat}$ = 24 kg/h to + 5 % for $\dot{m}_{heat}$ = 60 kg/h) than for the plug flow model with fixed inlets. This behavior is expected because the plug flow model with variable inlets inserts fluid from the heat source that is colder than the segment(s) at the top of the tank below these segment(s) which ultimately results in a lower return temperature to the heat source than obtained for the plug flow model with fixed inlets. For the plug flow model with fixed inlets the top of the tank is cooled down by mixing if the temperature of the heat source fluid is lower than the temperature(s) of the top segment(s). Therefore the bottom segments are less influenced by a low temperature of the heat source flow. The plug flow model, which includes plume entrainment, underpredicts the relative error in the energy

input to the tank by values between - 5 % and - 3 %. No flow rate dependence is observed.

The multi-node model with fixed inlets underpredicts the energy input to the tank for all four tests. The degree of underprediction depends on the number of nodes. A high number of nodes results in closer agreement with the experiments. QI increases for increasing $\dot{m}_{heat}$ and a two-node model because the amount of stratification in the tank decreases for increasing $\dot{m}_{heat}$. Therefore the two-node model, which introduces a considerable amount of mixing, gives better results. QI decreases for increasing heat source flow rate and fifteen nodes. The value of QI undergoes higher changes for a low value of $\dot{m}_{heat}$ when the number of nodes is changed than for a higher value of $\dot{m}_{heat}$ (- 28 % to - 0.5 % for 24 kg/h compared to - 23 % to - 7 % for 60 kg/h), suggesting that the higher the flow rate, the less crucial is the choice of the number of nodes. The multi-node model with variable inlets predicts higher values for the energy input to the tank than the multi-node model with fixed inlet options. The same reasoning as already discussed in connection with the plug flow model with variable inlets applies. However, the multi-node model with variable inlets still mostly underpredicts the measured energy input to the tank. QI increases as the number of nodes is increased. As for the multi-node model with fixed inlets, the extent that QI depends on the number of nodes becomes smaller for the multi-node model with variable inlets as $\dot{m}_{heat}$ increases (- 26 % to + 3 % for 24 kg/h compared to -20 % to - 0.5 % for 60 kg/h). The multi-node model including plume entrainment predicts lower values for the energy input into the tank than the multi-node model with fixed inlets. Thus the multi-node model with plume entrainment always underpredicts the measured values. The values of QI increase as the number of nodes increases. As for both, the multi-node models with fixed and variable inlets the range of QI as a function of the number of nodes becomes smaller for the multi-node model with plume entrainment as the heat source flow rate increases (- 33 % to - 1 % for 24 kg/h compared to -25 % to - 8 % for 60 kg/h).

The value of the measured delivered energy is highly underpredicted by the fully mixed tank model. The value of QD becomes larger as the heat source flow rate is increased (- 48 % for 24 kg/h compared to - 35 % for 60 kg/h). The assumption of a uniform temperature gives better results for high values of $\dot{m}_{heat}$ because the tank is less stratified.

The plug flow model with fixed inlets overpredicts the value of the delivered energy for $\dot{m}_{heat}$ = 24 kg/h by + 12 %. For the other flow rates the value of QD is about + 5 % regardless of the value of the flow rate. The plug flow model with the variable inlet option gives a value of + 20 % for QD at the heat source flow rate of 24 kg/h. For all other flow rates the value of QD is about + 13 % regardless of the value of $\dot{m}_{heat}$. The tank top temperature predictions are higher for the plug flow model with variable inlets than for the plug flow model with fixed inlets because no mixing is introduced at the top of the tank. The plug flow model, including plume entrainment, yields values between 0 % and + 3 % for all values of $\dot{m}_{heat}$. These results show that including plume entrainment into the plug flow model works well for the considered conditions.

The predictions of the delivered energy for the multi-node model with fifteen nodes are within ± 1 % for tests #1 to 4. The two-node model predictions improve as $\dot{m}_{heat}$ increases (- 30 % for 24 kg/h and - 19 % for 60 kg/h), concurring with the experimental results that less stratification is observed for higher heat source flow rates. The multi-node model with variable inlets underpredicts the values of delivered energy for small (<5) numbers of nodes and overpredicts for a high (>10) numbers of nodes. Thus, the values of QD for the variable inlet option are higher than those for the fixed inlet option because no mixing at the top of the tank is introduced when the entering fluid is colder than the top node(s). The number of nodes which gives the best predictions decreases as the flow rate increases (eight nodes for 24 kg/h and five nodes for 60 kg/h). Less stratification is modeled for the higher heat source flow rates as observed in the experiments. The value for QD for a fifteen-node model is + 6 % to + 8 % for all flow rates considered. The two-node model predictions improve as the heat source flow rate increases (- 27 % for 24 kg/h and -15 %

for 60 kg/h). The multi-node model, including plume entrainment, underpredicts the experimental delivered energy for all number of nodes and all flow rates considered. The values are below those for the multi-node model with fixed inlets. The fifteen-node model with plume entrainment gives values of - 2 % or better for all flow rates. The two-node model predictions improve as the flow rate is increased (- 35 % for 24 kg/h compared to - 21 % for 60 kg/h).

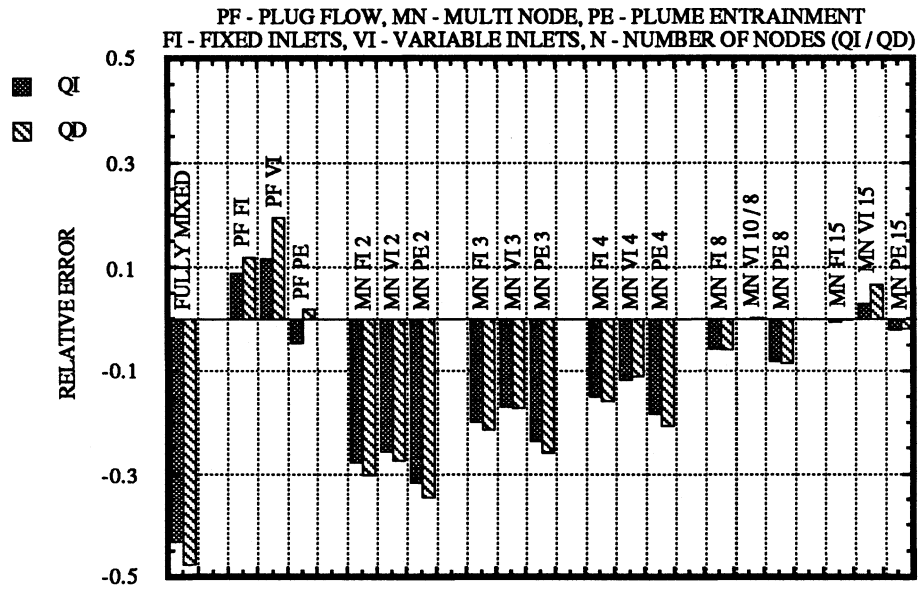

Fig. 5.1 Results for QI and QD for the Low Flow Test #1

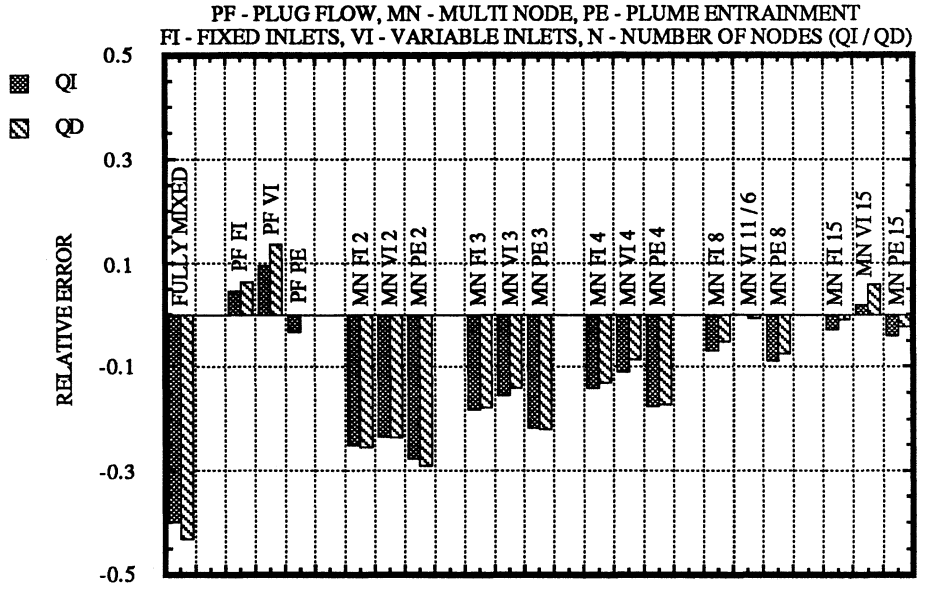

Fig. 5.2 Results for QI and QD for the Low Flow Test #2

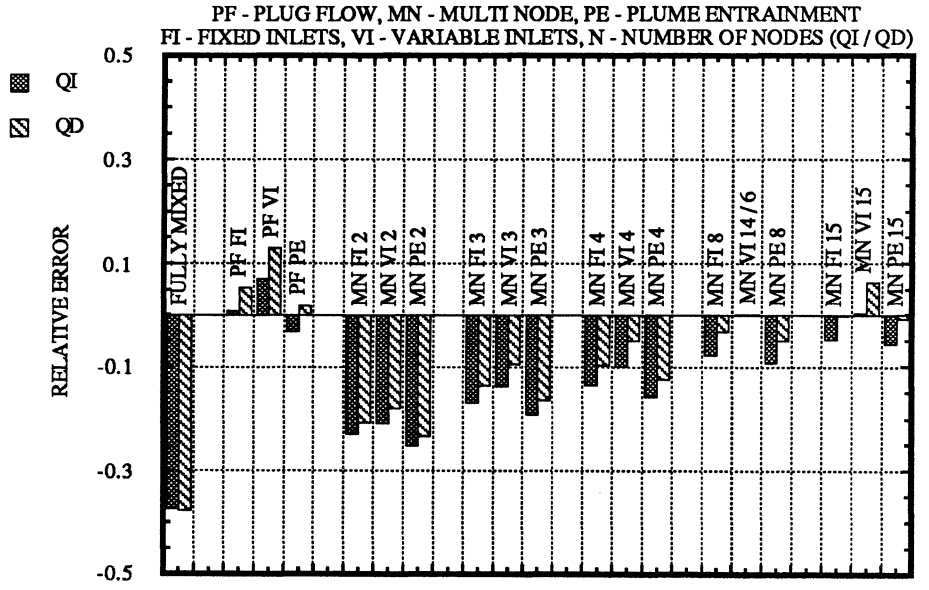

Fig. 5.3 Results for QI and QD for the Low Flow Test #3

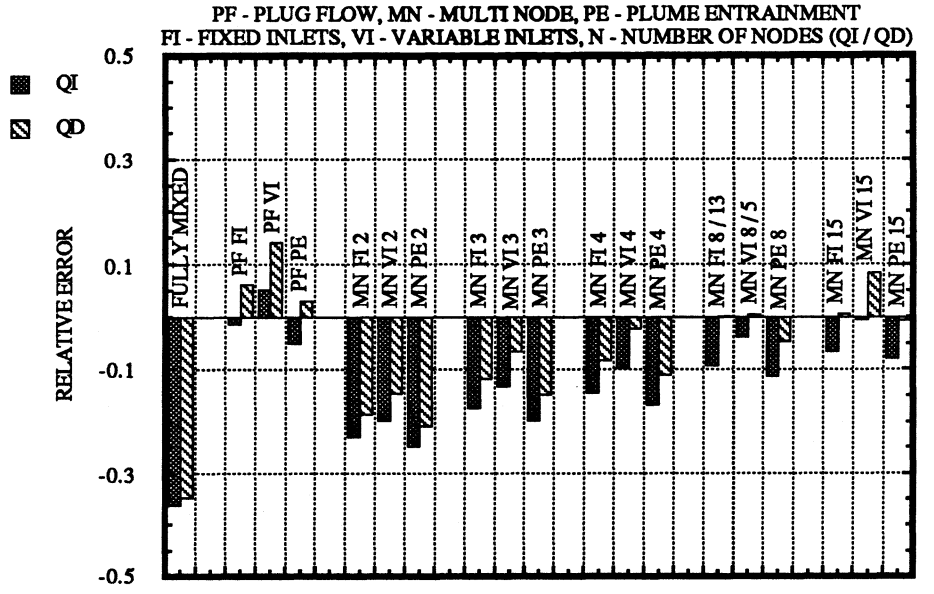

Fig. 5.4 Results for QI and QD for the Low Flow Test #4

The results of test #6 are discussed next in order to see how the increase in both the heat source flow rate and the load volume (but not the load characteristics (cf. Table 3.1)), affect the performance of the different tank models. Fig. 5.5 shows the values for QI and QD for the tank models under investigation.

The fully mixed tank model underpredicts the value of the measured energy input by - 35 %. This value of QI is higher than the values predicted for tests #1 to 4 by the same model. This result can be explained because a higher degree of mixing in the tank due to the higher heat source flow and load volume is represented better by the assumption of a uniform temperature.

The plug flow model with fixed inlets predicts a value of + 3 % for QI which is between the values for tests #2 and 3. The plug flow model with variable inlets overpredicts the energy input to the tank by + 11 %, which is a higher value than the values

obtained with tests #1 to 4 indicating that neglecting mixing for the flows of test #6 results in incorrect energy values. The value of QI (+ 1.5 %) for the multi-node model with plume entrainment is higher than for tests #1 to 4 but shows good performance.

The values of QI for the multi-node models with fixed inlets, variable inlets and plume entrainment are slightly higher than those for test #4. They change by the same amount when the number of nodes is increased as in test #4, suggesting that the further increases in the heat source flow and load volume for these "higher" values does not affect the model predictions very much.

The value of the delivered energy is underpredicted by the fully mixed tank model by - 37 %. This value is close to the results obtained for tests #3 and 4.

For the plug flow model with fixed inlets the value of QD is + 9 %. The reason for this overprediction is seen in the fact that the model does not take enough mixing at the top into account. This is even more the case for the plug flow model with variable inlets which yields a value of + 18 % for QD. Also the plug flow model with plume entrainment does not satisfactorily account for the mixing at the top of the tank and results in + 8 % overprediction for the higher heat source flow rate and load volume.

The values of QD for the multi-node models with fixed inlets, variable inlets and plume entrainment are close to the values obtained for tests #3 and 4. This suggests that the further increase in the heat source flow rate and load volume for these "higher" values does not affect the model predictions very much.

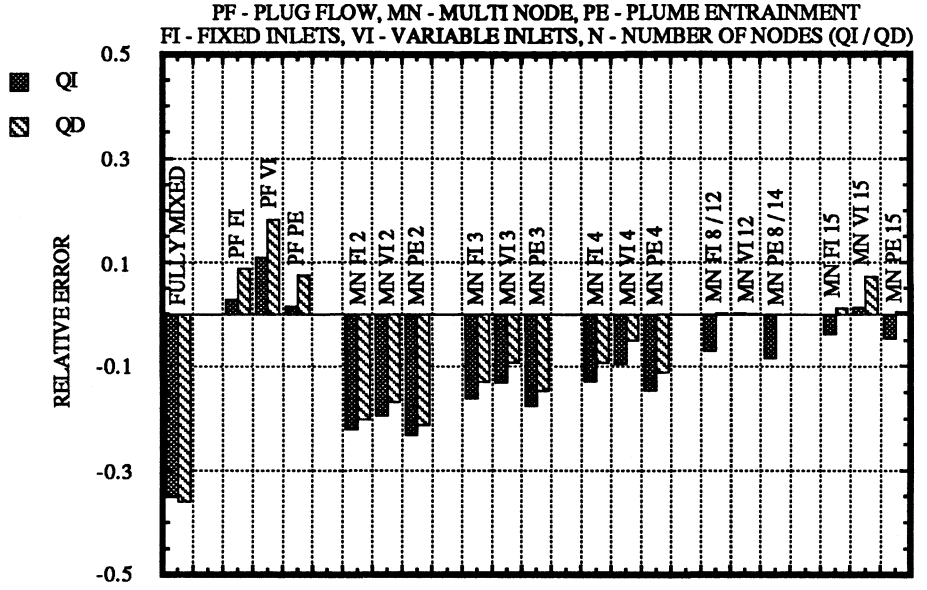

Fig. 5.5 Results for QI and QD for the Low Flow Test #6

Fig. 5.6 shows the results for the test #5 in which the load draw is done at the end of the day.

The fully mixed tank model greatly underpredicts the the energy input to the tank as well as the delivered energy. The value of QI is - 34 % and the value of QD is - 40 %. These results show that too much mixing is introduced which is not appropriate for the time when the tank is charged and the time when the tank is discharged because during charging and discharging there are considerable amounts of stratification in the tank as shown in Fig. 5.7.

The plug flow model with fixed inlets gives the same results as the plug flow models with variable inlets or with plume entrainment. This is because the temperatures of the tank during the day rise continually causing that T_{heat} is always greater than the temperature at the top of the tank so that neither the variable inlet option nor plume entrainment are

employed. Also the temperature of the mains water is the lowest temperature in the system so that the variable inlet option is not used during the load draws. The values for both, QI and QD (- 0.5 % and + 1.5 %, respectively) show good performance for the plug flow models.

All of the multi-node models also give the same values for QI and QD for a fixed number of nodes. The reason for that is already discussed in connection with the plug flow models. The values for QI change from - 22 % to - 6 % as the number of nodes increases from two to fifteen. The values for QD change from - 26 % to - 6 % as the number of nodes is increased from two to fifteen. The underprediction for both QI and QD is attributed to the fact that too much mixing is introduced by the multi-node models. The multi-node models with two nodes introduce more mixing than the multi-node models with fifteen nodes, hence the two-node models give poorer performance.

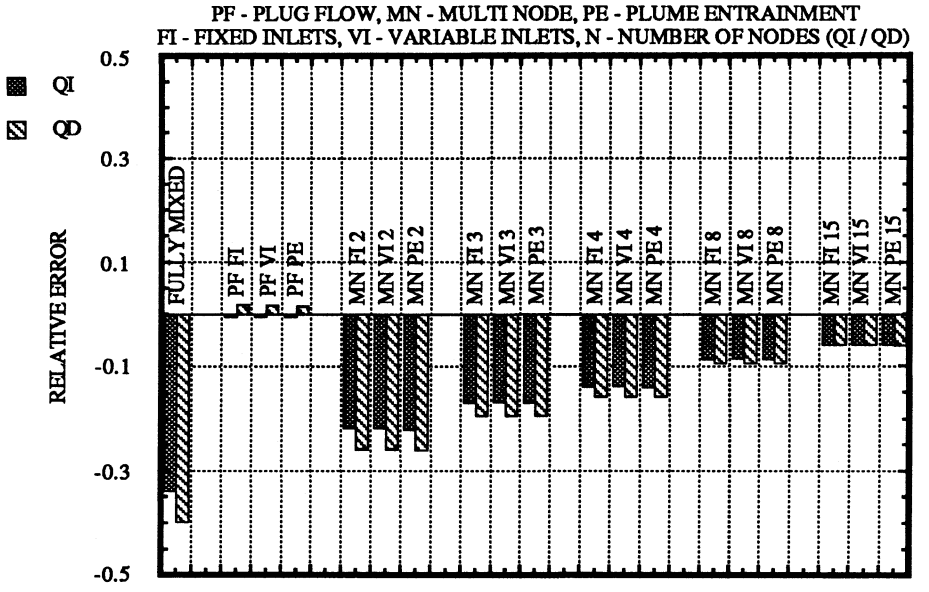

Fig. 5.6 Results for QI and QD for the Low Flow Test #5

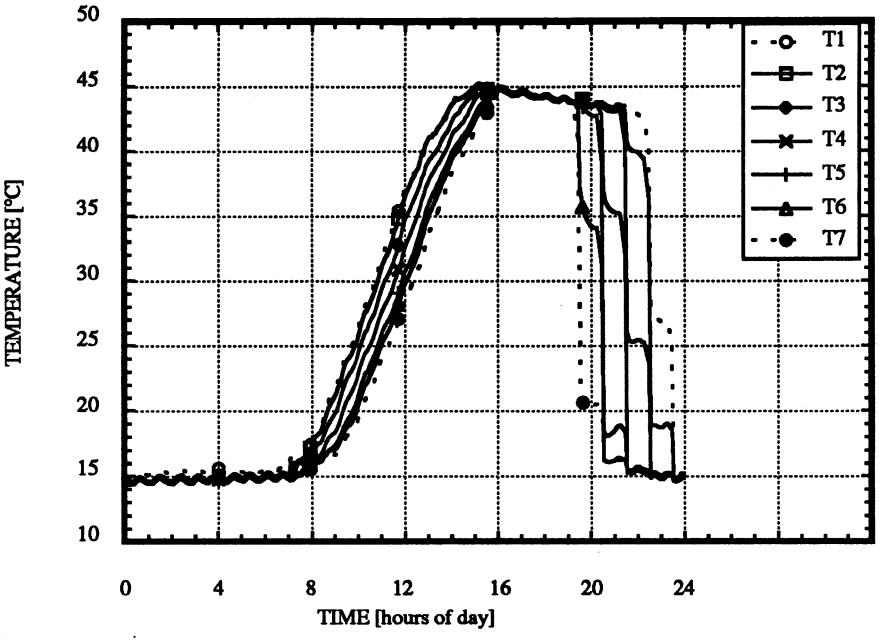

Fig. 5.7 Tank Temperatures for the Low Flow Test #5

5.1.2 Comparisons for the High Flow System

This section presents a discussion of the model predictions for the experimental energy quantities as measured by Colorado State University and described in detail in section 3.2. The results for either QI or QD will be discussed together for tests #1 to 8. They are shown in Figs 5.8 to 5.15.

In investigating the results obtained for the predictions of the energy quantities it was observed that the tests can be divided into two groups, characterized by the two different values of the heat source flow rate. All tests having odd test numbers correspond to a heat source flow rate, $\dot{m}_{heat}$, of 171 kg/h and all tests with even test numbers correspond to $\dot{m}_{heat}$ = 342 kg/h. Similar results were obtained for the two groups of tests that differ in

the value of the heat source flow rate. The range of the values for QI and QD for the tests with $\dot{m}_{heat}$ = 171 kg/h is larger than the range of the values for the tests with $\dot{m}_{heat}$ = 342 kg/h. This observation indicates that choosing a particular model for the higher heat source flow rate (342 kg/h) is less crucial than choosing a model for the lower heat source flow rate (171 kg/h). No pattern corresponding to the two different collector areas (amount of energy input), the two different tank volumes or the two different collector flow rates (cf. Table 3.3) could be found.

The fully mixed tank model significantly underpredicts the energy input into the tank for all eight tests. The values of QI for $\dot{m}_{heat}$ = 171 kg/h range from - 21 % to - 15 % and the values of QI for the heat source flow rate of 342 kg/h range from - 20 % to - 18 %. The values of QI show that no improvements are obtained for the tests with the higher heat source flow rate, suggesting that the fully mixed tank model is never appropriate to be used as a thermal storage tank model.

The plug flow model with fixed inlets overpredicts the energy input into the tank for all eight tests. The values of QI depend on the values of the heat source flow rate. For $\dot{m}_{heat}$ = 171 kg/h the values of QI range from + 12 % to + 21 %. For $\dot{m}_{heat}$ = 342 kg/h the values of QI are lower and range from + 3 % to + 4 %. The plug flow model with variable inlets gives higher values for QI than the plug flow model with fixed inlets. For the lower heat source flow rate, the values of QI range from + 21 % to + 29 % and for the higher heat source flow rate the values of QI range from + 12 % to + 15 %. The differences between the higher values of QI for the plug flow model with variable inlet positions and the lower values of QI for the plug flow model with fixed inlet positions result mainly from the time after the load draw at hour 12 of the day when the variable inlet option is employed. The values of QI for the plug flow model with plume entrainment are close to those for the plug flow model with fixed inlets (less than 1.5 % difference for all eight tests). This observation can be explained because plume entrainment does not significantly change the

temperatures of a tank that is nearly at uniform temperature during the time of heat source flow.

The values of QI for the multi-node model with fixed inlets and two nodes are between - 5 % and + 3 % for $\dot{m}_{heat}$ = 171 kg/h and between - 7 % and - 4 % for $\dot{m}_{heat}$ = 342 kg/h. As the number nodes increases the values of QI increase and reach values between + 13 % and + 23 % for the lower heat source flow rate and between + 4 % and + 8 % for the higher heat source flow rate when fifteen nodes are used. The number of nodes for which the values of the energy input into the tank best represent the experimental data range from two to five. The multi-node models with these numbers of nodes model the same amount of mixing as observed in the experiments. The results obtained for QI for the multi-node model with variable inlets are close to those for the multi-node model with fixed inlets if the number of nodes is small (less than 0.8 % if two or three nodes are employed). The differences in QI between the multi-node model with fixed inlets and the multi-node model with variable inlets increase as the number of nodes increases but does not exceed 2 % for the tests with $\dot{m}_{heat}$ = 171 kg/h and 5 % for the tests with $\dot{m}_{heat}$ = 342 kg/h when fifteen nodes are employed. The higher values of QI are obtained for the variable inlet option. The multi-node model with two nodes including plume entrainment yields values of QI that are between 4 % and 6 % lower than the values obtained for the multi-node model with two nodes and fixed inlets. The differences in QI between both models reduce to less than 1 % when the number of nodes is increased to fifteen.

For the relative error in the delivered energy, QD, the fully mixed tank model gives values between - 26 % and - 23 % for the heat source flow rate of 171 kg/h and values between -23 % and - 20 % for $\dot{m}_{heat}$ = 342 kg/h. As before, these results suggest that the fully mixed tank model is never appropriate to be used as a thermal storage tank model.

The plug flow model with fixed inlets overpredicts the delivered energy for all eight tests. The values of QD depend on the values of the heat source flow rate. For $\dot{m}_{heat}$ = 171 kg/h QD lies between + 9 % and + 19 %. For $\dot{m}_{heat}$ = 342 kg/h the values of QD are

lower than the values of QD for $\dot{m}_{heat}$ = 171 kg/h and range from + 6 % to + 9 %. The plug flow model with variable inlets predicts higher values for the delivered energy than the plug flow model with fixed inlets. For the lower heat source flow rate the values of QD range from + 23 % to + 26 % and for the higher heat source flow rate the values of QD are between + 16 % and + 20 %. The values of QD for the plug flow model with plume entrainment are close to those for the plug flow model with fixed inlets (less than 2 % difference for all eight tests). The same reasoning as already discussed in connection with QI applies.

The values of QD for the multi-node model with two nodes and fixed inlets are between - 7 % and - 4 % for $\dot{m}_{heat}$ = 171 kg/h and between - 7 % and - 2.5 % for $\dot{m}_{heat}$ = 342 kg/h. As the number of nodes increases, the values of QD increase and reach values between + 13 % and + 17 % for the lower heat source flow rate and values between + 6 % and + 12 % for the higher heat source flow rate when fifteen nodes are used. The numbers of nodes for which the values of the delivered energy represent the experimental data best are three if $\dot{m}_{heat}$ = 171 kg/h and two or four if $\dot{m}_{heat}$ = 342 kg/h. Thus, two to four nodes model the same amount of mixing as observed in the experiments. Based on QI it was found that the number of nodes for the multi-node model with fixed inlets which represent the experimental data best are two to five. The results obtained for QD for the multi-node model with variable inlets are close to those for the multi-node model with fixed inlets if the number of nodes is small (less than 0.9 % difference when two or three nodes are employed). The differences in QD between the multi-node model with fixed inlets and the multi-node model with variable inlets increase as the number of nodes increases but does not exceed 2.5 % for the tests with $\dot{m}_{heat}$ = 171 kg/h and 5 % for the tests with $\dot{m}_{heat}$ = 342 kg/h when fifteen nodes are used. The higher values of QD are obtained for the variable inlet option. The multi-node model with two nodes including plume entrainment yields values of QD that are between 4 % and 7 % lower than the values obtained for the multi-

node model with two nodes and fixed inlets. The differences in QD between both models reduce to less than 1 % when the number of nodes is increased to fifteen.

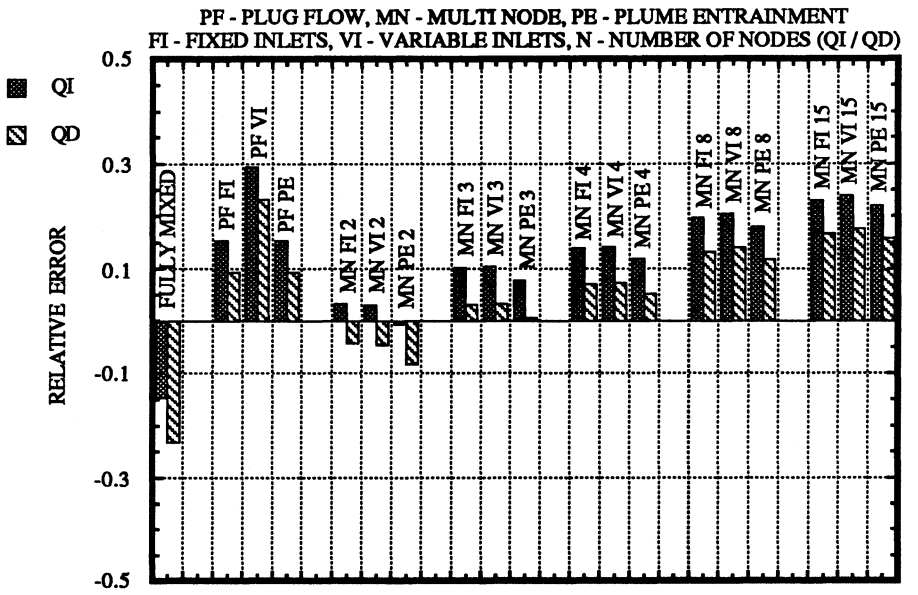

Fig. 5.8 Results for QI and QD for the High Flow Test #1

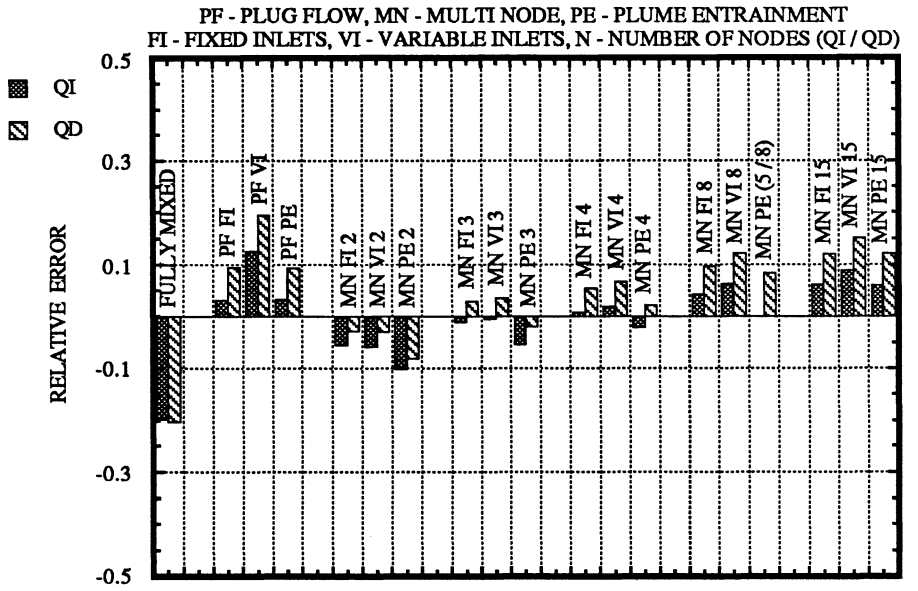

Fig. 5.9 Results for QI and QD for the High Flow Test #2

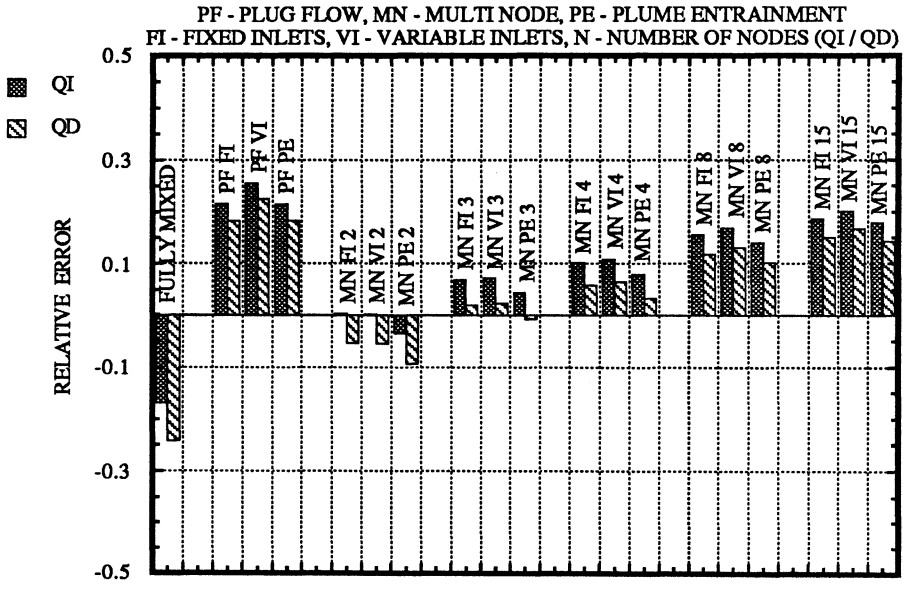

Fig. 5.10 Results for QI and QD for the High Flow Test #3

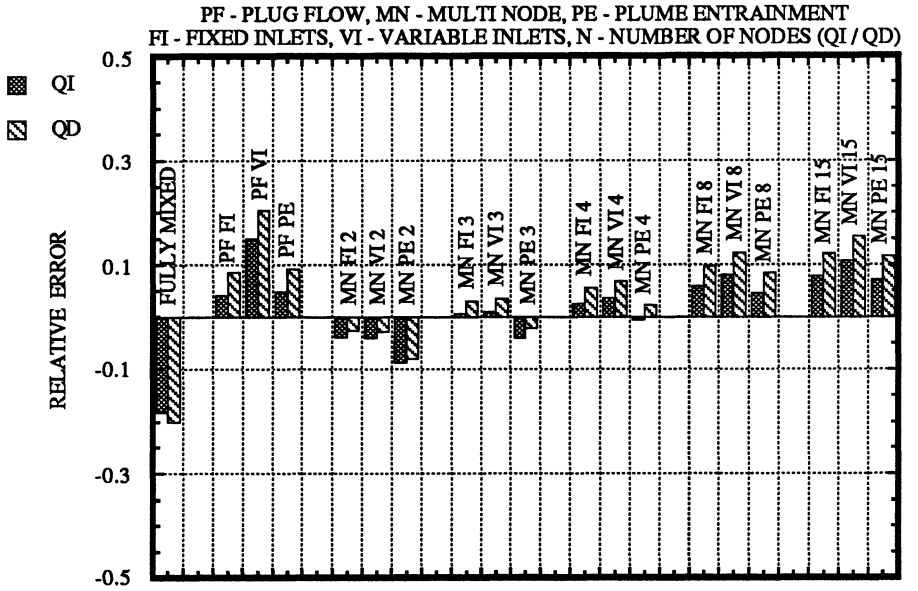

Fig. 5.11 Results for QI and QD for the High Flow Test #4

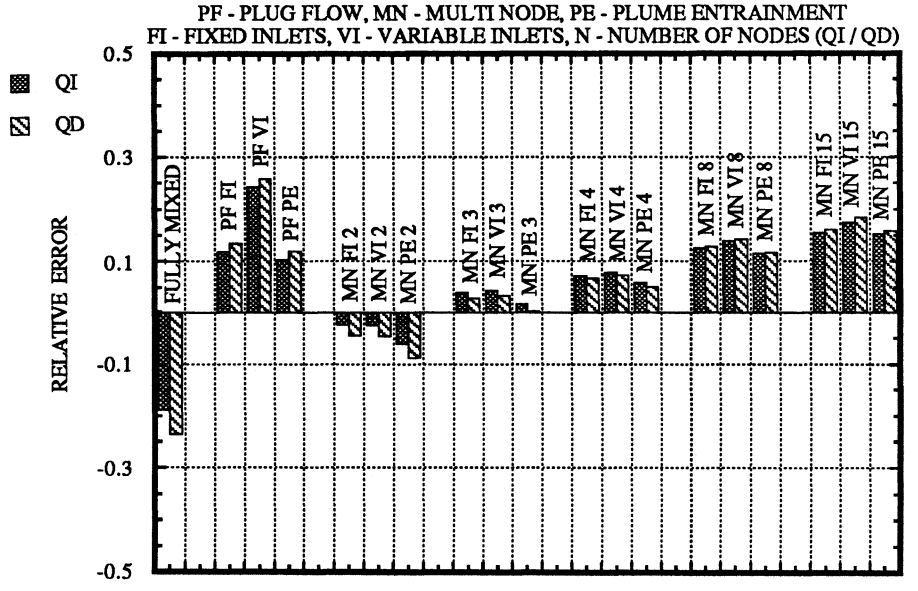

Fig. 5.12 Results for QI and QD for the High Flow Test #5

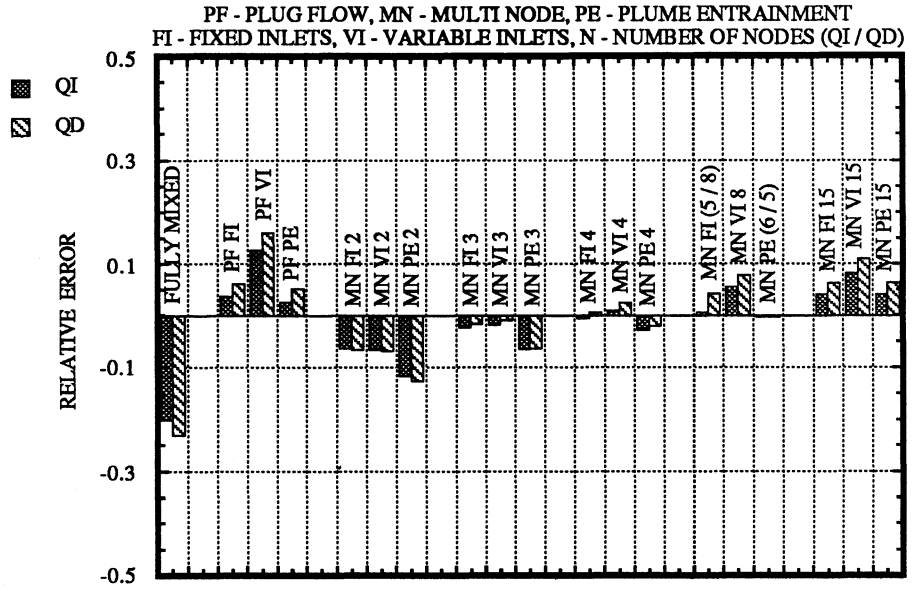

Fig. 5.13 Results for QI and QD for the High Flow Test #6

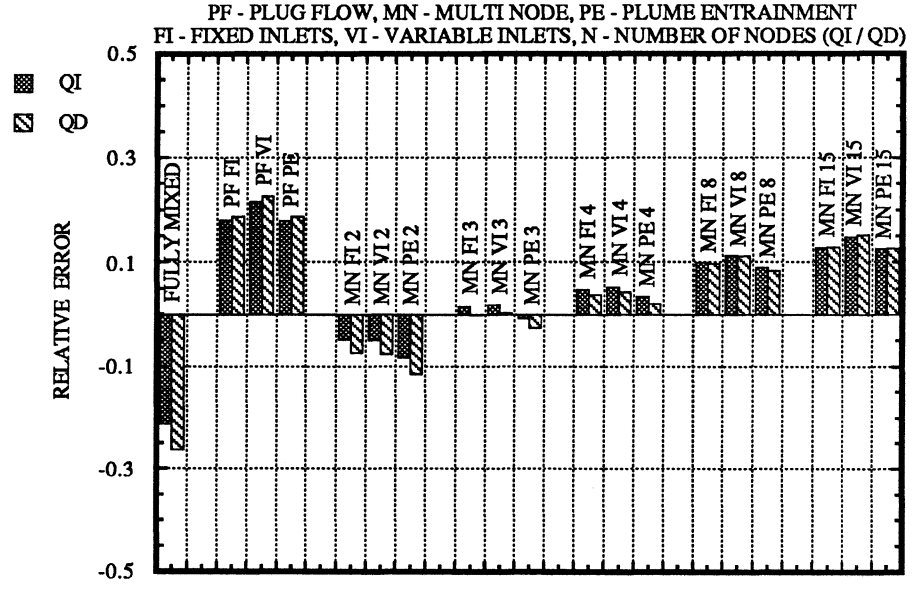

Fig. 5.14 Results for QI and QD for the High Flow Test #7

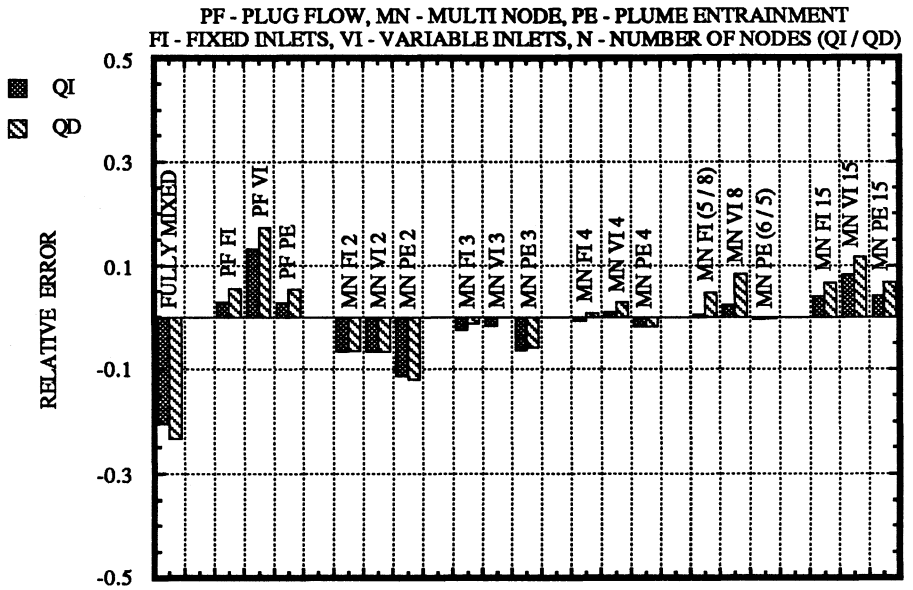

Fig. 5.15 Results for QI and QD for the High Flow Test #8

5.2 Heat Source Return Temperature

In this section the results for the ability of the different tank models to represent the heat source return temperature as measured in the experiments are discussed. The measure used to describe the performance of the different tank models is the dimensionless performance number P which is defined in Eqns (4.1.3) and (4.1.4) as the square root of the sum of the errors in the energy input squared divided by the total energy input. The reader is reminded that high values of P, indicating poor performance, can be caused by either high values of the heat source flow rate or large deviations of the simulated heat source return temperature from the measured heat source return temperature. As for the relative errors in the energy quantities, the results for the performance number P are plotted for the multi-node models

with two, three and four nodes. Then the best value of P for the corresponding number of nodes between five and fourteen is shown (or the value of P for the eight-node model if the best case is not obtained for the multi-node model with a number of nodes between five and fourteen). Finally the value of P is plotted for the fifteen-node model to show the results for the maximum number of nodes.

5.2.1 Comparisons for the Low Flow System

This section presents the results for the performance number P obtained with the experimental data measured at Queen's University, Kingston, Ontario.

The results for tests #1 to 4 will be analyzed first in order to see the effect on P when the heat source flow rate, $\dot{m}_{heat}$, is increased for a given load profile (cf. Table 3.1). Figs 5.16 to 5.19 show the values of P for the tests #1 to 4.

The values of P obtained for the fully mixed tank model are between 0.0298 and 0.0338. The fully mixed tank model gives the highest values of P (poorest performance) of all the models for all four tests.

The plug flow model with fixed inlets yields a value of 0.0126 for P if $\dot{m}_{heat}$ = 24 kg/h. The values of P increase to 0.0334 as the heat source flow rate is increased to 60 kg/h. The values of P for the plug flow model with variable inlets are between 4 % and 16 % lower than the corresponding values for the plug flow model with fixed inlets. The differences in P decrease as $\dot{m}_{heat}$ increases. The values of P obtained for the plug flow model with plume entrainment are between 6 % lower and 11 % higher than the values for the plug flow model with fixed inlets. An observation for all the plug flow models is that the performance improves (P decreases) as the heat source flow rate decreases.

The multi-node model with two nodes and fixed inlet positions yields values of P between 0.0189 and 0.0246 for tests #1 to 4. The values of P decrease for all four tests as

the number of nodes is increased. The numbers of nodes for which P reaches the lowest values depend on the heat source flow rate and and is fifteen if the heat source flow rate is 24 kg/h or 36 kg/h. For $\dot{m}_{heat}$ = 48 kg/h the number of nodes showing the best performance is thirteen and for $\dot{m}_{heat}$ = 60 kg/h eleven nodes give the lowest values of P. For the latter two tests, P increases again when the number of nodes is further increased. The best values of P for the multi-node model with fixed inlets are between 0.0063 and 0.0149. The multi-node model with two nodes and variable inlet positions predicts values of P that are between 5 % and 15 % lower than the values obtained with the two-node with fixed inlets. The difference in P between the two-node models with fixed and variable inlets increases as the heat source flow rate increases. The values of P for the multi-node model with variable inlet positions decrease for all four tests as the number of nodes is increased. The numbers of nodes for which P reaches its lowest values depend on the heat source flow rate. Fifteen nodes yield the best value of P for $\dot{m}_{heat}$ = 24 kg/h. For each further increase in the heat source flow rate by 12 kg/h the number of nodes giving the best value for P drops by three until six nodes are reached for $\dot{m}_{heat}$ = 60 kg/h. The best values of P for the multi-node model with variable inlet positions are between 0.0059 and 0.0139. The values of P for the multi-node model with plume entrainment are always higher (by up to 38 %) than the values of P for the multi-node model with fixed inlets. Thus, no improvement is achieved by adding plume entrainment to the multi-node model. An observation for all the multi-node models is that the numbers of nodes which result in the best values for P decrease as the heat source flow rate increases.

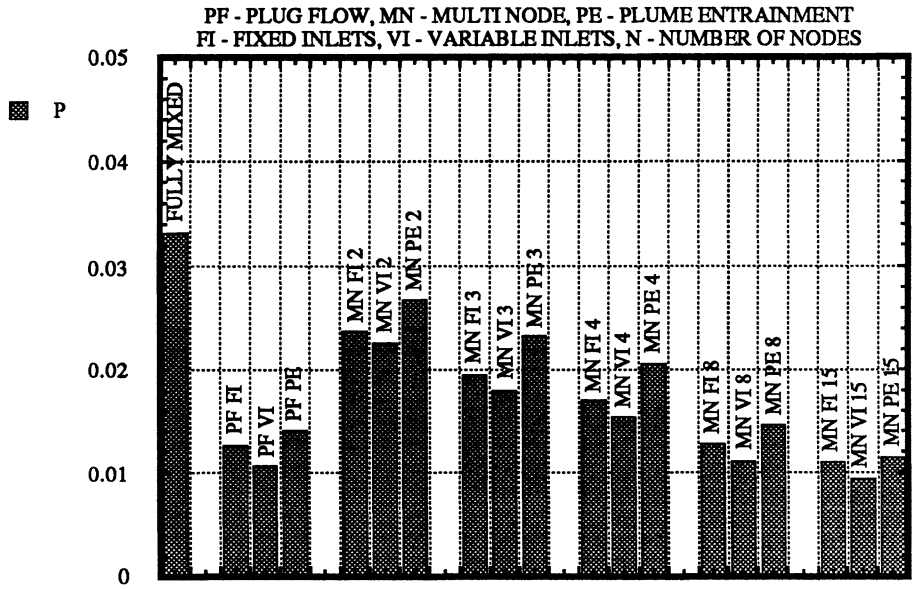

Fig. 5.16 Results for P for the Low Flow Test #1

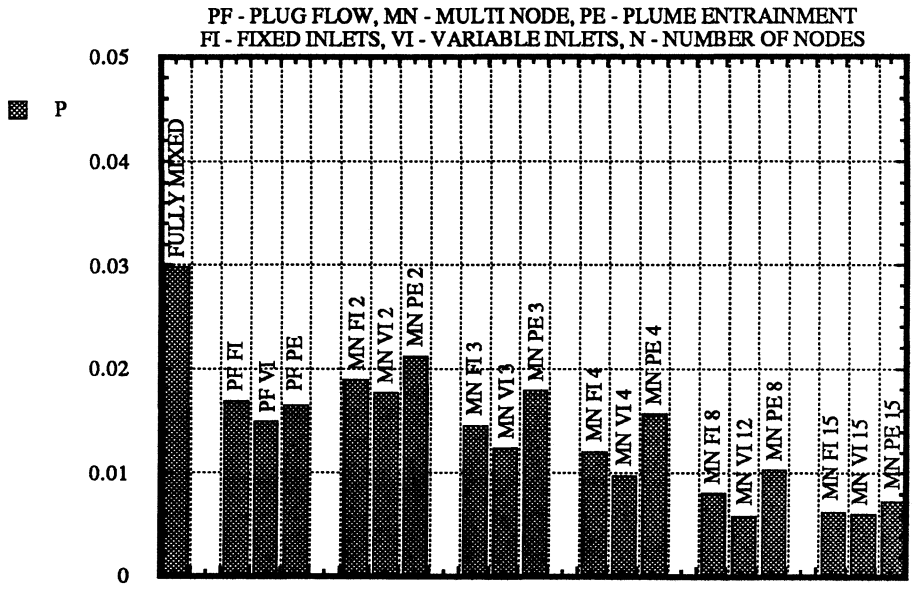

Fig. 5.17 Results for P for the Low Flow Test #2

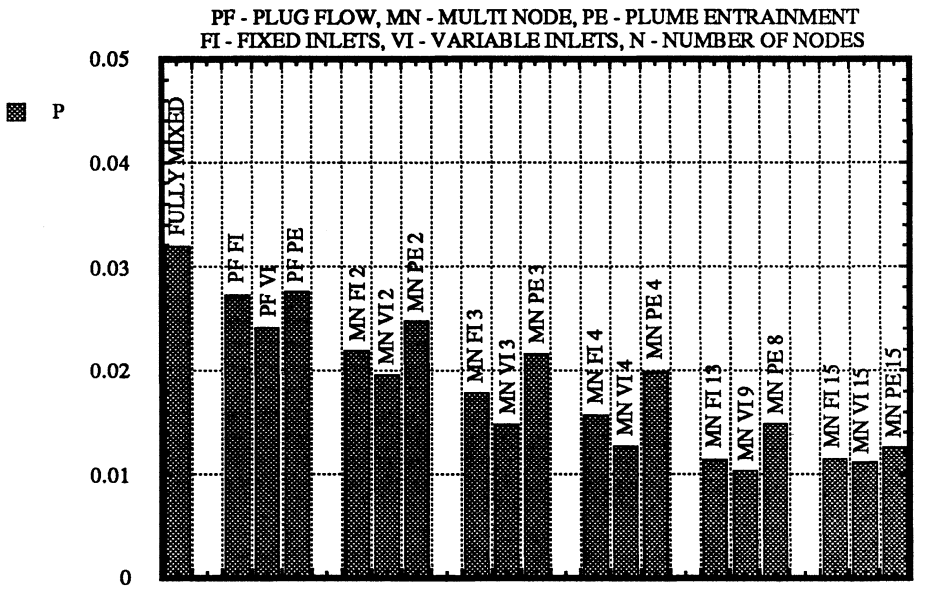

Fig. 5.18 Results for P for the Low Flow Test #3

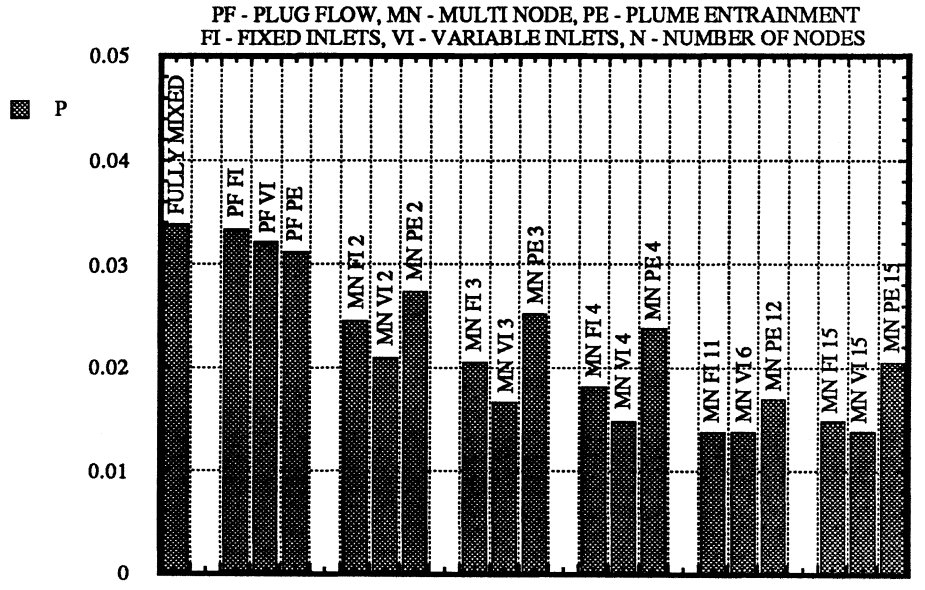

Fig. 5.19 Results for P for the Low Flow Test #4

The results for test #6 are discussed next in order to see how the increase in both the heat source flow rate and the load volume (but not the load characteristics (cf. Table 3.1)) affect the values of P for the different tank models. Fig. 5.20 shows the results of P for test #6.

The fully mixed tank model gives a value for P of 0.0347 which is less than 3 % higher than the value obtained with test #4.

The increase in the heat source flow rate and load volume results in a further increase in P for all the plug flow models compared to the values obtained for test #4. The increase in P for the plug flow model with fixed inlets is 25 % and for the plug flow model with variable inlets the increase is 15 %. The value of P is increased by 25 % for the plug flow model with plume entrainment. The values of P for the plug flow model exceed the value of P for the fully mixed tank model for test #6.

The values of P for test #6 for the multi-node models are higher than the values of P for the corresponding models in test #1 to 4. The increases in P lie between 2.5 % and 301 % (!) and depends on the particular tests and models that are compared. The range of change of P for the multi-node models in test #6 lies between 23 % and 27 % (with respect to the lowest value of P) when the number of nodes is changed. The range of change of P for the multi-node models in tests #1 to 4 as the number of nodes is varied is higher and is found between 51 % and 199 %. The numbers of nodes for which P reaches the best values for test #6 are lower than those obtained for tests #1 to 4. For the multi-node model with fixed inlets six nodes give the best values of P and the multi-node model with variable inlets yields the best value of P when five nodes are used. The number of nodes for which P reaches its lowest value is seven for the multi-node model with plume entrainment. The best value of P for test #6 and the multi-node model with fixed inlets is 48 % higher than the best value of P for test #4 and the multi-node model with fixed inlets. For the multi-node model with variable inlets the best value of P is increased by 41 % for test #4 if it is compared with test #6.

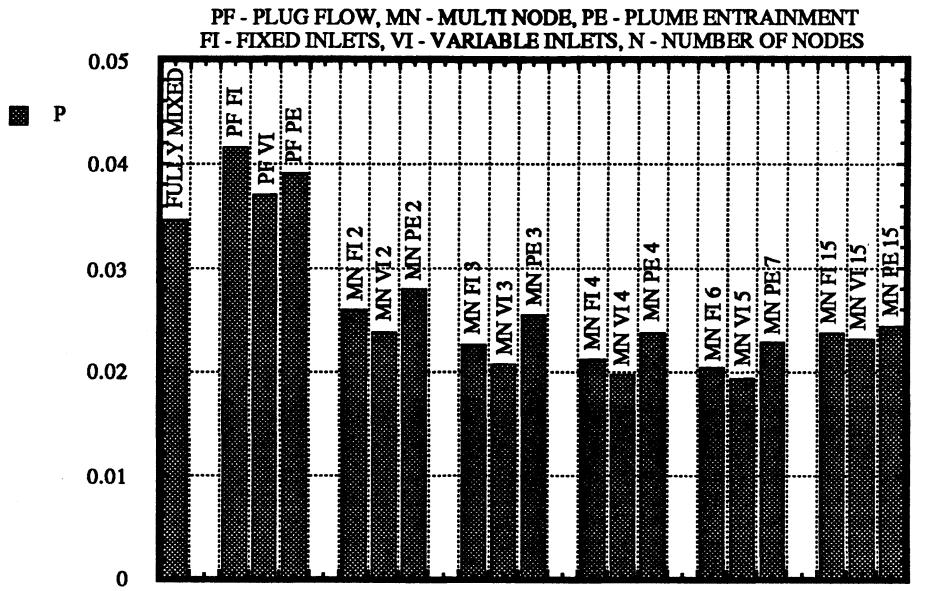

Fig. 5.20 Results for P for the Low Flow Test #6

Fig. 5.21 shows the results for the test #5 in which the load draw is done at the end of the day.

The fully mixed tank model gives a value for P of 0.0309. This value lies within the range of the values of P obtained for the fully mixed tank model in tests #1 to 4 and test #6.

The values of P for test #5 for the plug flow models are higher than the values of P for the fully mixed tank model. The highest value of P is obtained for the plug flow model with fixed inlets and is 0.0403. The values of P for the plug flow models with variable inlets or with plume entrainment are 5 % or 7 % lower than the value of P for the plug flow model with fixed inlets, respectively.

The multi-node model with two nodes and fixed inlets yields a value for P of 0.0209. The values of P obtained for the two-node models with variable inlets or with plume entrainment are within 2.5 % of the value of P for the two-node model with fixed inlets.

The values of P decrease for all the multi-node models as the number of nodes is increased. Fifteen nodes give the best values of P for all the multi-node models. The values of P for the fifteen-node models are between 0.0055 and 0.0059. Thus for test #5 the multi-node models show considerably better performance than either the fully mixed tank model or the plug flow models.

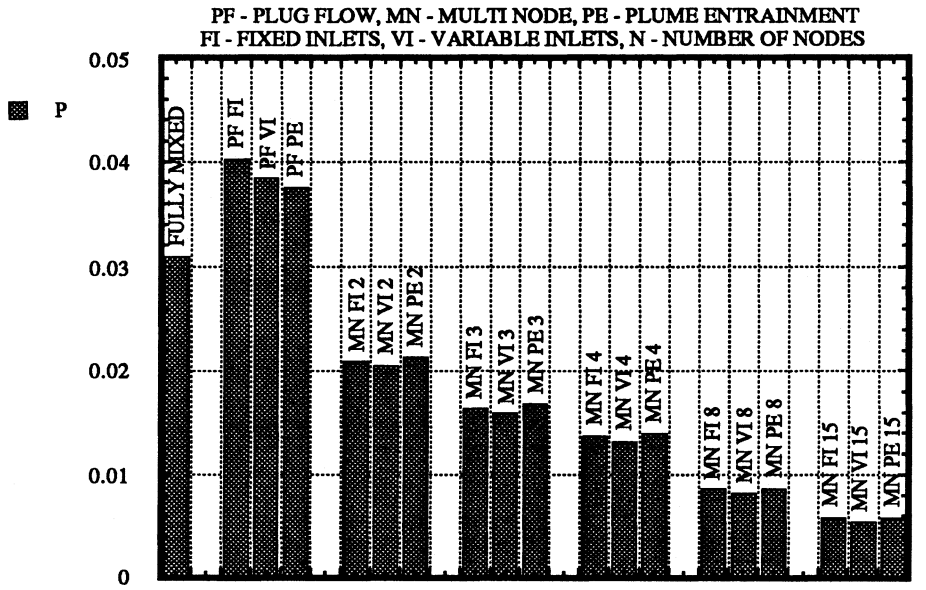

Fig. 5.21 Results for P for the Low Flow Test #5

5.2.2 Comparisons for the High Flow System

This section presents the results for the performance number P obtained with the experimental data as measured by Colorado State University. The values of P for the different tank models are plotted in Figs 5.22 to 5.29 for all eight tests.

The tests can be divided into two groups characterized by the two different values of the heat source flow rate, as also done for the discussion of the results for the energy predictions. Tests with odd test numbers correspond to a heat source flow rate, $\dot{m}_{heat}$, of 171 kg/h and tests with even test numbers correspond to $\dot{m}_{heat}$ = 342 kg/h. The values of P for the two groups characterized by the values of $\dot{m}_{heat}$ differ roughly by a factor of two. The tests having the higher heat source flow rate (342 kg/h) give the higher values of P and the tests with the lower heat source flow rate (171 kg/h) result in the lower values of P. This observation suggests that the difference in P results from the value of the heat source flow rate rather than from the deviations of the simulated heat source return temperature from the measured heat source return temperature (cf. Eqn (4.13)). Within each of the two groups characterized by different values of $\dot{m}_{heat}$ it can also be observed that the values of P for the tests with the small collector area (low energy input; tests #1 , 2, 5 and 6) are higher than the values of P for the tests with the large collector area (high energy input; tests #3, 4, 7 and 8). However the differences due to the different amounts of energy input are less marked than the differences due to the different heat source flow rates. The results for tests #1 to 8 will be discussed together and the differences resulting from different values of the heat source flow rate or the collector area, A_c, will be pointed out as necessary.

The values of P for the fully mixed tank model are between 0.0372 and 0.0598. The fully mixed tank model shows the least dependence for the range of the values of P on the heat source flow rate and the collector area.

The values of P for the plug flow model with fixed inlets and for the tests with the lower heat source flow rate and the small collector area (2.78 m^2) are 17 to 26 % higher than the values of P for the fully mixed tank model. The plug flow model with fixed inlets results in values of P that are between 7 % and 11 % lower than the values of P for the fully mixed tank model when $\dot{m}_{heat}$ = 171 kg/h and the collector area is large (5.56 m^2). For the higher heat source flow rate the plug flow model with fixed inlet positions predicts predicts values of P that are 33 % to 51 % higher than the values of P obtained for the fully

mixed tank model. The values of P for the plug flow model with variable inlets are less than 3 % higher than the values of P for the plug flow model with fixed inlets for the lower heat source flow rate and the large collector area. For all other tests the values of P for the plug flow model with variable inlets are lower than the values of P for the plug flow model with fixed inlets but no more than 13 %. The plug flow model with plume entrainment yields values of P that are between 0 % and 9 % lower than the values of P for the plug flow model with fixed inlets if $\dot{m}_{heat}$ = 171 kg/h. For $\dot{m}_{heat}$ = 342 kg/h the plug flow model with plume entrainment gives values of P that are between 14 % and 17 % lower than the values of P for the plug flow model with fixed inlets.

The multi-node model with two nodes and fixed inlets results in values of P between 0.0206 and 0.0241 for the lower heat source flow rate. The values of P for the higher heat source flow rate and the large collector area are 0.0442 and 0.0444 and for the higher heat source flow rate and the small collector area values of 0.0316 and 0.0290 are obtained. The values of P for the two-node model with variable inlets are within 6 % of the values of P for the two-node model with fixed inlets. The two-node model with plume entrainment results in values of P that are between 14 % and 34 % higher than the values of P for the two-node model with fixed inlets for all eight tests. As the number of nodes for all multi-node models is increased, the values of P change and after reaching a lowest value for a certain number of nodes the performance numbers P increase again when the number of nodes is further increased. The number of nodes which gives the best value of P for the multi-node model with fixed or variable inlet positions is four for $\dot{m}_{heat}$ = 171 kg/h and A_c = 5.76 m^2. For all other tests two or three nodes give the best results for the multi-node models with fixed or variable inlets. For the multi-node model with plume entrainment the numbers of nodes which yield the lowest values for P are four or five. The lowest values of P for the multi-node model with variable inlets are between 0 % and 13 % lower than the best values for the multi-node model with fixed inlet positions. The best values of P for the

multi-node model with plume entrainment are 0 % to 6 % higher than the lowest values of P for the multi-node model with fixed inlets.

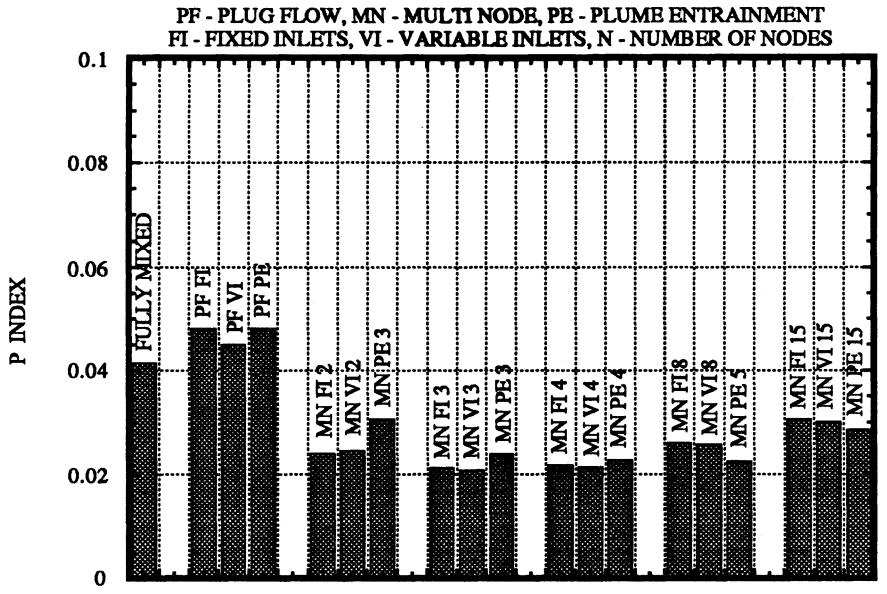

Fig. 5.22 Results for P for the High Flow Test #1

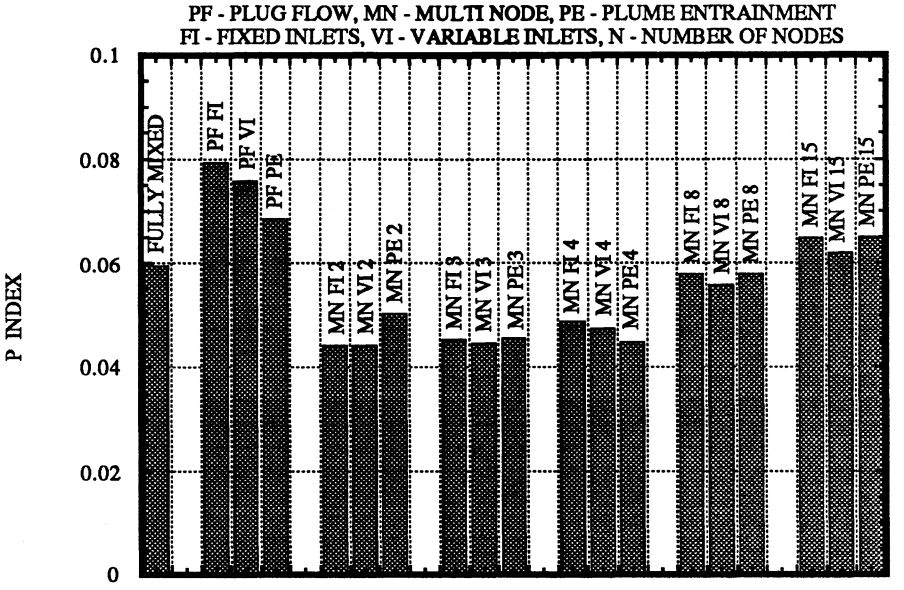

Fig. 5.23 Results for P for the High Flow Test #2

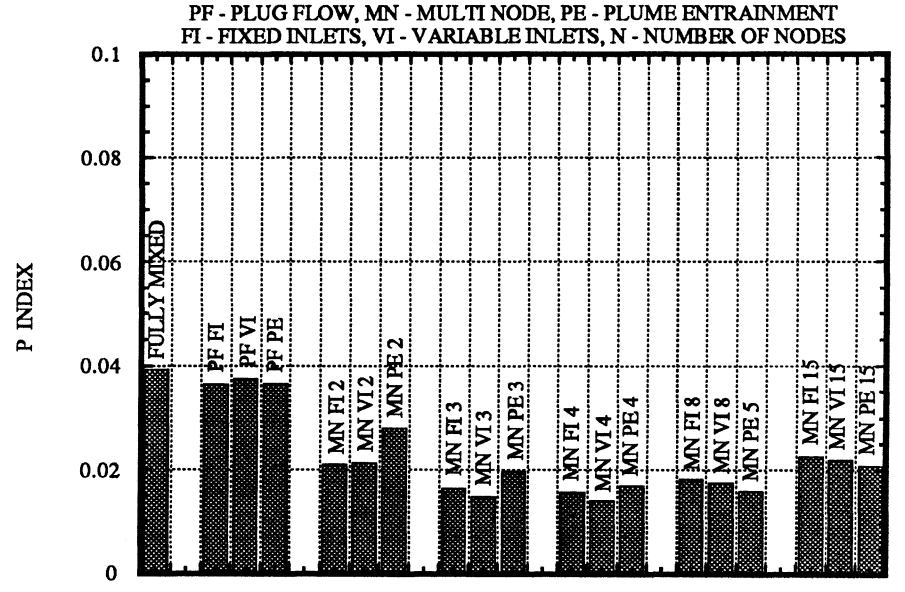

Fig. 5.24 Results for P for the High Flow Test #3

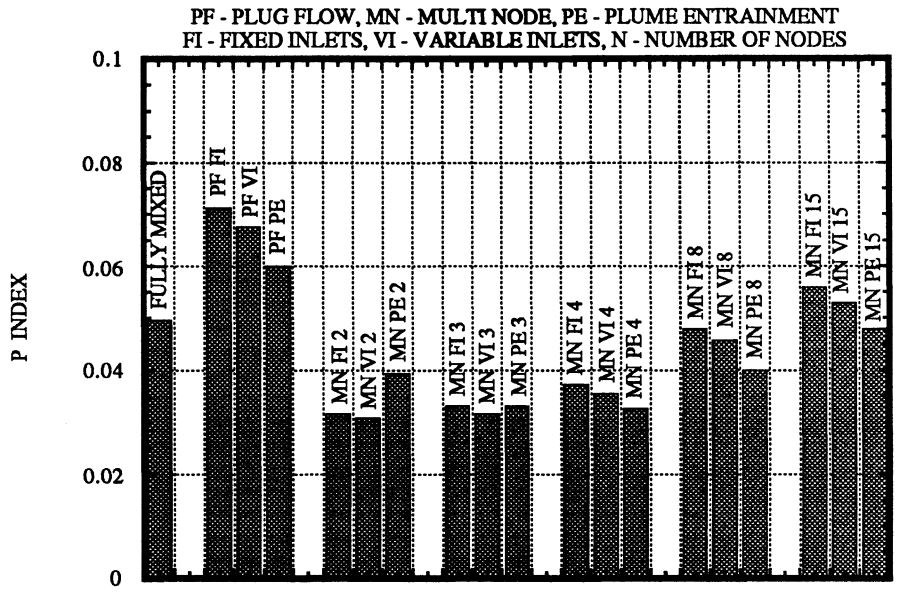

Fig. 5.25 Results for P for the High Flow Test #4

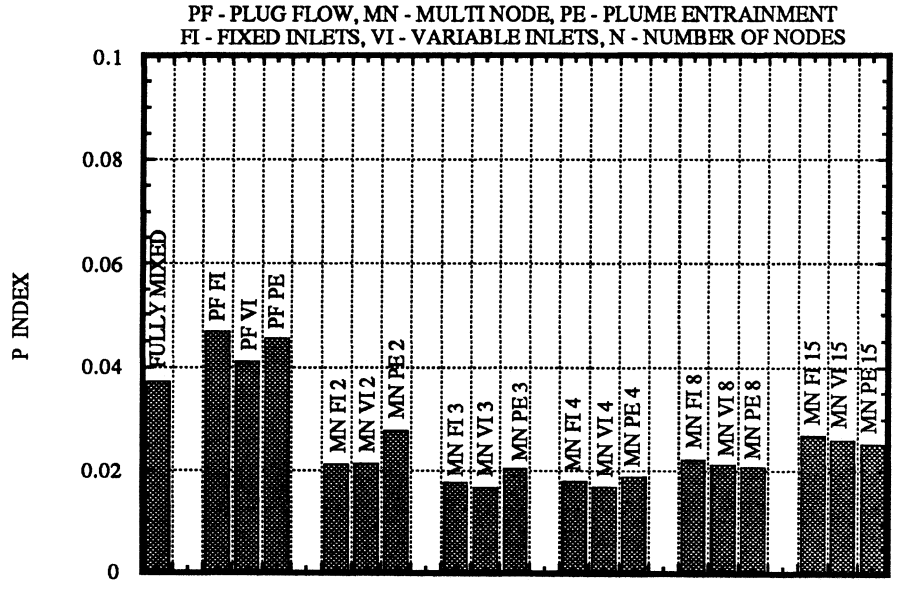

Fig. 5.26 Results for P for the High Flow Test #5

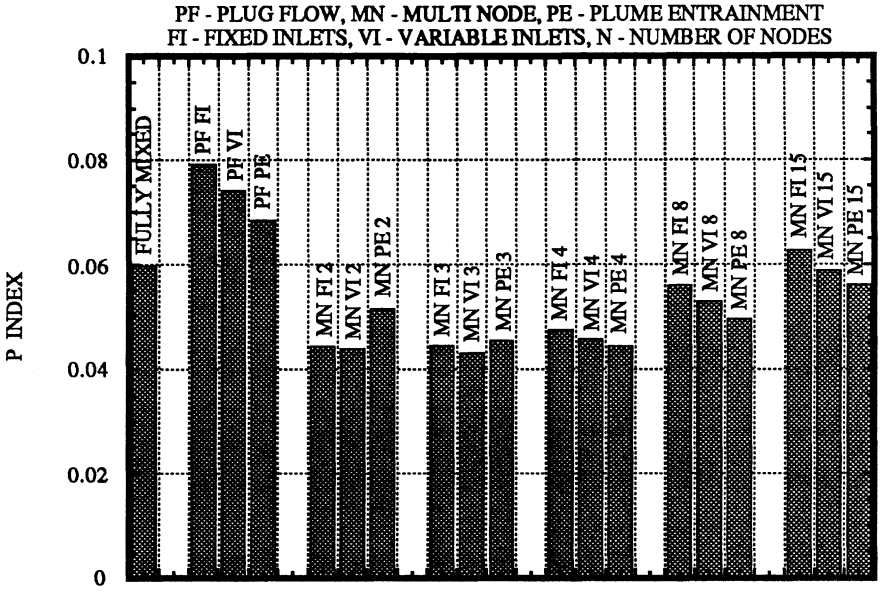

Fig. 5.27 Results for P for The High Flow Test #6

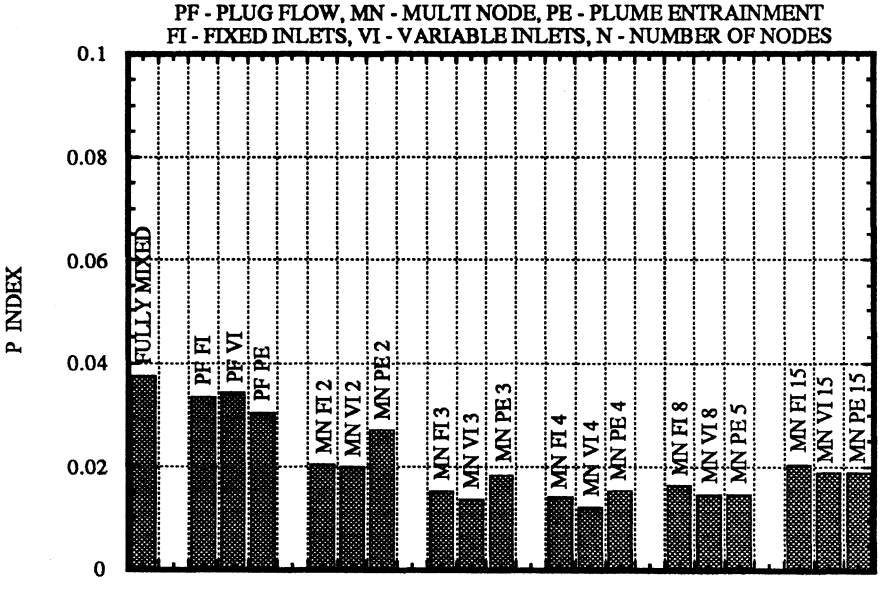

Fig. 5.28 Results for P for the High Flow Test #7

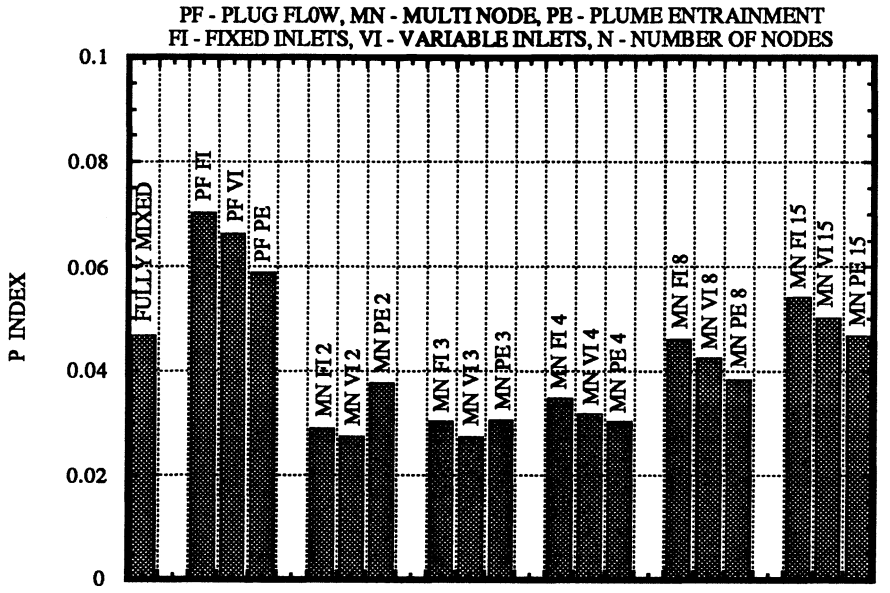

Fig. 5.29 Results for P for the High Flow Test #8

5.3 Choice of Number of Nodes

In the previous sections it has been seen that the performance of the multi-node models, as described by the relative errors in the energy input and the delivered energy, QI and QD, respectively, or the dimensionless performance number P, depends on the number of nodes chosen. In this section the attempt is made to find a relationship between the number of nodes to be used and the conditions under which the tank operates. The quantities that were varied significantly during the experiments or simulations are the values of the heat source flow rate, the load draw profiles (only for the low flow system), the collector area and the collector flow rate (the latter two quantities only for the high flow system). The variation of the collector area and the collector flow rate have been seen to have little influence on the results obtained for a multi-node model with a particular number of nodes. The parameters of the tanks (geometry, inlet positions and UA-value) are fixed and the ambient temperature was nearly constant during the tests. To relate the number of nodes to be used with the heat source flow and load flow a mean number of tank turnovers, T, has been defined as

$$T = \frac{M_{heat} + M_{load}}{M_T} \tag{5.1}$$

M_{heat} represents the total daily mass of the fluid coming from the heat source and is defined as

$$M_{heat} = \int_{day} \dot{m}_{heat}\, dt \tag{5.2}$$

Similarly, M_{load} stands for the total daily mass of the fluid removed to the load and is therefore

$$M_{load} = \int_{day} \dot{m}_{load}\, dt \tag{5.3}$$

M_T represents the mass of the fluid in the tank. Table 5.1 relates the values of T with the test numbers of the low flow tests and the high flow tests.

Low Flow System		High Flow System	
T	Test #	T	Test #
2.456	1	6.636	7
3.011	2	6.71	5
3.617	3	7.955	3
4.244	4	7.987	1
2.683	5	11.581	8
6.083	6	11.915	6
		14.094	2
		14.143	4

Table 5.1 Mean Number of Tank Turnovers for the Low Flow Tests and the High Flow Tests

The numbers of nodes which give the best values of QD, QI and P for each test are plotted in Figs 5.30 and 5.31 for all low flow and high flow tests as a function of T for the multi-node model with fixed inlet positions and the multi-node model with variable inlet positions, respectively. The multi-node model with plume entrainment was omitted from a similar analysis because it generally requires a larger number of nodes to represent the experimental data. Also the multi-node model with plume entrainment can become computationally expensive under certain conditions (cf. section 5.4). Considering Figs 5.30 and 5.31 several observations can be made.

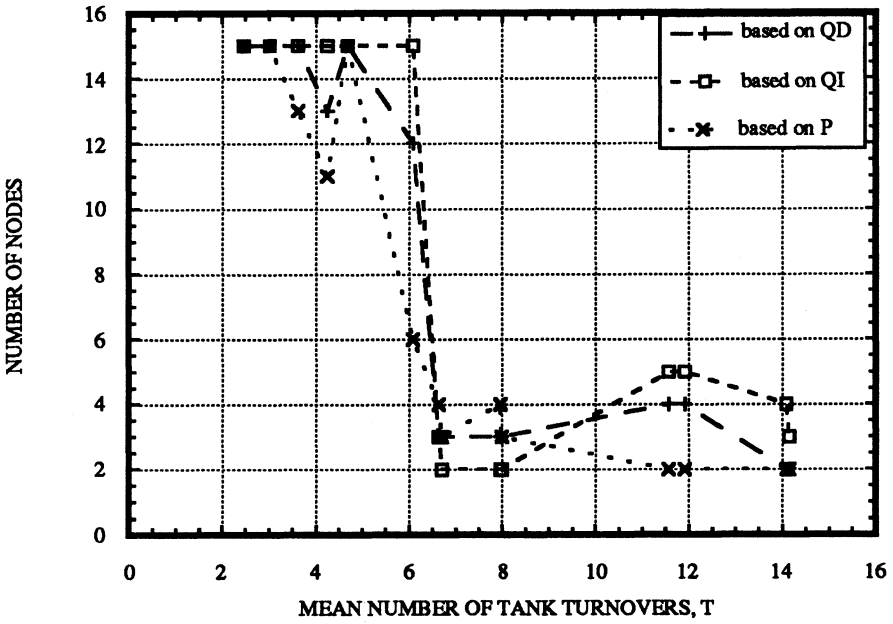

Fig. 5.30 Best Numbers of Nodes for the Multi-Node Model with Fixed Inlets

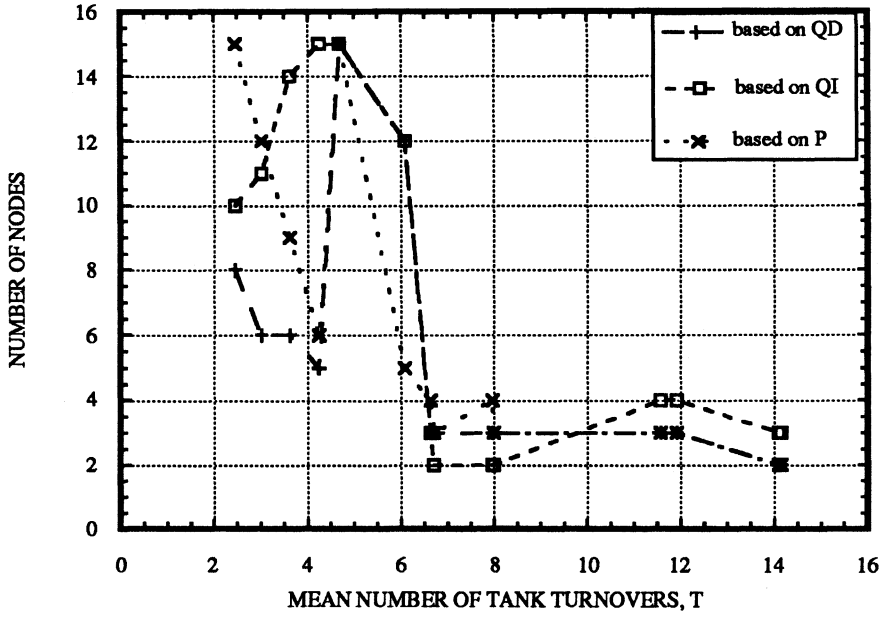

Fig. 5.31 Best Numbers of Nodes for the Multi-Node Model with Variable Inlets

The three different numbers used to describe the performance of the multi-node models do not give the same results for the best number of nodes for a particular test.

The model predictions (energy input, delivered energy and heat source return temperature) for the multi-node models with small (≤ 4) numbers of nodes differ more from each other than the results for the multi-node models with large (≥ 8) numbers of nodes (e.g. if the number of nodes is changed from two to three then this results in about 8 % difference in the energy quantities compared to about 1 % difference in the energy quantities if the number of nodes is changed from ten to twelve). This behavior influences the change in the values of the numbers used to describe the performance of the tank models as a function of the number of nodes and therefore results in a higher sensitivity of the best number of nodes to experimental errors if the best number of nodes is large.

If the best number of nodes is determined to be fifteen then this indicates that the results were continually improving as the number of nodes was increased. The values of the performance numbers might still have improved if the number of nodes could have been further increased (the maximum number of nodes in the current implementation is fifteen). From this point of view fifteen nodes is an "artificially" introduced maximum number of nodes.

Two different physical systems are plotted on one graph. The values of T for the low flow system range from 2.5 to 6.1. The values of T for the high flow system are between 6.6 and 14.1. A significant change in the best number of can be observed at the transition from the low flow system to the high flow system. The question what would happen if the values of T for the low flow system were further increased or if the values of T for the high flow system were further decreased remains unanswered.

A different approach has been taken to find a practical relationship between the mean number of tank turnovers and the number of nodes to be used. In Figs 5.32 and 5.33 the smallest numbers of nodes possible, for which the relative errors in the energy quantities do not exceed 5 % and the performance number P is less than 1.1 times the best value of P

(for a particular test), P_{best}, are plotted for the multi-node model with fixed inlets and the multi-node model with variable inlets, respectively. Since the multi-node models predict larger energy quantities as the number of nodes is increased, the 5 % tolerance for QI and QD means that not more than 5 % underprediction of the energy quantities is allowed. Introducing the above criteria for the choice of the appropriate number of nodes is motivated by two ideas. It was possible, in eleven out of seventeen cases, to get rid of the "artificial" limit of fifteen nodes which will help to find a more reasonable curve fit (number of nodes versus mean number of tank turnovers). The computational efficiency depends strongly on the number of nodes chosen (will be discussed in section 5.4). A large number of nodes requires more CPU-time. By using the tolerances defined above to find the appropriate number of nodes, rather than choosing the number of nodes which give the best results for QD, QI and P, the number of nodes could be reduced significantly (by up to eight nodes).

Power function curves optimized by the method of least squares were fitted to the numbers of nodes plotted in Figs 5.32 and 5.33 versus the mean number of tank turnovers. It can be observed that the multi-node model with fixed inlets results in higher values for the appropriate number of nodes than the multi-node model with variable inlets. The fitted curves based on QD, QI and P are close (propose the same number of nodes to be used) if the mean number of tank turnovers is less than five. Greater differences in the number of nodes to be used for a particular mean number of tank turnovers arise if T is further decreased, but the reader is reminded that the results obtained with the multi-node models with large numbers of nodes are close if the number of nodes is changed by one or two.

An investigation of the errors in predicting the energy quantities introduced when using the number of nodes as proposed by the fitted curves (an average number of nodes was taken for T less than five) has been performed. For the multi-node model with fixed inlets QI is greater than - 10 % and less than + 10 % and QD lies between - 12 % and + 7 % if the number of nodes is chosen according to the fitted curves in Fig. 5.32. For the multi-node

model with variable inlets the error in the energy input into the tank lies between - 12 % and + 10 % and the error in the delivered energy is found between - 13 % and + 7 % if the number of nodes proposed by the fitted curves of Fig. 5.33 is used.

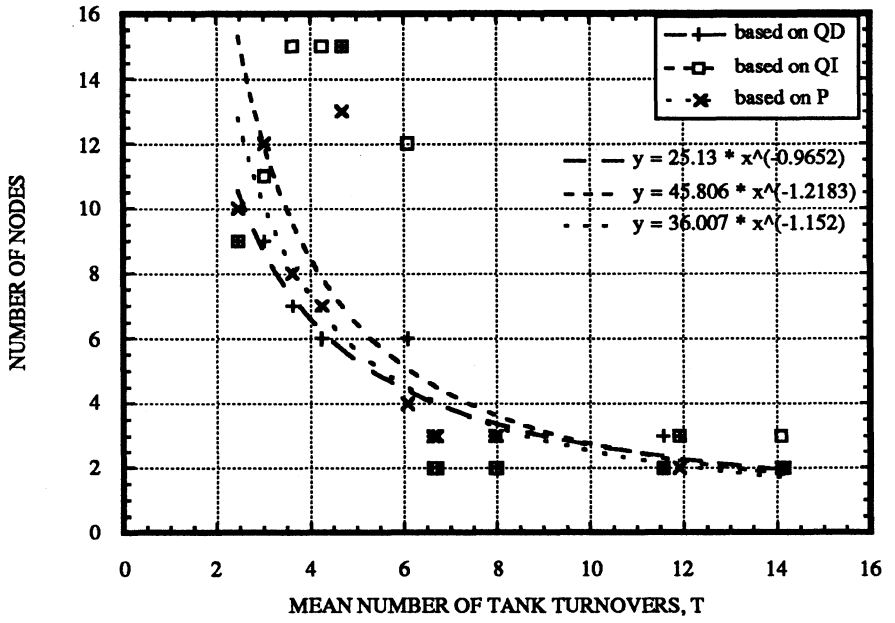

Fig. 5.32 Numbers of Nodes for the Multi-Node Model with Fixed Inlets based on less than 5 % Error in the Energy Quantities and $P < 1.1\ P_{best}$

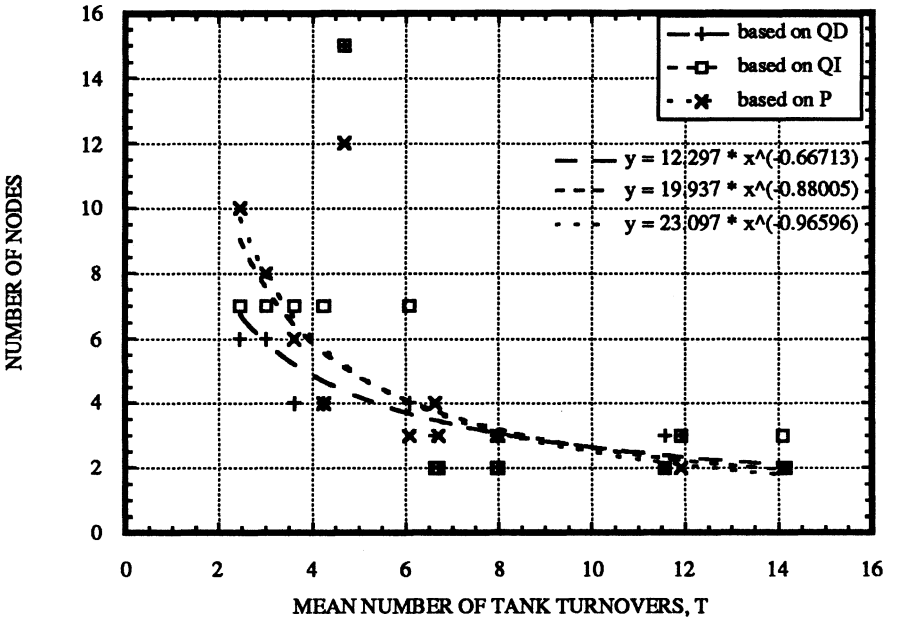

Fig. 5.33 Numbers of Nodes for the Multi-Node Model with Variable Inlets based on less than 5 % Error in the Energy Quantities and $P < 1.1\ P_{best}$

5.4 Computational Efficiency

The selected models were also compared with respect to their computational efficiency. Therefore a simple TRNSYS deck with three type 14 forcing functions, one type 24 integrator, one type 25 printer and the tank model under investigation was set up. Two hundred similar days for various heat source flow rates and time steps were simulated. The heat source flow rate was operating eight hours per day. The temperature of the fluid from the heat source was specified as hourly step profile with first rising and then falling temperatures in order to force the variable inlet option and plume entrainment to be employed. An hourly load profile was specified with four equal draws equally distributed

during the time of the heat source flow. The load flow rate was chosen to be half of the heat source flow rate. The tank parameters were the same as those specified in Tables 4.1 and 4.2 for the tank of the low flow system. The simulations were performed on a VAXstation 3100 Model 38. Table 5.2 shows the CPU-seconds for the different tank models which was obtained by subtracting the CPU-time for simulating the deck without tank model from the CPU-time for simulating the deck including the tank model. Several observations can be made.

Tank Model[1)]	Heat Source Flow Rate			
	25 kg/h		200 kg/h	
	Simulation Time Step		Simulation Time Step	
	1 h	0.1 h	1 h	0.1h
PF FI	3.01 s	40.72 s	2.21 s	25.81 s
PF VI	5.05 s	71.5 s	2.32 s	26.53 s
PF PE	2.95 s	42.06 s	3.48 s	28.48 s
FULLY MIXED	3.7 s	37.77 s	3.56 s	38.83 s
MN FI 3	6.37 s	64.53 s	6.35 s	63.77 s
MN VI 3	6.45 s	64.18 s	6.05 s	66.63 s
MN PE 3	7.05 s	71.48 s	14.09 s	71.03 s
MN FI 15	17.2 s	177.27 s	17.5 s	181.23 s
MN VI 15	19.16 s	179.97 s	18.15 s	180.07 s
MN PE 15	21.47 s	174.74 s	51.57 s	191.81 s

Table 5.2 CPU-Seconds for the different Tank Models on a VAXstation 3100 Model 38

The plug flow models are faster for the higher heat source flow rate (200 kg/h) than for the lower heat source flow rate (25 kg/h) since the number of segments employed when the heat source flow rate is high is smaller than the number of segments used when the heat

1) PF - Plug Flow Model, MN - Multi Node Model, PE - Plume Entrainment Model, FI - Fixed Inlets, VI - Variable Inlets, N - Number of Nodes

source flow rate is low. The CPU-times for the multi-node models depend strongly on the number of nodes specified (increase of the CPU-time by a factor of five if the number of nodes is increased from one to fifteen for the multi-node model with fixed inlets), but not on the value of the heat source flow rate. The plug flow models are faster than the multi-node models. Comparable values of CPU-time for the plug flow models and the fully mixed tank model (multi-node model with one node) are obtained for the lower heat source flow rate. For the lower heat source flow rate the plug flow model with variable inlets uses significantly more CPU-time than the other plug flow models (increase by a factor of 1.7) due to a large number of segments involved in the algorithms for finding the heat source flow inlet position. Including plume entrainment significantly increases the CPU-time (two to three times) for the large simulation time step and the high heat source flow rate (cf. Eqn (2.3.36)) for the multi-node models. The small increase in CPU-time for the plug flow model including plume entrainment for a high heat source flow rate and a large simulation time step is due to the fact that the number of segments employed is very low (mostly one).

Chapter 6

Recommendations

Several one-dimensional models for stratified thermal storage tanks (all available in TRNSYS) have been investigated and compared to experimental data for a wide range of conditions. The goal of this project was to give some recommendations as to which tank model should be used under which conditions. Experimental errors outside the specified accuracy of the measurements or the absence of error estimates introduce some uncertainties in the conclusions.

It has been seen that the assumption of a uniform tank temperature (instantaneous mixing) leads to a considerable underprediction of the energy input into the tank and the delivered energy under all conditions considered. Thus, the fully mixed tank model is never appropriate to be used as a thermal storage tank model when stratification affects are important for the overall system performance.

Relationships between the number of nodes to be used for the multi-node models with fixed and variable inlet positions and the mean number of tank turnovers have been developed. These relationships are useful as a guideline for choosing the most appropriate number of nodes for given operating conditions. It is recommended to use the multi-node model with variable inlets since this model results in less nodes to be used than the multi-node model with fixed inlets and is therefore computationally more efficient. The use of the multi-node model with plume entrainment is not recommended because it has been shown that including plume entrainment does not improve the model predictions and results in less computational efficiency.

The plug flow models have been seen to be computationally more efficient than the multi-node models. Since the plug flow models with fixed and variable inlets tend to overpredict the energy quantities it is recommended to use the plug flow model including plume entrainment as an alternative for the multi-node with variable inlets for a mean number of tank turnovers less than five. The reader is reminded that the results obtained with the plug flow models depend on the simulation time step chosen as discussed in section 2.4.4, which introduces some uncertainty.

Future work could provide insight in how the use of inlet diffusers in the experiments influences the recommendations obtained with data which were obtained without the use of specific inlet manifolds.

Since drawing the load at the end of the day gave results which did not quite fit into the pattern observed for the tests where the load draws were done (mainly) throughout the day it is of interest if this observation can be confirmed. Therefore performing more experiments in which the load draw is done at the end of the day and applying the performance study for the different tank models as described in chapter 4 is recommended.

Appendix A

Derivation of the Energy Equations for the Stream and the Tank

in Δt:

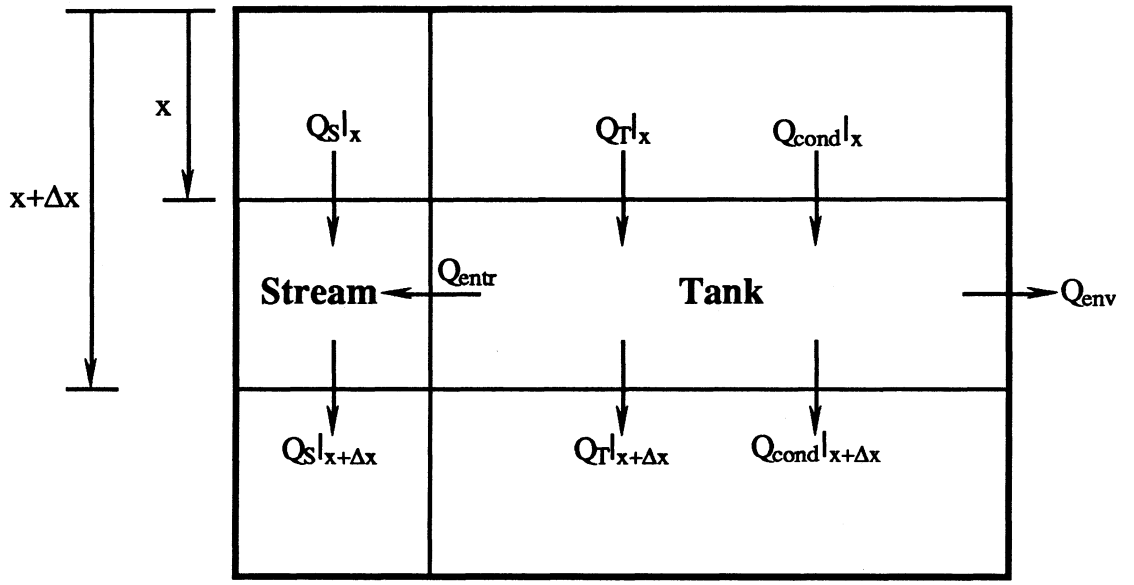

Stream Energy Balance:

$$0 = - Q_S |_{x+\Delta x} + Q_S |_x + Q_{entr}$$

Tank Energy Balance:

$$\Delta U = - Q_T |_{x+\Delta x} + Q_T |_x - Q_{entr} - Q_{cond} |_{x+\Delta x} + Q_{cond} |_x - Q_{env}$$

with

$$\Delta U = \rho_f A \Delta x (Tl_{t+\Delta t} - Tl_t)$$

$$Qs\,|_{x+\Delta x} = (\dot{m}_S T_S)\,|_{x+\Delta x}\, C_f \Delta t$$

$$Qs\,|_x = (\dot{m}_S T_S)\,|_x\, C_f \Delta t$$

$$Q_{entr} = (\dot{m}_S\,|_{x+\Delta x} - \dot{m}_S\,|_x)\, \overline{T}_T\,|_x^{x+\Delta x}\, C_f \Delta t = -(\dot{m}_T\,|_{x+\Delta x} - \dot{m}_T\,|_x)\, \overline{T}_T\,|_x^{x+\Delta x}\, C_f \Delta t$$

$$Q_T\,|_{x+\Delta x} = (\dot{m}_T T_T)\,|_{x+\Delta x}\, C_f \Delta t$$

$$Q_T\,|_x = (\dot{m}_T T_T)\,|_x\, C_f \Delta t$$

$$Q_{cond}\,|_{x+\Delta x} = k_f A \frac{T_T\,|_{x+\frac{\Delta x}{2}} - T_T\,|_{x+\frac{3\Delta x}{2}}}{\Delta x} \Delta t$$

$$Q_{cond}\,|_x = k_f A \frac{T_T\,|_{x-\frac{\Delta x}{2}} - T_T\,|_{x+\frac{\Delta x}{2}}}{\Delta x} \Delta t$$

$$Q_{env} = U_L P_L \Delta x (\overline{T}_T\,|_x^{x+\Delta x} - T_{env}) \Delta t$$

Substituting the above terms in the energy balances for the stream and the tank, dividing both equations by Δt and Δx and then allowing $\Delta t \rightarrow 0$ and $\Delta x \rightarrow 0$ leads to Eqns (2.3.1) and (2.3.2)

Appendix B

Determination of the UA-value by a cool-down test

The UA-value for a hot liquid storage tank is determined by measuring the rate of tank temperature decay over time for an initially heated up tank. The tank is assumed to be at uniform temperature during the entire cool-down test (actually this approximation will not quite be the case since the heat losses are higher at the top, the bottom and near the side walls of the tank and convective flows will be induced). The value of the tank temperature is obtained by taking the average value of the thermocouple tree temperatures inside the tank. The decay can be characterized by the following equations which result from an energy balance for the tank.

For T_{env} = const

$$\frac{dU}{dt} = - UA\,(T_T - T_{env}) = M_T\,C_f \frac{d\,T_T}{dt} = M_T\,C_f \frac{d\,(T_T - T_{env})}{dt}$$

With $T_T - T_{env} = \Delta T_c$ we obtain

$$- UA\,\Delta T_c = M_T\,C_f \frac{d\,\Delta T_c}{dt}$$

$$\frac{d\,\Delta T_c}{\Delta T_c} = - \frac{UA}{M_T\,C_f}\,dt$$

which upon integration gives

$$\ln(\Delta T_c) = -\frac{UA}{M_T C_f} t + \text{constant}$$

The quantity ΔT_c is measured as a function of time. Then $\ln(\Delta T_c)$ is plotted versus time which results in a straight line. The slope of $\ln(\Delta T_c)$ vs time is equal to $(-UA/(M_T C_f))$. The quantity $(M_T C_f)$ may also be increased by the appropriate amount (e.g. 1 %) to take into account the mass of the material of the storage tank.

Appendix C

Example TRNSYS Deck

```
**************************************************************
* DECK SET UP TO FORCE INPUTS FOR LOW FLOW TEST #6       *
* LOAD PROFILE 3 (300 LITERS)                            *
* AND HEAT SOURCE FLOW RATE OF "84" KG/H                 *
**************************************************************

EQUATIONS  3
* number of simulation days
  DAYS=10.
* number of simulation hours
  HOURS=DAYS*24.
* simulation time step
  STEP=.05

SIMULATION      0.000E+00   2.400E+02   5.000E-02

TOLERANCES      1.000E-03   1.000E-03

LIMITS  50  4  51

UNIT 14   TYPE 14    HEAT SOURCE MASS FLOW RATE FORCING FUNCTION
PARAMETERS 228
0.000E+00  0.000E+00  7.020E+00  0.000E+00  7.100E+00  8.994E+01  7.180E+00  9.078E+01
7.270E+00  9.018E+01  7.350E+00  8.892E+01  7.440E+00  8.928E+01  7.520E+00  8.910E+01
7.600E+00  8.838E+01  7.690E+00  8.970E+01  7.770E+00  8.898E+01  7.850E+00  8.832E+01
7.940E+00  8.874E+01  8.020E+00  8.904E+01  8.110E+00  8.898E+01  8.200E+00  8.814E+01
8.280E+00  8.982E+01  8.370E+00  9.006E+01  8.450E+00  9.078E+01  8.530E+00  9.024E+01
8.620E+00  9.018E+01  8.700E+00  8.964E+01  8.790E+00  8.982E+01  8.870E+00  9.084E+01
```

8.950E+00	9.018E+01	9.040E+00	9.084E+01	9.200E+00	8.976E+01	9.280E+00	8.988E+01
9.370E+00	9.018E+01	9.450E+00	8.988E+01	9.540E+00	8.994E+01	9.620E+00	9.090E+01
9.700E+00	8.994E+01	9.790E+00	8.970E+01	9.870E+00	8.406E+01	9.960E+00	8.262E+01
1.004E+01	8.298E+01	1.025E+01	8.280E+01	1.034E+01	8.160E+01	1.042E+01	8.214E+01
1.050E+01	8.202E+01	1.059E+01	8.220E+01	1.067E+01	8.262E+01	1.076E+01	8.268E+01
1.084E+01	8.250E+01	1.092E+01	8.262E+01	1.101E+01	8.286E+01	1.109E+01	8.304E+01
1.120E+01	8.388E+01	1.128E+01	8.178E+01	1.137E+01	8.214E+01	1.145E+01	8.208E+01
1.154E+01	8.238E+01	1.162E+01	8.244E+01	1.170E+01	8.202E+01	1.179E+01	8.238E+01
1.187E+01	8.238E+01	1.196E+01	8.250E+01	1.204E+01	8.298E+01	1.216E+01	8.232E+01
1.224E+01	8.208E+01	1.233E+01	8.190E+01	1.241E+01	8.178E+01	1.250E+01	8.220E+01
1.258E+01	8.196E+01	1.266E+01	8.244E+01	1.275E+01	8.298E+01	1.283E+01	8.268E+01
1.292E+01	8.316E+01	1.300E+01	8.244E+01	1.308E+01	8.238E+01	1.317E+01	8.202E+01
1.325E+01	8.142E+01	1.334E+01	8.166E+01	1.342E+01	8.190E+01	1.350E+01	8.124E+01
1.359E+01	8.148E+01	1.367E+01	8.190E+01	1.376E+01	8.040E+01	1.384E+01	8.070E+01
1.392E+01	8.004E+01	1.401E+01	8.088E+01	1.409E+01	8.070E+01	1.417E+01	8.010E+01
1.426E+01	7.992E+01	1.434E+01	7.992E+01	1.443E+01	8.016E+01	1.451E+01	7.974E+01
1.459E+01	7.926E+01	1.468E+01	7.956E+01	1.476E+01	7.974E+01	1.485E+01	7.986E+01
1.493E+01	7.956E+01	1.501E+01	7.962E+01	1.510E+01	7.938E+01	1.518E+01	7.938E+01
1.527E+01	7.926E+01	1.535E+01	7.926E+01	1.543E+01	7.896E+01	1.552E+01	7.944E+01
1.560E+01	7.926E+01	1.569E+01	7.920E+01	1.577E+01	7.938E+01	1.585E+01	7.920E+01
1.594E+01	7.926E+01	1.602E+01	7.926E+01	1.611E+01	7.962E+01	1.619E+01	7.494E+01
1.627E+01	7.956E+01	1.636E+01	7.902E+01	1.644E+01	7.908E+01	1.653E+01	6.606E+01
1.663E+01	0.000E+00	2.400E+01	0.000E+00				

UNIT 15 TYPE 14 HEAT SIDE INPUT TEMPERATURES FORCING FUNCTION

PARAMETERS 232

0.000E+00	0.000E+00	7.020E+00	0.000E+00	7.020E+00	2.061E+01	7.100E+00	1.980E+01
7.180E+00	1.794E+01	7.270E+00	1.749E+01	7.350E+00	1.784E+01	7.440E+00	1.819E+01
7.520E+00	1.864E+01	7.600E+00	1.884E+01	7.690E+00	1.912E+01	7.770E+00	1.954E+01
7.850E+00	1.977E+01	7.940E+00	1.996E+01	8.020E+00	2.051E+01	8.110E+00	2.140E+01
8.200E+00	2.261E+01	8.280E+00	2.115E+01	8.370E+00	2.225E+01	8.450E+00	2.275E+01
8.530E+00	2.310E+01	8.620E+00	2.373E+01	8.700E+00	2.449E+01	8.790E+00	2.534E+01
8.870E+00	2.612E+01	8.950E+00	2.681E+01	9.040E+00	2.719E+01	9.200E+00	2.744E+01
9.280E+00	2.442E+01	9.370E+00	2.508E+01	9.450E+00	2.551E+01	9.540E+00	2.585E+01
9.620E+00	2.650E+01	9.700E+00	2.722E+01	9.790E+00	2.800E+01	9.870E+00	2.929E+01
9.960E+00	3.002E+01	1.004E+01	3.082E+01	1.025E+01	3.114E+01	1.034E+01	2.800E+01

1.042E+01 2.759E+01 1.050E+01 2.797E+01 1.059E+01 2.817E+01 1.067E+01 2.834E+01
1.076E+01 2.853E+01 1.084E+01 2.882E+01 1.092E+01 2.946E+01 1.101E+01 3.066E+01
1.109E+01 3.206E+01 1.120E+01 3.299E+01 1.128E+01 3.025E+01 1.137E+01 2.998E+01
1.145E+01 3.049E+01 1.154E+01 3.079E+01 1.162E+01 3.132E+01 1.170E+01 3.237E+01
1.179E+01 3.372E+01 1.187E+01 3.480E+01 1.196E+01 3.548E+01 1.204E+01 3.597E+01
1.216E+01 3.645E+01 1.224E+01 3.441E+01 1.233E+01 3.346E+01 1.241E+01 3.439E+01
1.250E+01 3.536E+01 1.258E+01 3.653E+01 1.266E+01 3.733E+01 1.275E+01 3.757E+01
1.283E+01 3.778E+01 1.292E+01 3.818E+01 1.300E+01 3.849E+01 1.308E+01 3.880E+01
1.317E+01 3.907E+01 1.325E+01 3.589E+01 1.334E+01 3.616E+01 1.342E+01 3.732E+01
1.350E+01 3.793E+01 1.359E+01 3.864E+01 1.367E+01 3.929E+01 1.376E+01 3.991E+01
1.384E+01 4.052E+01 1.392E+01 4.084E+01 1.401E+01 4.098E+01 1.409E+01 4.124E+01
1.417E+01 4.137E+01 1.426E+01 4.143E+01 1.434E+01 4.127E+01 1.443E+01 4.139E+01
1.451E+01 4.180E+01 1.459E+01 4.218E+01 1.468E+01 4.222E+01 1.476E+01 4.219E+01
1.485E+01 4.230E+01 1.493E+01 4.235E+01 1.501E+01 4.209E+01 1.510E+01 4.188E+01
1.518E+01 4.183E+01 1.527E+01 4.177E+01 1.535E+01 4.144E+01 1.543E+01 4.146E+01
1.552E+01 4.156E+01 1.560E+01 4.146E+01 1.569E+01 4.150E+01 1.577E+01 4.172E+01
1.585E+01 4.174E+01 1.594E+01 4.165E+01 1.602E+01 4.174E+01 1.611E+01 4.166E+01
1.619E+01 4.193E+01 1.627E+01 3.061E+01 1.636E+01 2.819E+01 1.644E+01 2.975E+01
1.653E+01 3.183E+01 1.663E+01 3.143E+01 1.663E+01 0.000E+00 2.400E+01 0.000E+00

UNIT 16 TYPE 14 LOAD MASS FLOW FORCING FUNCTION

PARAMETERS 148

0.000E+00 0.000E+00 7.000E+00 0.000E+00 7.000E+00 2.000E+02 7.050E+00 2.000E+02
7.050E+00 0.000E+00 8.000E+00 0.000E+00 8.000E+00 4.000E+02 8.050E+00 4.000E+02
8.050E+00 1.000E+02 8.100E+00 1.000E+02 8.100E+00 0.000E+00 9.000E+00 0.000E+00
9.000E+00 4.000E+02 9.050E+00 4.000E+02 9.050E+00 1.000E+02 9.100E+00 1.000E+02
9.100E+00 0.000E+00 1.000E+01 0.000E+00 1.000E+01 4.000E+02 1.010E+01 4.000E+02
1.010E+01 1.000E+02 1.015E+01 1.000E+02 1.015E+01 0.000E+00 1.100E+01 0.000E+00
1.100E+01 4.000E+02 1.105E+01 4.000E+02 1.105E+01 1.000E+02 1.110E+01 1.000E+02
1.110E+01 0.000E+00 1.200E+01 0.000E+00 1.200E+01 2.000E+02 1.205E+01 2.000E+02
1.205E+01 0.000E+00 1.300E+01 0.000E+00 1.300E+01 1.000E+02 1.305E+01 1.000E+02
1.305E+01 0.000E+00 1.600E+01 0.000E+00 1.600E+01 3.000E+02 1.605E+01 3.000E+02
1.605E+01 0.000E+00 1.700E+01 0.000E+00 1.700E+01 4.000E+02 1.705E+01 4.000E+02
1.705E+01 1.000E+02 1.710E+01 1.000E+02 1.710E+01 0.000E+00 1.800E+01 0.000E+00
1.800E+01 4.000E+02 1.810E+01 4.000E+02 1.810E+01 1.000E+02 1.815E+01 1.000E+02
1.815E+01 0.000E+00 1.900E+01 0.000E+00 1.900E+01 4.000E+02 1.905E+01 4.000E+02

1.905E+01 1.000E+02 1.910E+01 1.000E+02 1.910E+01 0.000E+00 2.000E+01 0.000E+00
2.000E+01 4.000E+02 2.005E+01 4.000E+02 2.005E+01 2.000E+02 2.010E+01 2.000E+02
2.010E+01 0.000E+00 2.100E+01 0.000E+00 2.100E+01 2.000E+02 2.105E+01 2.000E+02
2.105E+01 0.000E+00 2.200E+01 0.000E+00 2.200E+01 1.000E+02 2.205E+01 1.000E+02
2.205E+01 0.000E+00 2.400E+01 0.000E+00

UNIT 17 TYPE 14 MAINS WATER TEMPERATURE FORCING FUNCTION
PARAMETERS 116

0.000E+00 0.000E+00 7.000E+00 0.000E+00 7.000E+00 1.473E+01 7.150E+00 1.473E+01
7.150E+00 0.000E+00 8.000E+00 0.000E+00 8.000E+00 1.470E+01 8.150E+00 1.474E+01
8.150E+00 0.000E+00 9.000E+00 0.000E+00 9.000E+00 1.462E+01 9.150E+00 1.462E+01
9.150E+00 0.000E+00 1.000E+01 0.000E+00 1.000E+01 1.460E+01 1.015E+01 1.460E+01
1.015E+01 0.000E+00 1.100E+01 0.000E+00 1.100E+01 1.469E+01 1.115E+01 1.469E+01
1.115E+01 0.000E+00 1.200E+01 0.000E+00 1.200E+01 1.569E+01 1.215E+01 1.569E+01
1.215E+01 0.000E+00 1.300E+01 0.000E+00 1.300E+01 1.761E+01 1.315E+01 1.761E+01
1.315E+01 0.000E+00 1.600E+01 0.000E+00 1.600E+01 1.635E+01 1.615E+01 1.635E+01
1.615E+01 0.000E+00 1.700E+01 0.000E+00 1.700E+01 1.490E+01 1.715E+01 1.490E+01
1.715E+01 0.000E+00 1.800E+01 0.000E+00 1.800E+01 1.457E+01 1.815E+01 1.457E+01
1.815E+01 0.000E+00 1.900E+01 0.000E+00 1.900E+01 1.474E+01 1.915E+01 1.474E+01
1.915E+01 0.000E+00 2.000E+01 0.000E+00 2.000E+01 1.449E+01 2.015E+01 1.449E+01
2.015E+01 0.000E+00 2.100E+01 0.000E+00 2.100E+01 1.502E+01 2.115E+01 1.502E+01
2.115E+01 0.000E+00 2.200E+01 0.000E+00 2.200E+01 1.515E+01 2.215E+01 1.515E+01
2.215E+01 0.000E+00 2.400E+01 0.000E+00

UNIT 18 TYPE 14 ENVIRONMENTAL TEMPERATURE FORCING FUNCTION
PARAMETERS 500

0.000E+00 1.924E+01 6.000E-02 1.924E+01 1.500E-01 1.941E+01 2.500E-01 1.949E+01
3.400E-01 1.921E+01 4.300E-01 1.951E+01 5.300E-01 1.986E+01 6.200E-01 2.014E+01
7.200E-01 2.040E+01 8.100E-01 2.061E+01 9.000E-01 2.076E+01 1.000E+00 2.029E+01
1.090E+00 1.982E+01 1.190E+00 1.944E+01 1.280E+00 1.964E+01 1.370E+00 1.993E+01
1.470E+00 1.977E+01 1.560E+00 1.939E+01 1.660E+00 1.915E+01 1.750E+00 1.929E+01
1.840E+00 1.963E+01 1.940E+00 1.984E+01 2.030E+00 1.946E+01 2.130E+00 1.942E+01
2.220E+00 1.973E+01 2.310E+00 1.949E+01 2.410E+00 1.918E+01 2.500E+00 1.912E+01
2.600E+00 1.943E+01 2.690E+00 1.976E+01 2.780E+00 2.005E+01 2.880E+00 2.030E+01
2.970E+00 2.055E+01 3.070E+00 2.071E+01 3.160E+00 2.083E+01 3.250E+00 2.070E+01
3.350E+00 2.002E+01 3.440E+00 1.955E+01 3.540E+00 1.961E+01 3.630E+00 1.988E+01

3.720E+00	1.966E+01	3.820E+00	1.929E+01	3.910E+00	1.902E+01	4.010E+00	1.931E+01
4.100E+00	1.967E+01	4.190E+00	1.993E+01	4.290E+00	2.020E+01	4.380E+00	2.043E+01
4.480E+00	2.061E+01	4.570E+00	2.028E+01	4.660E+00	1.966E+01	4.760E+00	1.919E+01
4.850E+00	1.935E+01	4.950E+00	1.965E+01	5.040E+00	1.997E+01	5.140E+00	1.979E+01
5.230E+00	1.936E+01	5.320E+00	1.898E+01	5.420E+00	1.911E+01	5.510E+00	1.942E+01
5.610E+00	1.973E+01	5.700E+00	2.005E+01	5.790E+00	2.027E+01	5.890E+00	2.045E+01
5.980E+00	2.035E+01	6.080E+00	1.975E+01	6.170E+00	1.924E+01	6.260E+00	1.923E+01
6.360E+00	1.952E+01	6.450E+00	1.979E+01	6.550E+00	2.007E+01	6.640E+00	1.992E+01
6.730E+00	1.944E+01	6.830E+00	1.899E+01	6.920E+00	1.928E+01	7.020E+00	1.953E+01
7.100E+00	1.983E+01	7.180E+00	2.011E+01	7.270E+00	2.027E+01	7.350E+00	2.021E+01
7.440E+00	1.967E+01	7.520E+00	1.922E+01	7.600E+00	1.901E+01	7.690E+00	1.927E+01
7.770E+00	1.952E+01	7.850E+00	1.982E+01	7.940E+00	2.002E+01	8.020E+00	2.023E+01
8.110E+00	2.001E+01	8.200E+00	1.935E+01	8.280E+00	1.902E+01	8.370E+00	1.914E+01
8.450E+00	1.939E+01	8.530E+00	1.964E+01	8.620E+00	1.987E+01	8.700E+00	2.007E+01
8.790E+00	2.024E+01	8.870E+00	2.006E+01	8.950E+00	1.951E+01	9.040E+00	1.910E+01
9.200E+00	1.910E+01	9.280E+00	1.959E+01	9.370E+00	1.979E+01	9.450E+00	2.001E+01
9.540E+00	2.022E+01	9.620E+00	1.994E+01	9.700E+00	1.943E+01	9.790E+00	1.906E+01
9.870E+00	1.917E+01	9.960E+00	1.940E+01	1.004E+01	1.964E+01	1.025E+01	1.983E+01
1.034E+01	2.034E+01	1.042E+01	2.023E+01	1.050E+01	1.966E+01	1.059E+01	1.923E+01
1.067E+01	1.924E+01	1.076E+01	1.952E+01	1.084E+01	1.970E+01	1.092E+01	1.997E+01
1.101E+01	2.020E+01	1.109E+01	2.023E+01	1.120E+01	1.988E+01	1.128E+01	1.915E+01
1.137E+01	1.919E+01	1.145E+01	1.947E+01	1.154E+01	1.973E+01	1.162E+01	1.996E+01
1.170E+01	2.015E+01	1.179E+01	2.032E+01	1.187E+01	2.035E+01	1.196E+01	1.994E+01
1.204E+01	1.949E+01	1.216E+01	1.945E+01	1.224E+01	1.975E+01	1.233E+01	1.998E+01
1.241E+01	2.019E+01	1.250E+01	2.037E+01	1.258E+01	2.053E+01	1.266E+01	2.045E+01
1.275E+01	1.992E+01	1.283E+01	1.954E+01	1.292E+01	1.958E+01	1.300E+01	1.979E+01
1.308E+01	1.998E+01	1.317E+01	1.974E+01	1.325E+01	1.936E+01	1.334E+01	1.916E+01
1.342E+01	1.941E+01	1.350E+01	1.964E+01	1.359E+01	1.987E+01	1.367E+01	2.011E+01
1.376E+01	2.028E+01	1.384E+01	2.046E+01	1.392E+01	2.061E+01	1.401E+01	2.073E+01
1.409E+01	2.082E+01	1.417E+01	2.078E+01	1.426E+01	2.032E+01	1.434E+01	1.988E+01
1.443E+01	1.980E+01	1.451E+01	2.001E+01	1.459E+01	2.003E+01	1.468E+01	1.971E+01
1.476E+01	1.940E+01	1.485E+01	1.950E+01	1.493E+01	1.975E+01	1.501E+01	1.996E+01
1.510E+01	2.015E+01	1.518E+01	2.031E+01	1.527E+01	2.051E+01	1.535E+01	2.067E+01
1.543E+01	2.084E+01	1.552E+01	2.097E+01	1.560E+01	2.104E+01	1.569E+01	2.113E+01
1.577E+01	2.121E+01	1.585E+01	2.129E+01	1.594E+01	2.138E+01	1.602E+01	2.141E+01
1.611E+01	2.146E+01	1.619E+01	2.149E+01	1.627E+01	2.155E+01	1.636E+01	2.162E+01

1.644E+01 2.164E+01 1.653E+01 2.164E+01 1.663E+01 2.173E+01 1.672E+01 2.167E+01
1.682E+01 2.108E+01 1.691E+01 2.056E+01 1.701E+01 2.032E+01 1.710E+01 2.005E+01
1.722E+01 1.973E+01 1.731E+01 1.959E+01 1.741E+01 1.985E+01 1.750E+01 1.977E+01
1.759E+01 1.952E+01 1.769E+01 1.940E+01 1.778E+01 1.927E+01 1.787E+01 1.920E+01
1.797E+01 1.923E+01 1.806E+01 1.950E+01 1.828E+01 1.964E+01 1.837E+01 1.930E+01
1.846E+01 1.910E+01 1.856E+01 1.937E+01 1.865E+01 1.965E+01 1.875E+01 1.987E+01
1.884E+01 2.008E+01 1.893E+01 2.027E+01 1.903E+01 2.048E+01 1.912E+01 2.040E+01
1.923E+01 1.938E+01 1.932E+01 1.938E+01 1.942E+01 1.960E+01 1.951E+01 1.978E+01
1.960E+01 2.000E+01 1.970E+01 2.021E+01 1.998E+01 1.923E+01 2.007E+01 1.943E+01
2.025E+01 1.970E+01 2.034E+01 2.014E+01 2.053E+01 2.060E+01 2.063E+01 2.078E+01
2.081E+01 2.099E+01 2.091E+01 2.104E+01 2.110E+01 2.117E+01 2.120E+01 2.123E+01
2.130E+01 2.086E+01 2.139E+01 2.025E+01 2.158E+01 1.963E+01 2.167E+01 1.988E+01
2.177E+01 2.008E+01 2.186E+01 2.003E+01 2.205E+01 1.932E+01 2.223E+01 1.978E+01
2.233E+01 1.962E+01 2.242E+01 1.942E+01 2.251E+01 1.964E+01 2.261E+01 1.981E+01
2.270E+01 1.943E+01 2.280E+01 1.913E+01 2.289E+01 1.930E+01 2.308E+01 1.978E+01
2.327E+01 2.026E+01 2.346E+01 2.050E+01 2.355E+01 1.999E+01 2.374E+01 1.939E+01
2.383E+01 1.961E+01 2.400E+01 1.961E+01

UNIT 38 TYPE 38 PLUG FLOW TANK MODEL
PARAMETERS 12
1.000E+00 1.800E-01 9.200E-01 9.200E-01 4.190E+00 1.000E+03 0.000E+00
1.000E+00 1.645E+01 1.000E+00 1.500E+01 1.270E-02
INPUTS 5
15,1 14,1 17,1 16,1 18,1
0.000E+00 0.000E+00 0.000E+00 0.000E+00 0.000E+00

UNIT 24 TYPE 24 INTEGRATOR ENERGIES AND FLOWS
PARAMETERS 1
2.400E+01
INPUTS 5
38,9 38,6 38,5 38,2 38,4
0.000E+00 0.000E+00 0.000E+00 0.000E+00 0.000E+00

UNIT 25 TYPE 25 PRINTER TEMPERATURES AND HEAT SOURCE FLOW RATE
PARAMETERS 4
5.000E-02 2.231E+02 2.326E+02 1.000E+01

```
INPUTS  3
38,1            15,1            14,1
TRET            THEAT           MHEAT

UNIT 26    TYPE 25    PRINTER INTEGRATED ENERGIES AND FLOWS
PARAMETERS  4
2.400E+01   0.000E+00   2.400E+02   1.100E+01
INPUTS  5
24,1            24,2            24,3            24,4            24,5
QIN             QDEL            QENV            HEATFL          LOADFL

END
```

References

1. Z. Lavan and J. Thompson, *Experimental Study of Thermally Stratified Hot Water Storage Tanks*, Solar Energy, Vol. 19, pp. 519 - 524, 1977

2. H. N. Gari and R. I. Loehrke, *A Controlled Buoyant Jet for Enhancing Stratification in a Liquid Storage Tank*, Journal of Fluids Engineering, Vol. 104, pp. 475 - 481, 1982

3. C. W. Miller, *Effect of a Conducting Wall on a Stratified Fluid in a Cylinder*, Heat Transfer and Thermal Control Systems, Progress in Astronautics and Aeronautics, Vol. 60, pp. 190 - 208, 1977

4. Y. Jaluria and S. K. Gupta, *Decay of Thermal Stratification in a Water Body for Solar Energy Storage,* Solar Energy, Vol. 28, pp. 137 - 143, 1982

5. C. F. Hess and C. W. Miller, *An Experimental and Numerical Study on the Effect of the Wall in a Thermocline-Type Cylindrical Enclosure-I*, Solar Energy, Vol. 28, pp. 145 - 152, 1982

6. C. Sherman, B. D. Wood and J. Mason, *Effect of Vertical Wall Conduction on Temperature Relaxation in Thermally Stratified Liquid Thermal Storage Tanks*, Sun II, Proceedings of the International Solar Energy Society Silver Jubilee Congress, Atlanta, pp. 591 - 595, Pergamon Press, New York, 1979

7. B. J. Sliwinski, A. R. Mech and R. S. Shih, *Stratification in Thermal Storage during Charging*, 6th International Heat Transfer Conference, Toronto, Vol. 4, pp. 149 - 154, 1978

8. R. I. Loehrke and J. C. Holzer, *Stratified Thermal Storage Experiments*, Technical Report HT-TS793, Prepared for the Boeing Computer Services Company, Seattle, Washington, July 1979

9. J. A. Duffie and W. A. Beckman, *Solar Engineering of Thermal Processes*, Wiley Interscience, New York, 1980

10. M. K. Sharp and R. I. Loehrke, *Stratified Thermal Storage in Residential Solar Energy Applications*, Journal of Energy, Vol. 3(2), pp. 106 - 113, 1979

11. C. W. J. Van Koppen, J. P. S. Thomas and W. B. Veltkamp, *The Actual Benefits of Thermally Stratified Storage in a Small and Medium Size Solar System*, Sun II, Proceedings ISES Biennial Meeting, Atlanta, Georgia, Vol. 2, pp. 576 - 580, Pergamon Press, New York, 1979

12. R. J. Briggs and J. E. Ferguson, *Effects of Stratification Enhancement on Performance of a Solar DHW System*, Proceedings for SESCI '84 Calgary Conference, pp. 63 - 66, 1984

13. A. H. Fanney and S. A. Klein, *Thermal Performance Comparisons for Solar Hot Water Systems Subjected to Various Collector and Heat Exchanger Flow Rates*, Solar Energy, Vol. 40, pp. 1 - 11, 1988

14. H. C. Hottel and A. Whillier, *Evaluation of Flat-Plate Solar Heat Collectors*, Proc. Conference on the Use of Solar Energy, Vol. 2, p. 74, University of Arizona, Tucson, 1955

15. W. F. Phillips and R. N. Dave, *Effects of Stratification on the Performance of Liquid-Based Solar Heating Systems*, Solar Energy, Vol. 29, pp. 111 - 120, 1982

16. Li-Yun Wu and R. B. Bannerot, *An Experimental Study of the Effect of Water Extraction on Thermal Stratification in Storage*, Solar Engrg. - 1987, Proc. of the ASME-JSME-JSES Solar Energy Conf., March 22 -27, 1987, Honululu, Hawaii

17. S. M. Koldhekar, *Temperature Stratification in Hot Water Solar Thermal Preheat Storage Tanks*, M.S. Thesis, Department of Mechanical and Aerospace Engineering, Arizona State University, Tempe, Arizona

18. R. W. Bliss, *The Derivation of Several 'Plate-Efficiency Factors' Useful in the Design of Flat-Plate Solar Heat Collectors*, Solar Energy, Vol. 3 (No. 4), pp. 55, - 64, 1959

19. S. A. Klein, *A Design Procedure for Solar Heating Systems*, Ph. D. Thesis., Department of Chemical Engineering, University of Wisconsin-Madison, 1976

20. S. A. Klein et al., *TRNSYS 13.1 User's Manual*, Engineering Experiment Station Report 38-13, Solar Energy Laboratory, University of Wisconsin-Madison, 1990

21. J. K. Kuhn, G. F. VanFuchs and A. P. Zob, *Developing and Upgrading of Solar System Thermal Energy Storage Simulation Models*, Draft Report for DOE, Boeing Computer Services Company, August 31, 1980

22. S. M. Han and S. T. Wu, *Computer Simulation of a Solar Energy System with a Viscous-Entrainment Liquid Storage Tank Model*, Proceedings of the Third Southeastern Conference on Application of Solar Energy, S. T. Wu, D. L. Christensen and R. R. Head, eds., pp. 165 - 182, 1978

23. W. F. Phillips and R. A. Pate, *Mass and Energy Transfer in a Hot Liquid Energy Storage System*, Proceedings of the American Section of the International Solar Energy Society, Orlando, Florida, 1977

24. M. Lightstone, *Mathematical Model of Plume Entrainment*, Solar Thermal Research Laboratory, University of Waterloo, Ontario, Canada, December 1987

25. R. L. Cole and F. O. Bellinger, *Natural Thermal Stratification in Tanks*, Argonne National Laboratory Report ANL-82-5, Februar 1982

26. Y. H. Zurigat, P. R. Liche and A. J. Ghajar, *Turbulent Mixing Correlations for a Thermocline Thermal Storage Tank*, AICHE Symposium Series, S. B. Yilmaz, ed., AICHE, No. 263, Vol. 84, pp. 160 - 168, 1988

27. F. J. Oppel, A. J. Ghajar and P. M. Moretti, *A Numerical and Experimental Study of Stratified Thermal Storage*, ASHRAE Transactions, Vol. 92, Part 2, pp. 293 - 309, 1986

28. M. K. Sharp, *Thermal Stratification in Liquid Sensible Heat Storage*, M.S. Thesis, Colorado State University, Fort Collins, Colorado, 1978

29. D. J. Close, *A Design Approach for Solar Processes*, Solar Energy, Vol. 11, No. 2, pp. 112 - 122, 1967

30. M. W. Wildin and C. R. Truman, *Evaluation of Stratified Chilled-Water Storage Technique*, EPRI Report EPRI EM-4352, December 1985

31. A. Cabelli, *Storage Tanks - A Numerical Experiment*, Solar Energy, Vol. 19, pp. 45 - 54, 1977

32. K. L. Gu and S. T. Wu, *Numerical Study of Flow and Temperature Stratifications in a Liquid Thermal Storage Tank*, ASME Journal of Solar Energy Engineering, Vol. 107, pp. 15 - 20, 1985

33. A. M. C. Chan, P. S. Smereka and D. Giusti, *A Numerical Study of Transient Mixed Convection Flows in a Thermal Storage Tank*, ASME Journal of Solar Energy Engineering, Vol. 105, pp. 246 - 253, 1983

34. W. T. Sha, E. I. H. Lin, R. C. Schmitt, K. V. Lin, J. R. Hull, J. J. Oras, Jr.and H. M. Domanus, *COMMIX-SA-1: A Three-Dimensional Thermohydrodynamic Computer Program for Solar Applications*, Argonne National Lab. Report ANL-80-8, November 1980

35. M. F. Lightstone, G. D. Raithby and K. G. T. Hollands, *Numerical Simulation of the Charging of Liquid Storage Tanks: Comparison with Experiment*, ASME Journal of Solar Energy Engineering, Vol. 111, pp. 225 - 231, 1989

36. K. DenBraven, *An Analytical Model of Stratification for Liquid-Based Solar Systems*, ASME Journal of Solar Energy Engineering, Vol. 108, pp. 105 - 110, 1986

37. R. A. Pate, Ph. D. Thesis, Utah State University, 1977

38. H. Schlichting, *Boundary Layer Theory*, Sixth Edition, McGraw-Hill, New York, 1968

39. B. J. Hill, *Measurements of Local Entrainment Rate in the Initial Region of Axisymmetric Turbulent Air Jet*, Journal of Fluid Mechanics, Vol. 51, pp. 773 - 779, 1972

40. S. V. Patankar, *Numerical Heat Transfer and Fluid Flow*, Hemisphere, Washington, D. C., 1980

41. *WATSUN User's Manual and Program Documentation Version 12.0/90-04*, WATSUN Simulation Lab, University of Waterloo, Ontario, Canada, 1990

42. R. J. Cataford and S. J. Harrison, *Experimental Investigation of the Effects of Storage Tank Stratification on SDHW System Performance*, ISES '89, Kobe, Japan, 1989